Volume 66
June 2023
ISSN 2217-8139 (Print)
ISSN 2335-0229 (Online)
UDK: 06.055.2:62-03+620.1+624.001.5(497.1)=861

GRAĐEVINSKI MATERIJALI I KONSTRUKCIJE

BUILDING MATERIALS AND STRUCTURES

2

Society for Materials and Structures Testing of Serbia
University of Belgrade Faculty of Civil Engineering
Association of Structural Engineers of Serbia

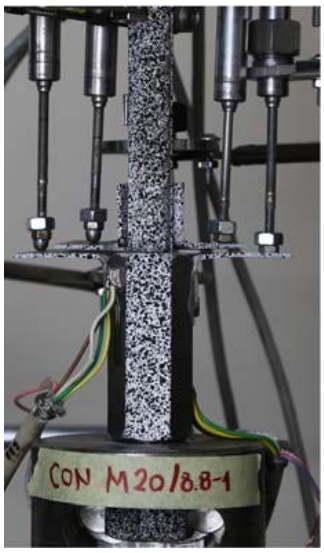

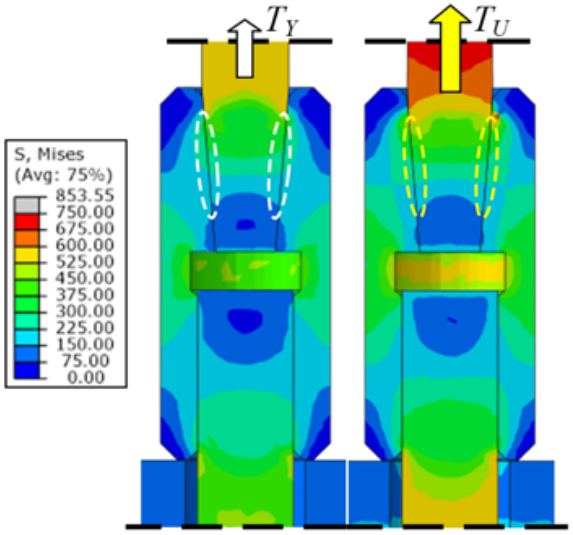

GRAĐEVINSKI MATERIJALI I KONSTRUKCIJE

BUILDING MATERIALS AND STRUCTURES

ISSN 2217-8139 (PRINT)
ISSN 2335-0229 (Online)

VOLUME 66(2)
June 2023

CONTENTS

GRAĐEVINSKI MATERIJALI I KONSTRUKCIJE

BUILDING MATERIALS AND STRUCTURES

ISSN 2217-8139 (PRINT)
ISSN 2335-0229 (Online)

VOLUME 66(2)
June 2023

EDITORIAL BOARD

Aims and scope

Building Materials and Structures aims at providing an international forum for communication and dissemination of innovative research and application in the field of building materials and structures. Journal publishes papers on the characterization of building materials properties, their technologies and modeling. In the area of structural engineering Journal publishes papers dealing with new developments in application of structural mechanics principles and digital technologies for the analysis and design of structures, as well as on the application and skillful use of novel building materials and technologies.

The scope of Building Materials and Structures encompasses, but is not restricted to, the following areas: conventional and non-conventional building materials, recycled materials, smart materials such as nanomaterials and bio-inspired materials, infrastructure engineering, earthquake engineering, wind engineering, fire engineering, blast engineering, structural reliability and integrity, life cycle assessment, structural optimization, structural health monitoring, digital design methods, data-driven analysis methods, experimental methods, performance-based design, innovative construction technologies, and value engineering.

Publishers Society for Materials and Structures Testing of Serbia, Belgrade, Serbia, veb sajt: www.dimk.rs
University of Belgrade Faculty of Civil Engineering, Belgrade, Serbia, www.grf.bg.ac.rs
Association of Structural Engineers of Serbia, Belgrade, Serbia, dgks.grf.bg.ac.rs

Print Razvojno istraživački centar grafičkog inženjerstva, Belgrade, Serbia

Edition quarterly

Peer reviewed journal

Journal homepage www.dimk.rs

Cover **Connector appearance during and after the tensile test and connector stresses in case coupler-rebar connection modelled with „Tie“ constraint,** *from Local behaviour of the connector with mechanical coupler and rebar anchor under tension load* by Ivan Milićević, Branko Milosavljević, Milan Spremić, Rastislav Mandić and Marko Popović

Financial support Ministry of Education, Science and Technological Development of Republic of Serbia
University of Belgrade Faculty of Civil Engineering
Institute for testing of materials-IMS Institute, Belgrade
Faculty of Technical Sciences, University of Novi Sad, Department of Civil Engineering
Serbian Chamber of Engineers

CIP - Каталогизација у публикацији
Народна библиотека Србије, Београд

620.1

GRAĐEVINSKI materijali i konstrukcije = Building materials and structures / editor-in-chief Snežana Marinković
. - God. 54, br. 3 (2011)- . - Belgrade : Society for Materials and Structures Testing of Serbia : University of Belgrade, Faculty of Civil Engineering : Association of Structural Engineers of Serbia, 2011- (Belgrade : Razvojno istraživački centar grafičkog inženjerstva). - 30 cm

Tromesečno. - Je nastavak: Materijali i konstrukcije = ISSN 0543-0798. - Drugo izdanje na drugom medijumu: Građevinski materijali i konstrukcije (Online) = ISSN 2335-0229
ISSN 2217-8139 = Građevinski materijali i konstrukcije
COBISS.SR-ID 188695820

Građevinski materijali i konstrukcije
Building Materials and Structures
journal homepage: www.dimk.rs

https://doi.org/10.5937/GRMK2300001R UDK: 624.21.042
625.745.11

Invited paper

Emerging research on vibration serviceability assessment of pedestrian structures

Vitomir Racić*[1)]

[1)] *University of Belgrade, Faculty of Civil Engineering, Bulevar kralja Aleksandra 73, 11000 Belgrade, Serbia*

Article history
Received: 17 January 2023
Received in revised form:
25 February 2023
Accepted: 27 March 2023
Available online: 05 May 2023

Keywords
human-structure dynamic interaction,
walking forces,
crowd dynamic loading,
ground reaction forces

ABSTRACT

Despite an increasing number of reported vibration serviceability problems caused by pedestrians walking on newly built footbridges, floors, and staircases around the world, there is still a lack of adequate codes of practice. There are three key issues that a new generation of relevant design guidelines should urgently address: (1) the absence of a universal model that accounts for the entire energy spectrum of walking loading as well as inter- and intra-subject variability of individual walking forces; (2) the effect of human bodies on the dynamic properties of a structure; and (3) pedestrian "intelligent" interaction with the surrounding people and environment. This article provides a brief overview of the relevant state-of-the-art research that has great potential to change this unsatisfactory state of affairs.

1 Introduction

Substantial developments in workmanship and structural materials aided by digitalisation of structural analysis have enabled daring architects and structural engineers to promote elegant but lightweight and flexible structures. As structures are becoming slenderer than ever, vibration serviceability assessment under pedestrian-induced dynamic excitation has become a routine requirement requirement in contemporary design [1-5]. While running and jumping produce more dramatic vibration responses [6,] walking is the most common form of locomotion and can be sustained for longer periods of time. Having reduced the natural frequency, this means an increased likelihood of a resonant response.

Predicting vibration responses reliably is a vital component of structural design. Retrofits after construction come at a high price and take time. For example, using tune-mass dampers to solve the lateral sway problem of the London Millennium Bridge increased the structure's cost by 30% and took two years to complete [7, 8]. Extra material is frequently added in common engineering practice to increase stiffness and/or mass in order to shift natural frequencies. For instance, an additional concrete topping is frequently placed on floor slabs and bridge decks to increase their weight. Regarding the global campaign to urgently reduce unnecessary embodied carbon emissions from the structure, the addition of excess material is increasingly deemed unacceptable [9].

Generally speaking, the formal procedure for the design of any structure for which pedestrian dynamic loading is a major concern involves: (1) establishing acceptance criteria, (2) determining the dynamic design loads, (3) creating a structural model, (4) simulating the structure´s response to the loads, (5) comparing results against the acceptance criteria, and (6) if necessary, adjusting the structural model, then repeating steps (4), (5) and (6) until satisfactory performance is achieved. Of all these steps, determining the design load has the greatest uncertainty, and to this end, there have been numerous attempts to provide reliable and practical descriptions of pedestrian induced forces. This issue will be elaborated in Section 2.

There is a widespread yet utterly wrong assumption that walking people affect structural vibrations only through the inertia of their moving body mass, thereby acting only as the dynamic excitation [6]. In reality, human bodies are mechanisms with mass, stiffness, and damping. When attached to the structure, they have the power to alter the modal properties of the empty structure [10]. Generally known as “human-structure interaction” (HSI), this aspect of the human influence on structural vibration will be discussed in Section 3.

A single pedestrian walking is a hardly relevant load case scenario for footbridges. Pedestrian groups and ultimately crowds are a far more likely source of dynamic excitation in urban environments. However, due to multiple pedestrian occupants, there is a severe lack of reliable force and HSI models, as will be revealed in Section 4.

2 Dynamic loading due to individuals walking

The modern design guidelines and codes of practice model a pedestrian as a moving force F(t) generated at the point of contact between the feet and the supporting structure, known as "ground reaction force" or GRF (Figure 1). It is traditionally modelled as a deterministic and perfectly periodic function (Figure 2), presentable by the sum of the first few dominant Fourier harmonics [6, 11, 12]:

* Corresponding author:
E-mail address: vracic@grf.bg.ac.rs

$$F(t) = W + \sum_{n=1}^{N} A_n \sin(2\pi n f_p + \theta_n) \quad (1)$$

Here, f_p is walking frequency (also called pacing rate), W is the mean value (equivalent to the body weight of a pedestrian), A_n are harmonic amplitudes, θ_n are the corresponding phase angles, and N determines the number of harmonics considered in a model. One harmonic is tuned to match the frequency of a target mode of the structure to induce resonance (Figure 1a). The simplest such model is a single sinusoidal function and can be found in the current UK [13] and Canadian [14] design codes for footbridges. On the other hand, vibration design guidelines primarily for floors [15-18] provide for up to four harmonics. There are models comprising even the sixth harmonic [19]. In the time domain, vibration analysis of the structure is assumed to be linearly elastic. Based on the principles of modal decomposition, the vibration response of each mode can be studied separately using harmonic loads described by the appropriate mode shape to account for the moving load [20].

The weight-normalised coefficients $\alpha_n = A_n/W$ are commonly reported in the literature as dynamic load factors (DLFs), which depend on walking frequency f_p and a person's manner of walking [6]. In a comprehensive experimental study of walking DLFs, Kerr [21] observed a wide variability of DLF values among different pedestrians while walking at different walking frequencies, so called "inter-subject variability". Based on Kerr's dataset, Young [22] fitted a frequency-dependent mean and coefficient of variation for the first four DLFs. These deterministic DLF functions are most widely used in the design of pedestrian structures [6]. Deterministic means that there is a uniform force model for naturally diverse individuals, thereby neglecting the true stochastic nature of walking loading.

The random nature of phase angles θ_n has been utilised very little in design practice. This is because vibration analysis focuses mostly on the resonance due to a single harmonic, so the phase angles have no influence on the overall response. However, when the modes are closely spaced phase angles determine if the responses due to each harmonic result in an increase or decrease in the overall vibration level.

The Fourier modelling approach described by Equation (1) seems too good to be true. Years of experimental and analytical research, as well as application in design practice, have shown that the Fourier characterization is insufficient to reliably describe walking loading. Brownjohn et al. [23] showed that perfect periodicity oversimplifies reality, yielding inaccuracies as high as 50% between simulated and measured vertical vibrations. Rare studies [24] addressed the randomness of inter-subject variability by providing statistical distributions of DLFs. However, a model of intra-subject variability that would address the near-periodic nature of successive footfalls is yet to be seen.

Modern research laboratories and hospitals increasingly accommodate equipment sensitive to even micro-levels of non-resonant vibration. The high-frequency content of walking has become relevant for the design of "high-frequency floors", i.e., when the natural frequency of the fundamental mode of vibration is far above the average pacing rate. Their vibration response has a series of transient decays due to each footfall (Figure 1c). No resonant buildup of vibrations (Figure 1a) can be developed due to the high level of damping that is typical for HFF [25].

The difference in the nature of resonant and transient vibration responses (Figure 1a and 1c) has led to a requirement for two conceptually distinct walking force models used in the design guidelines of low-frequency and high-frequency structures. For floors, the most-up-to date guidance is available in Appendix G [17] of the Concrete Society Technical Report 43 (CSTR43). It provides design values of DLFs for single pedestrians on low-frequency floors (i.e., if f_n<10 Hz) and equivalent impulse values (Equation 2) for high-frequency floors (i.e., if f_n>10 Hz).

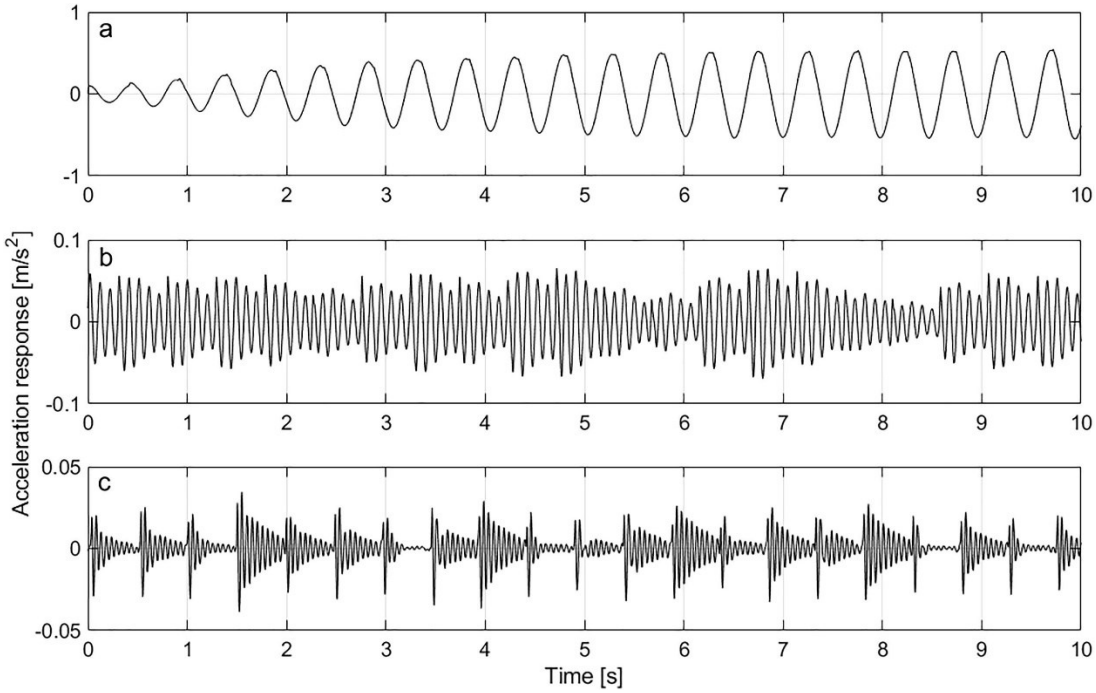

Figure 1. Measured vibration responses of a floor with the fundamental frequency a) 2 Hz, b) 10 Hz and c) 20 Hz due to an individual walking at f_p=2 Hz (after [33])

$$I_{eff} = 54\frac{f_p^{1.43}}{f_n^{1.3}} \quad (2)$$

This artificial division proves unreliable when the fundamental frequency of a floor is close to the cut-off frequency between the low-frequency and high-frequency floors (Figure 1b), which clearly indicates the need for a uniform model capable of taking into account the complete frequency content of walking forces [6, 11]. In an attempt to overcome this problem, Zivanovic and Pavic [26] merged together the Appendix G impulses and their previously published low-frequency force model based on the Fourier approach [27]. The new model takes into account the differences in the walking force induced by different people and, as a result, can estimate the probability distribution of vibration responses generated by a pedestrian population. However, Middleton [28] showed that inter-subject variations do not affect the dynamic response as much as variations in an individual's pace rate for successive steps. This randomness is called "intra-subject variability", which essentially means that people do not walk regularly like robots. In the case of high-frequency floors, a lack of these variations can overestimate response by up to 40%. Various authors [23, 29-31] showed that the actual narrow-band nature of the forces could be described in the frequency domain via auto-spectral density (ASD). However, predicted acceleration provides no information about the expected performance of the structure in real time. For instance, when and where do the peak responses happen? Therefore, a reliable time-domain model of walking forces is clearly the way forward.

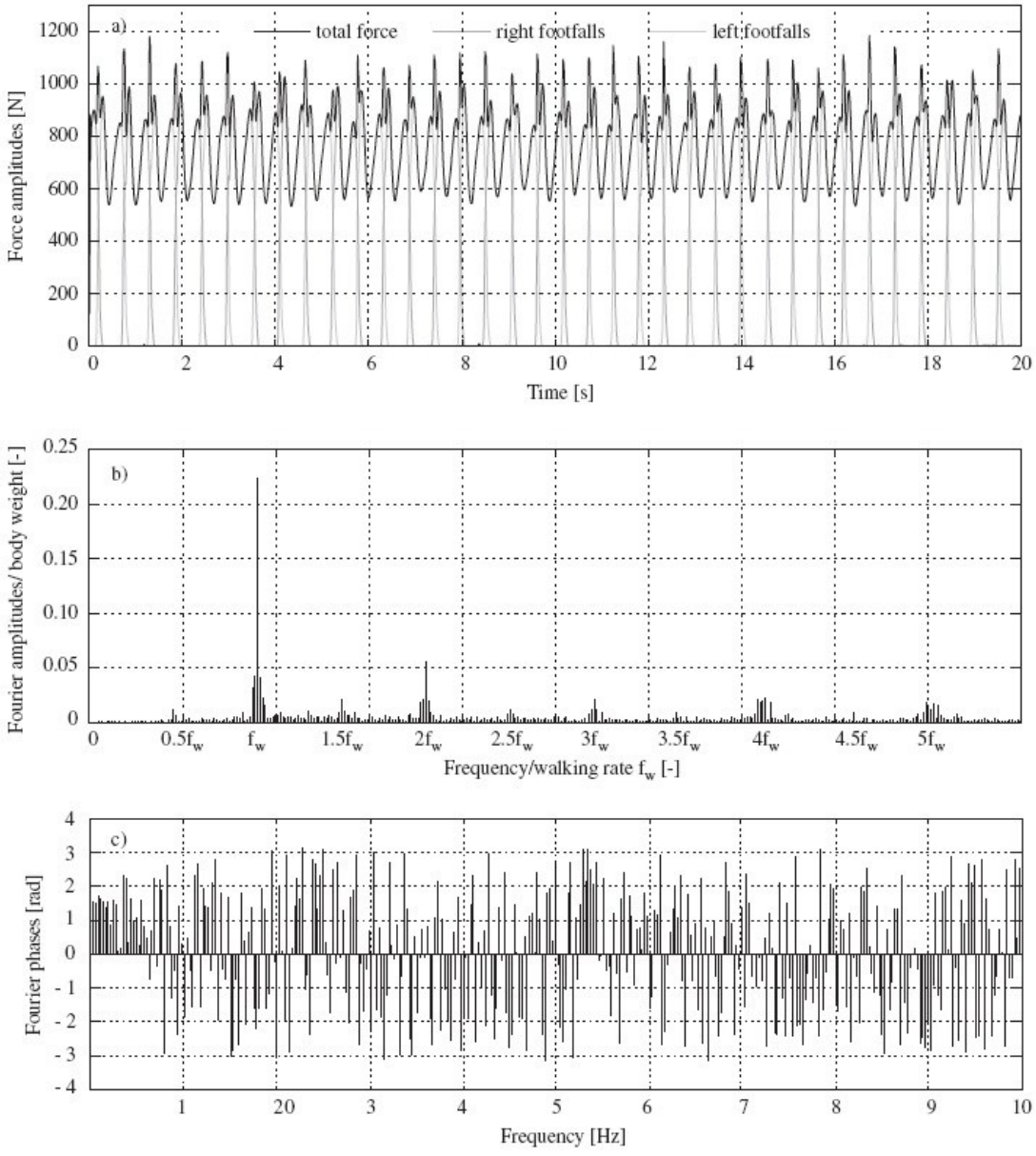

Figure 2. Vertical walking force record. After Racic and Brownjohn [11]

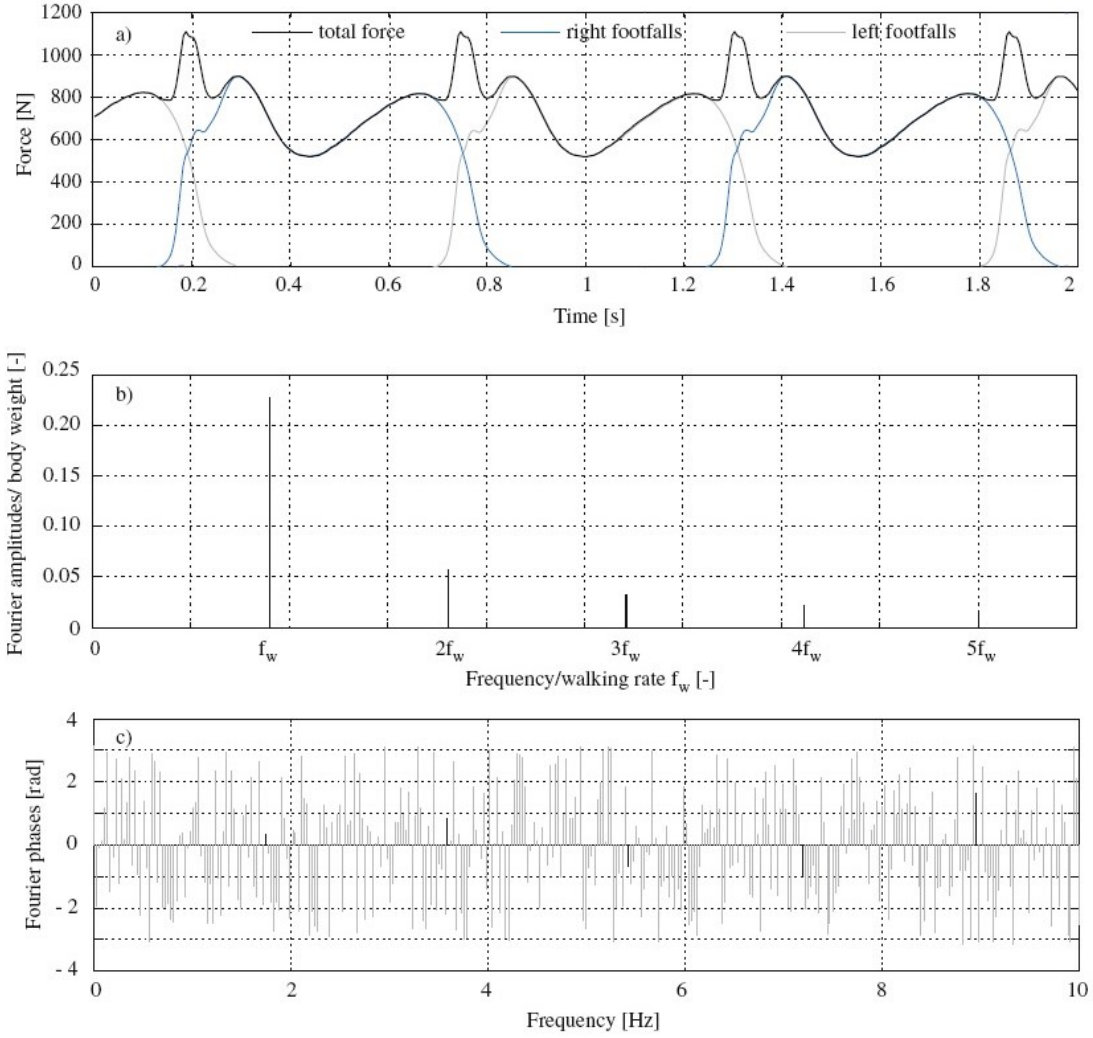

Figure 3. Periodic approximation of the force record shown in Figure 1. After Racic and Brownjohn [11]

A significant move toward a more realistic description of individual walking loads was made recently by taking into account the inter- and intra-subject variability of the pedestrians as a stochastic process. While the models of Racic et al. [11, 12] , Zivanovic et al. [27] , García-Diéguez et al. [32], and Muhammad et al.[33] all provide the best-to-date estimations of vibration levels, they require extensive and time consuming coding. The luxury of time is not often given to structural engineers in everyday design practice. Van Nimmen et al. [34] studied the vibration response records of real footbridges to prove that the variation in the individual footfall rate is the key force parameter needed for simulating accurately the shape of the vibration response (Figure 4). Moreover, they speculated that the apparent differences between measured and simulated vibration amplitudes could be attributed to the HSI phenomenon, which will be discussed in the next section.

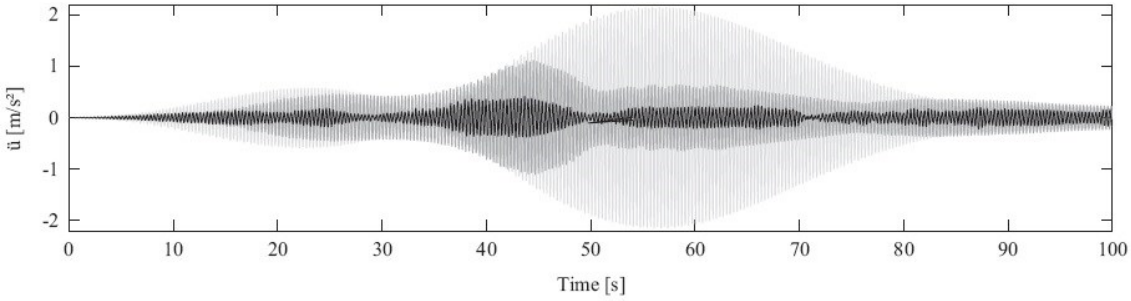

Figure 4. Vertical acceleration at the mid-span of a bridge: measured (black), simulated using perfectly periodic force of a kind shown in Figure 2 (light grey) and simulated using identical footfall shapes but different footfall rates (dark grey). After van Nimmen et al. [34]

3 Human-structure interaction

The HSI has been intensively studied in the lateral direction [35-37] since the infamous vibration problem of the London Millennium Bridge in 2000 [7]. It is now widely accepted that pedestrians are complex, vibration-sensitive dynamic systems whose lateral motion and corresponding contact forces are likely to be influenced by the lateral sway of the supporting structure. Moreover, they often synchronise their footfalls with the lateral structural motion (the so-called "lateral lock-in" effect), and thereby supply energy within the coupled pedestrian-structure dynamic system while acting as negative dampers [8]. On the other hand, very little is known about HSI in the vertical direction. Rare studies indicate that the individuals mainly add damping to vertical vibrations without necessarily involving the vertical lock-in effect [36].

Two types of coupled pedestrian-structure models have been proposed so far to describe HSI in the vertical direction (Figure 5). Transferred and adopted from the biomechanics of human gait, the first modelling approach represents a pedestrian as a simple inverted pendulum that oscillates in the vertical plane while moving along a bridge (Figure 5a). This modelling concept was first used by Macdonald [35] to simulate HSI on laterally swaying bridges, then adapted by Bocian et al. [36] to describe the vertical vibration. Apart from the lack of adequate experimental validation, the non-linear interaction mechanism, which is an essential part of these models, is not straightforward for implementation in design practice. Moreover, the credibility of the results of IP models is usually compromised by the large number of assumptions.

The other type of HSI model couples a single-degree-of-freedom (SDOF) model of a structure with a moving (usually) SDOF mass-spring-damper (MSD) oscillator representing a pedestrian walking (Figure 5b). Zivanović et al. [38] did a series of frequency response function (FRF) measurements on a test footbridge and studied the changes in the dynamic properties of the structure in the vertical direction due to the presence of either all standing or all walking groups of people (Figure 6). They reported a slight increase in the natural frequency and a three-fold increase in the damping of the occupied structure relative to the empty structure. Moreover, the authors observed that the walking people added less damping to the structure than the stationary people. Shahabpoor et al. [10] carried out more elaborate tests on the same structure and showed that the natural frequency of a vertical mode of the occupied structure can either increase or decrease depending on the frequency of the human SDOF system , while damping of the structure always increases. These changes appeared prominent especially when the natural frequency of the human SDOF system was close to the modal frequency of the empty structure. Note that all the available studies focus on a single structure and have very limited group sizes. There is no fully developed and experimentally verified universal model to reliably simulate the changes in the modal properties of an empty structure for a diverse range of loading scenarios and structural designs. This is because collecting the key experimental data for walking people still remains a challenge, mainly due to the lack of adequate technology.

4 Crowd loading

In the case of multi-pedestrian traffic, the net force is most commonly modelled by multiplying the individual walking force described by Equation (1) by factor(s) which often depend on the pedestrian density on the structure [5]. On the other hand, crowds are portrayed as the equivalent of uniformly distributed loading in the French guideline Setrà [2]. The most notable drawback specific to these models is their deterministic nature.

Moving from a stochastic models of a single walking person [] to multi-pedestrian walking traffic, the random nature of relevant modelling parameters needs to be considered. Variability of the human mass, stiffness, and damping between different people and even for the same person under different walking scenarios, interaction of people with each other and time-varying location of people on the structure (Figure 7), all make the pedestrian traffic-structure system highly complex. Modelling the scale and character of the net crowd dynamic load on the structure remains a challenge, mainly due to the shortage of knowledge on the proportion of individuals who interact with each other, and the effect of the surrounding environment on the pedestrian gait and walking trajectories. Pedestrians are "intelligent" agents who react to what they perceive around

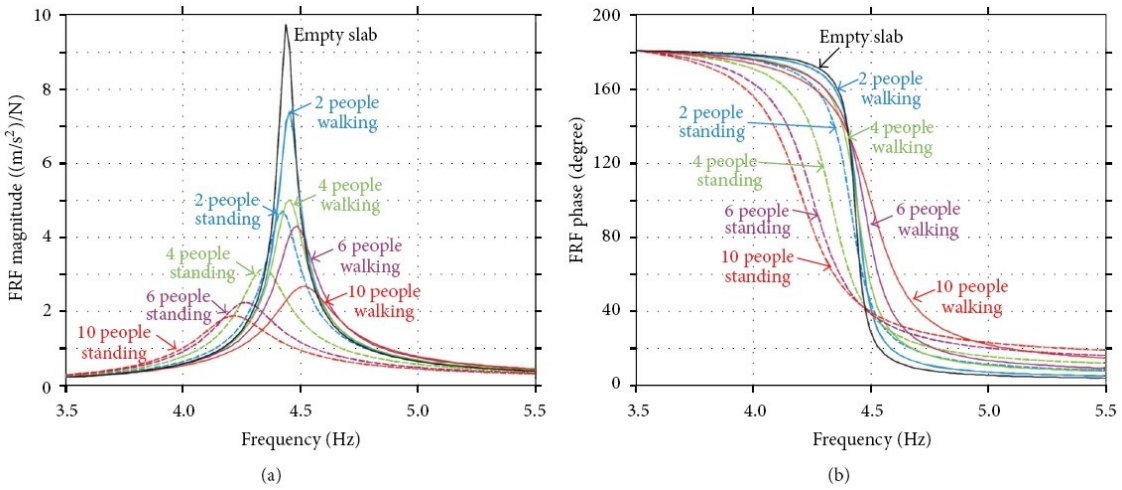

Figure 5. FRF magnitude and phase graphs of a footbridge when occupied by different number of standing/walking groups of people. After Zivanovic et al. [38]

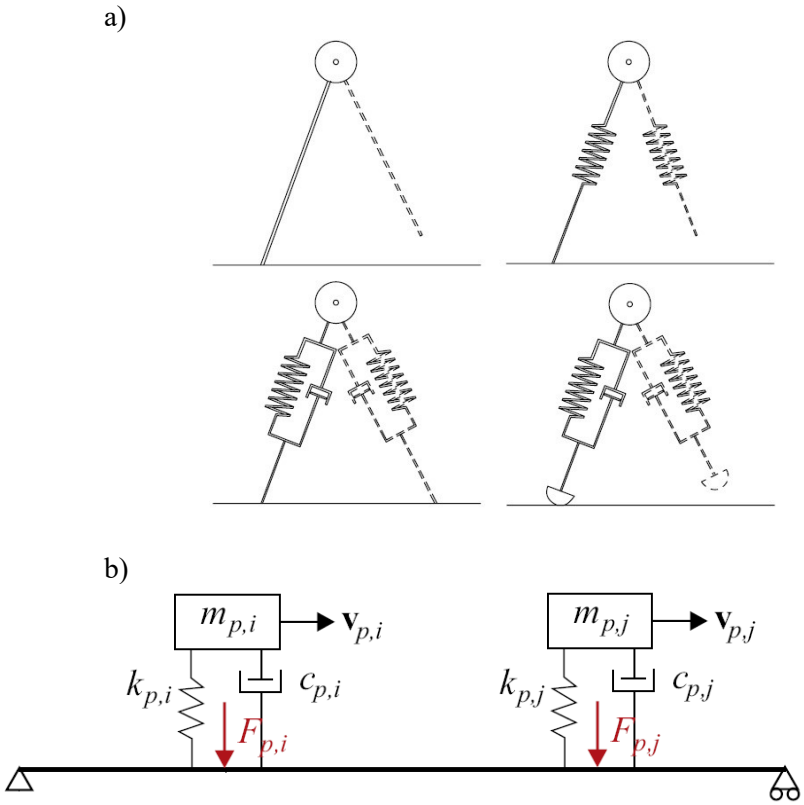

Figure 6. Examples of models suggested in the literature for modelling pedestrian-structure interaction in the vertical direction (a) IPM models and (b) a moving MSD model (i and j represent different individuals)

them. There is strong evidence that peripheral stimuli, such as visual, auditory and tactile, have an equal impact on pedestrian gait [5]. Since the early sixties, applied mathematicians and transportation engineers have proposed several mathematical models of pedestrian behaviour in crowds to address issues relevant to urbanism, evacuation of public buildings, and public safety. They can be divided into two main categories: macroscopic models based on the analogy between a pedestrian flow and the flow of a continuous fluid, and microscopic models, which describe the time-varying position and velocity of each individual in a crowd. Macroscopic models imply a coarse approximation of reality due to the "granular" nature of the crowd, so they can be appropriate (only) in cases of high pedestrian density. Moreover, their modelling parameters do not target individuals but the whole crowd, such as the mean crowd density and velocity of the pedestrian traffic, thus they are not able to explicitly describe the inter-subject variability. Caroll et al. [20] and Venuti et al. [21] used successfully a microscopic approach to simulate lateral and vertical pedestrian loading, respectively. Figure 7:

Using the microscopic approach, Venutti et al. [40] proposed a modelling framework for simulating crowd excitation on footbridges, including the inter- and intra-variability as well as the HSI. Although the framework was demonstrated on the vertical vibrations, it can be applied to the lateral vibrations without losing generality. Each of its sub-models describing crowd dynamics, pedestrian moving bodies and walking forces is adapted or derived from the most reliable models and data available in the literature. The sub-models can be updated independently as soon as their better models have been published or the relevant experimental data have been made available for calibration and verification.

Figure 7. An example of simulated pedestrian traffic on a footbridge at an instant in time. Dots represent different individuals. After Venutti et al. [40]

5 Conclusions

The key impression at the end of this survey is that there is a colossal disconnect between academia and industry. The dissemination of research outcomes to industry is almost nonexistent, resulting in structural designers using outdated information. Academia needs to be engaged with industry and relevant professional institutes to provide up-to-date design guidance based on research best practices.

Future research in this area should be based on simultaneously collecting vibration data and pedestrian-structure and pedestrian-pedestrian interaction data on real structures under different walking traffic scenarios. Such datasets are needed for different types of footbridges and floor structures to identify and validate walking human models and analyse their robustness and versatility. The research findings need to be codified so the next generation of design guidelines can incorporate a realistic model of walking loading, crowd dynamics, and a comprehensive HSI model into a practical and inclusive modelling approach that can be used in everyday design practice.

References

[1] FIB (The International Federation for Structural Concrete), Guidelines for the design of footbridges, Lausanne, 2005.

[2] Sétra (Service d'Etudes Techniques des Routes et Autoroutes), Footbridges, assessment of vibrational behaviour of footbridges under pedestrian loading, Technical Guide, Paris, 2006.

[3] ISO (International Organization for Standardization), Bases for design of structures - Serviceability of buildings and walkways against vibration, ISO 10137, Geneva, 2007.

[4] BSI (British Standards Institution), U.K. national annex to Eurocode 1: Actions on structures - Part 2: Traffic loads on bridges. EN 1991-2:2003, London. 2008.

[5] HiVoSS (Human induced vibration of steel structures), Research fund for coal and steel, Design of footbridges, Technical report, Brussels: RFCS publications, 2008.

[6] V. Racic, A. Pavic, J.M.W. Brownjohn, Experimental identification and analytical modelling of human walking forces: literature review, Journal of Sound and Vibration 326 (2009) 1-49.

[7] A. Fitzpatrick, P. Dallard, S. le Bourva, A. Low, R. Ridsill Smith, M. Willford, Linking London: The Millennium Bridge, The Royal Academy of Engineering, London, 2001.

[8] P. Dallard, T. Fitzpatrick, A.Flint, A. Law, R. M. Ridsdill Smith, M. Willford, M. Roche, The London Millennium Bridge: pedestrian-induced lateral vibration, Journal of Bridge Engineering 6 (6) (2001) 412-417.

[9] C.F. Dunant, M.P. Drewniok, J.J. Orr, J.M. Allwood, Good early stage design decisions can halve embodied CO2 and lower structural frames' cost, Structures. 33 (2021) 343–354.

[10] E. Shahabpoor, A. Pavic, V. Racic, Identification of mass-spring-damper model of walking humans. Structures 5 (2016) 233-246.

[11] V. Racic, J.M.W. Brownjohn, Stochastic model of near-periodic vertical loads due to humans walking, Advanced Engineering Informatics 25 (2) (2011) 259-275.

[12] V. Racic, J.M.W. Brownjohn, Mathematical modelling of random narrow band lateral excitation of footbridges due to pedestrians walking, Computers & Structures 90-91 (2012) 116-130.

[13] British Standards Institution (BSI), Steel, Concrete and Composite Bridges. Part 2: Specification for Loads; Appendix C: Vibration Serviceability Requirements for Foot and Cycle Track Bridges (BS 5400), British Standards Institution, London, 1978.

[14] The Highway Engineering Division, Ontario Highway Bridge Design Code CAN/CSA-S6-06, The Canadian Standards Association, Toronto, 1983.

[15] T.A. Wyatt, Design Guide on the Vibration of Floors, The Steel Construction Institute, Construction Industry Research and Information Association, London,1989.

[16] D.E. Allen, T.M. Murray, Design criterion for vibrations due to walking, Engineering Journal AISC 30 (4) (1993) 117–129.

[17] A. Pavic, M.R. Willford, Appendix G: vibration serviceability of post-tensioned concrete floors, in: Post-Tensioned Concrete Floors Design Handbook, second ed., Concrete Society, Slough, 2005, pp. 99–107.

[18] A.L. Smith, S.J. Hicks, P.J. Devine, Design of floors for vibration: a new approach, SCI P354, The Steel Construction Institute, Askot, 2007. The Canadian Standards Association, Toronto, 1983

[19] B.R. Ellis, On the response of long-span floors to walking loads generated by individuals and crowds, The Structural Engineer 10 (78) (2000) 17–25.

[20] J.W. Smith, Vibration of Structures, Chapman and Hall, London, 1988.

[21] S.C. Kerr, Human Induced Loading on Staircases. Ph.D. Thesis, Department of Mechanical Engineering, University of London, UK, 1998.

[22] P. Young, Improved Floor Vibration Prediction Methodologies, ARUP Vibration Seminar, 4 October, London, 2001.

[23] J.M.W. Brownjohn, A. Pavic, P. Omenzetter, A spectral density approach for modelling continuous vertical forces on pedestrian structures due to walking, Canadian Journal of Civil Engineering 31 (2004) 65–77.

[24] A. E. Peters, V. Racic, S. Živanović, J. Orr, Fourier series approximation of vertical walking force-time history through frequentist and Bayesian inference, Vibration 5 (4) (2022) 883-913.

[25] C.J. Middleton, J.M.W. Brownjohn, Response of high frequency floors: a literature review, Engineering Structures 32 (2) (2009) 337–352.

[26] S. Živanović, A. Pavic, Probabilistic modelling of walking excitation for building floors, Journal of Performance of Constructed Facilities 23 (3) (2009) 132–143.

[27] S. Živanović, A. Pavic, P. Reynolds, Probability-based prediction of multi-mode vibration response to walking excitation, Engineering Structures 29 (6) (2007) 942-954.

[28] C.J. Middleton, Dynamic Performance of High Frequency Floors, PhD Thesis. University of Sheffield, UK, 2009.

[29] Brownjohn, J.M.W, Racic, V., Chen, J. (2016) Universal response spectrum procedure for predicting walking-induced floor vibration. Mechanical Systems and Signal Processing 70-71 (2016) 741-755.

[30] J. Chen, R. Xu, M. Zhang, Acceleration response spectrum for predicting floor vibration due to occupant walking, Journal of Sound and Vibration 333 (15) (2014) 3564-3579.
[31] J. Chen, J. Wang, and J. Brownjohn, Power Spectral-Density Model for Pedestrian Walking Load. ASCE Journal of Structural Engineering 145 (2) (2019).
[32] M. García-Diéguez, V. Racic, and J. L. Zapico-Valle, Complete statistical approach to modelling variable pedestrian forces induced on rigid surfaces, Mechanical Systems and Signal Processing 159 (2021).
[33] A. S. Mohammed, A. Pavic, and V. Racic, Improved model for human induced vibrations of high-frequency floors, Engineering Structures 168 (2018) 950-966.
[34] K. Van Nimmen , G. Lombaert, I. Jonkers, G. DeRoeck, P. Van den Broeck. Characterisation of walking loads by 3D inertial motion tracking. Journal of Sound and Vibration 333 (20) (2014) 5212-5226.
[35] J. Macdonald, Lateral excitation of bridges by balancing pedestrians, Proceedings of the Royal Society A - Mathematical, Physical and Engineering Sciences 465 (2009) 1055-1073.
[36] M. Bocian, J.Macdonald, J.Burn, Biomechanically-inspired modelling of pedestrian-induced vertical self-excited forces, ASCE Journal of Bridge Engineering 18 (12) (2012) 1336-1346.
[37] L. Bruno, F.Venuti, Crowd-structure interaction in footbridges: modelling, application to a realcase-study and sensitivity analyses, Journal of Sound and Vibration 323 (2009) 475-493.
[38] S. Zivanovic, I. M. Diaz, and A. Pavic, Influence of walking and standing crowds on structural dynamic properties, in Proceedings of the 27th Conference & Exposition on Structural Dynamics (IMAC XXVII), Orlando, USA, February 2009.
[39] S. P. Caroll, J. S.Owen, A. A. Hussein, A coupled biomechanical/discrete element crowd model of crowd-bridge interaction and application to the Clifton Suspension Bridge, Engineering Structures 49 (2013), 58-75.
[40] F. Venuti, V. Racic, A. Corbeta, Modelling framework for dynamic interaction between multiple pedestrians and vertical vibrations of footbridges, Journal of Sound and Vibration 379 (2016) 245-263.

Građevinski materijali i konstrukcije
Building Materials and Structures
journal homepage: www.dimk.rs

https://doi.org/10.5937/GRMK2300004N UDK: 624.072:624.012.45

Original scientific paper

Numerical modelling of concrete-filled steel tubular short columns under axial compression

Jelena Nikolić[*1)], Svetlana M. Kostić[1)], Saša Stošić[1)]

[1)] *University of Belgrade, Faculty of Civil Engineering, Department of Engineering Mechanics and Theory of Structure, Bulevar kralja Aleksandra 73, 11000 Belgrade, Serbia*

Article history
Received: 25 January 2023
Received in revised form: 07 April 2023
Accepted: 04 May 2023
Available online: 09 June 2023

Keywords
composite columns,
nonlinear analysis,
3D FEM model,
concrete material model,
Eurocode 4

ABSTRACT

The paper presents three-dimensional numerical models of short concrete-filled steel tubular circular columns that can successfully describe the column behaviour under axial compression. Several of the most commonly used material models for the steel part and a concrete portion of the column are evaluated in the models. In addition, the paper presents a new proposal for the extension of the Eurocode 2 stress-strain relation to make it suitable for describing the complex behaviour of concrete inside the steel tube. This model overcomes the current limitations of the Eurocode 2 design guide, referring to the limitation for the concrete curve in compression to 3.5‰ strain. The ultimate axial column strength obtained by the proposed model is compared to the ultimate column capacity calculated by a simplified method provided in Eurocode 4. All presented numerical models are validated on a set of experiments from the literature and demonstrate good agreement. The comments about the accuracy of each model are provided, along with the identified limitations.

1 Introduction

A concrete-filled steel tubular column (CFST) consists of an outer steel tube filled with concrete. The composite action between the two parts, the concrete core and steel tube, ensures that the concrete core stiffens the steel tube and postpones its local buckling. In turn, the outer steel tube acts as longitudinal and transverse reinforcement, permanent formwork, and confinement for the concrete core. CFST columns demonstrate excellent structural behaviour, such as high strength, stiffness, ductility, and good seismic behaviour [1], [2].

Due to their overall good performance, CFST columns have been widely used in different types of construction and are the subject of numerous ongoing research projects [1]. Various shapes and types of CFST columns have been constructed in the past [3]–[6]. The axial behaviour of these columns has been investigated experimentally and numerically. To date, several databases with experimental results exist, counting more than one thousand axially loaded specimens [7].

In general, there are three approaches to the numerical modelling of CFST columns. The first uses the simplified concentrated plasticity nonlinear beam/column elements [2], [7]. These elements are computationally very efficient but have some limitations since they require the expressions of the yield surface, which depend on the column cross-section. The second approach deals with the distributed plasticity fibre beam-column elements [8]–[10]. Although slightly less computationally efficient than elements from the first group, these numerical models are much more versatile and can account for numerous nonlinear effects, such as the nonlinear material behaviour of constituent parts, residual stresses, and nonlinear geometry. However, they can capture only indirectly the local buckling of the steel tube, the interaction of the steel tube with the concrete part, and the variable confinement effects of the concrete core. For these reasons, there is a need to develop reliable, sophisticated, 3D finite element models that can fully describe the complex nonlinear behaviour of the composite columns. These models can also predict other important information, such as failure modes and deformation patterns, or capture phenomena such as local buckling of the steel tube and confinement of the concrete part of the section [11]. This third approach is followed in this paper.

There are several 3D numerical models developed in the past [12]–[14] using the commercial program ABAQUS. The crucial differences among these models are the assumed material model behaviour, initial imperfections and residual stresses, modelling the steel tube–concrete core interface, and the boundary conditions. Most of these models proposed their own concrete material models [13], [15]–[17] or steel material models [10], [13], [15], [16]. However, there is a lack of numerical models that deploy the material models proposed by the Eurocode design guide. For that reason, the study presented in this paper provides a relatively simple 3D

[*] Corresponding author:
E-mail address jnikolic@grf.bg.ac.rs

numerical model developed in the commercial program ABAQUS that follows the general analysis method of Eurocode 4 (EC4) for the nonlinear analysis of axially loaded CFST columns. The proposal for the extension of the concrete material model suggested by Eurocode 2 (EC2) is developed to make it suitable for describing the complex behaviour of concrete inside the steel tube. The developed concrete material model is carefully evaluated and compared with other commonly employed concrete material models. Finally, the ultimate strength results are compared to the axial capacity of the short columns calculated by EC4 [18], [19].

2 Numerical modelling of short cfst columns

The study presented here is focused on the efficient numerical modelling of short CFST columns. These columns are expected to develop a cross-section's full plastic strength capacity without failing due to buckling. According to the Japanese standard AIJ [20], CFST columns are classified as short columns when the length-to-outer column diameter ratio is less than or equal to four ($L/D \leq 4$) and this boundary is commonly used among researchers for the classification [9].

The numerical model of the CFST columns needs to predict structural members' behaviour effectively and provide complex information regarding their structural response. On the other side, the model needs to be relatively simple because of its computational efficiency. This paper presents one such model for the CFST short columns under axial loading. The model considers the geometry, the test setup simulation, boundary conditions, and applied loading in a simplified way. It is validated based on selected test results from the literature and previously developed models by other authors. The analysis is performed as the displacement controlled in all these simulations and includes material and geometrical nonlinearities. A detailed description of the developed numerical model follows.

2.1 3D model description

Finite element analysis (FEA) was conducted using ABAQUS [21] version 6.9, which offers significant capabilities for the 3D nonlinear analysis of CFST columns. ABAQUS Standard solver was chosen due to the quasi-static nature of the loading and its ability to analyse such conditions accurately. The possible disadvantage of 3D modelling is that many elements in the model may require a long calculation time. For the sake of reasonable time for both developing the 3D model and the analysis, the intention here was to create a simple but reliable model that would provide highly accurate results.

The outer steel tube and the concrete core are modelled using the 3D8-node brick elements (C3D8R) with reduced integration (i.e., one integration point), Figure 1. The element has three translation degrees of freedom at each element node. The single-point reduced-integration scheme is based on the “uniform strain formulation”, meaning that the strains are obtained as the average strain over the element volume. The advantage of the reduced integration elements comes from the fact that strains and stresses are calculated at locations that provide optimal accuracy. A second advantage is that the reduced number of integration points decreases calculation time and storage requirements [21]. For the steel tube, shell elements might be used as well, since they are generally well-suited for analysing structures with thin to moderately thick walls. In the presented analysis, using the shell elements for modeling steel tube would not have an effect on the results, as shown in Figure 2a below for test CC-0 with Model 4.

The boundary conditions at column ends are considered by applying the constraints option available in ABAQUS. It connects all surface nodes to only one reference point (RP) defined in the centre of the column's top and bottom surfaces, as shown in Figure 1. Tests used to validate the FE models had steel plates for load application at both ends of the specimens. Some tests had these plates welded at both ends of specimens [11], [22], while others used plates in a

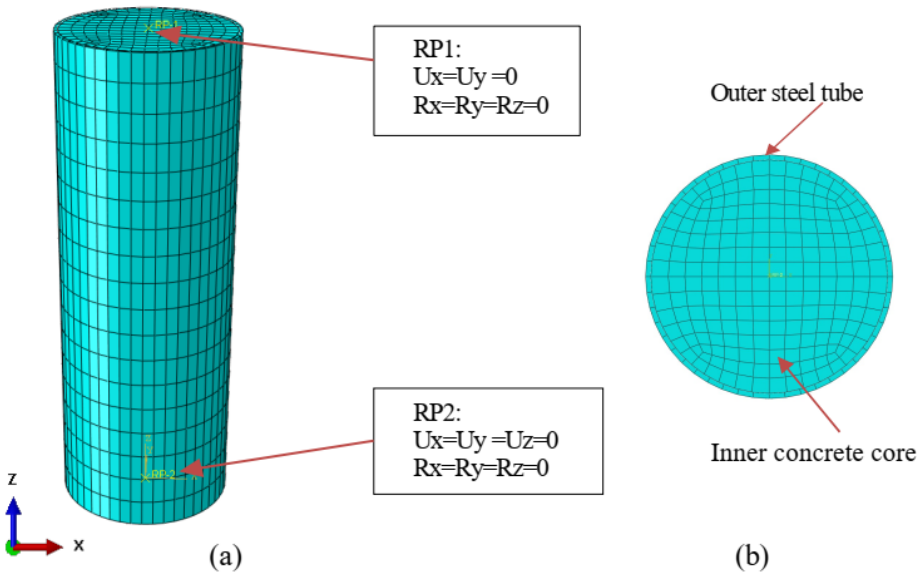

Figure 1. (a) 3D model of CFST column with RP1 and RP2 with BC; (b) Cross-section and meshing

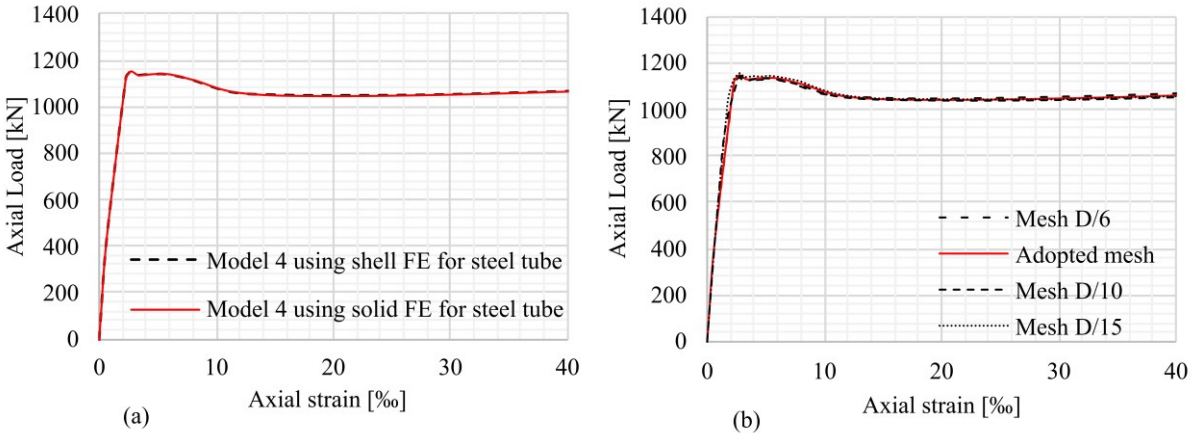

Figure 2.(a) Mesh type sensitivity analysis on specimen CC-0 using Model 4; (b) Mesh size sensitivity analysis on specimen CC-0 using Model 4

testing machine only to ensure load application to the whole cross-sections [23],[24]. Test boundary conditions are modelled numerically using the constraint option on specimen end surfaces. This is considered adequate since the steel plates were very stiff. The end surface behaves rigidly with a master node (RP). Boundary conditions (BC) are set to RP1 and RP2: all displacements are restrained except displacement in the loading direction at RP1. A displacement-controlled axial loading scheme is applied to the RP1 only.

The starting point for the selection of the FE mesh size were the conclusions from the mesh convergence studies presented in reference [13]. Accordingly, the optimal element size across the cross-section was determined to be $D/15$, where D represents the outer diameter of a circular column. The element size in the longitudinal direction was 2.5 times larger than that in the cross-section. However, a mesh sensitivity study was conducted to confirm the convergence of results as well as the total computational time required for the analysis. Figure 2b shows the FEM mesh size sensitivity analysis for Model 4 for specimen CC-0 using the adopted mesh size and three other meshes, namely $D/6$, $D/10$, and $D/15$. As demonstrated, the results confirm convergence, particularly considering that the model with $D/15$ took almost ten times longer to run.

Interaction between the steel tube and the concrete core is simulated using the surface-to-surface contact option. The inner steel tube surface is chosen as the master surface, while the concrete surface is defined as the slave surface. When two surfaces are in contact, they transmit shear and normal forces across their interface. The normal (radial) contact behaviour is defined using the "hard" contact option. This relationship minimises the penetration of the slave surface into the master surface in compression and allows separation after contact. The tangential behaviour between surfaces is defined using the friction formulation with “penalty”. It uses the classical isotropic Coulomb friction model, where the critical shear stress is obtained as a contact pressure multiplied by a coefficient of friction. Some studies have investigated this particular effect [25], and the literature reports a coefficient range of 0.5 to 0.6 for carbon steel tubes. Our own investigation revealed that values between 0.4 and 0.7 had little impact on axial resistance. Therefore, we have adopted a friction coefficient of 0.6 in our models, as suggested in [16].

The initial local or global imperfections were not considered in the model as their influence was negligible for the stub columns that are the subject of this paper. Namely, specimens with $L / D \leq 3$ do not demonstrate lateral deflections during failure tests, and the concrete infill reduces some possible local imperfections of the steel tube [11]. However, the behaviour of columns with a higher L/D ratio may be affected to a certain degree by global imperfections.

2.2 Material modelling

In this study, four different combinations of steel and concrete material models are assigned to the steel tube and the concrete core, as summarised in Table 1, and these models are evaluated. Therefore, all four 3D models, denoted as Models 1 to 4, have the same geometry, boundary conditions, and FE mesh but different assigned material models for steel tube and concrete core. Models 1, 2, and 3 follow the commonly applied material models as recommended by [13], [16], and [26], respectively. Model 4 is created using the material curves provided in Eurocode 3 (EC3) [27] for steel tubes and the proposed extended material model for concrete in Eurocode 2 (EC2) [28]. These modifications are explained in detail later in the paper.

Table 1. Numerical models with details of material modelling

Model	Structural steel	Concrete
Model 1	Tao et al. [13]	Tao et al. [13]
Model 2	Han et al. [16]	Han et al. [16]
Model 3	EC3 [27]	Ellobody [26]
Model 4	EC3 [27]	proposed extended EC2

2.2.1 Material modelling of concrete core in ABAQUS

Concrete under compression initially exhibits an elastic response. As the stress increases, non-recoverable (inelastic) strains occur, and the material's stiffness decreases. After ultimate stress is reached, the material softens until it can no longer carry any stress. In multiaxial stress states, these observations can be generalised through

surfaces of failure and ultimate strength surfaces in stress space. These surfaces are fitted to the experimental data.

Under low confining pressures, concrete behaves in a brittle manner, so the main failure mechanisms are cracking in tension and crushing in compression. The brittle behaviour of concrete disappears when the confining pressure is sufficiently large to prevent crack propagation. Under these circumstances, failure is driven by the consolidation and collapse of the concrete´s microporous microstructure, leading to a macroscopic response resembling a ductile material with work hardening.

In ABAQUS, the concrete damage plasticity (CDP) model for quasi-brittle materials is the constitutive model commonly adopted for concrete. This CDP model is a plasticity-based continuum model. The elastic response is assumed to be linear and isotropic, defined by the modulus of elasticity and Poisson‘s ratio. The plastic region requires the definition of stress-strain curves for both compression and tension behaviour. Input parameters are stress values and the corresponding inelastic strain. The following strain rate decomposition is assumed for the model:

$$\dot{\varepsilon} = \dot{\varepsilon}^{el} + \dot{\varepsilon}^{pl} \tag{1}$$

where $\dot{\varepsilon}$ is the total strain rate, $\dot{\varepsilon}^{el}$ is the elastic part of the strain rate while $\dot{\varepsilon}^{pl}$ is the plastic part of the total strain [21].

The CDP model also requires the input of five plasticity parameters: dilation angle (ψ), flow potential eccentricity (e), the ratio of the second stress invariant on the tensile meridian to that on the compressive meridian (K_c), a ratio of the compressive strength under biaxial loading to uniaxial compressive strength (f_{b0}/f_c'), and a viscosity parameter.

Due to the steel tube's passive confinement, concrete reaches a triaxial stress state when the CFST column is under axial compression [13]. This confinement effect is more significant in circular columns than square columns, as reported in [29].

The concrete elastic material´s behaviour is defined by the modulus of elasticity and Poisson‘s ratio. The plastic part requires the definition of a stress-strain curve for compression and tension in combination with plasticity parameters. The CDP model uses the concept of isotropic damage elasticity in combination with isotropic tensile and compressive plasticity to represent the inelastic behaviour of concrete. Modelling confined concrete behaviour in CFST columns has been challenging and investigated by many authors. The researchers proved that passive confinement would increase both the peak strain (ductility) and the strength of the concrete and the CFST column. One of the possibilities for including the confinement effect in ABAQUS is by modifying the uniaxial concrete stress-strain curve. It means including softening and hardening behaviour as a result of composite action during the lateral expansion of concrete.

2.2.2 Concrete models

As mentioned before, this study explores four different stress-strain concrete models. The first three models are the most commonly applied concrete material models in nonlinear 3D FEM analysis of CFST composite columns. The fourth model is the one that follows the concrete material model proposed by EC2 but is extended in order to be applicable for modelling the concrete core inside the steel tube. The corresponding curves for all four models are illustrated in Figure 3 for the geometry and material parameters of specimen 3HN [30], which will be analysed later. Here, f_c' refers to the 150 x 300 mm concrete cylinder compressive strength obtained from tests. A detailed description of all four models follows.

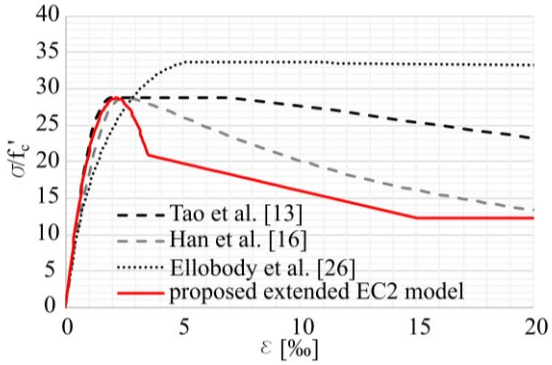

Figure 3.Concrete constitutive models 1-4 illustrated for material properties of specimen3HN

2.2.2.1 Concrete material model by Tao et al. [13]

The first evaluated model for concrete is a three-stage $\sigma - \varepsilon$ relation proposed by Tao et al. [13]. This model has been widely exploited as it considers the strain hardening/softening rule of concrete confined by a steel tube. However, it should be noted that this model includes passive confinement since there is an increase in the plastic strain only, and there is no increase in the concrete compressive strength, as presented in Figure 4.

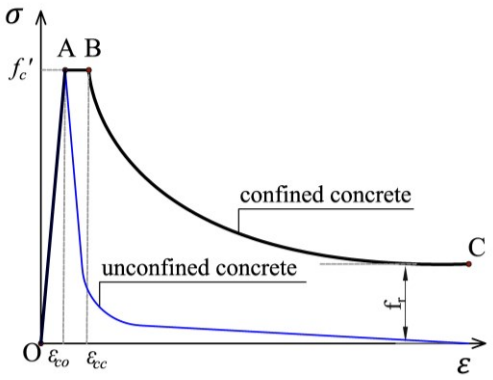

Figure 4. Stress-strain model for confined concrete used in Model 1

The first ascending stage between points O-A is defined by equations (2-3) until the peak stress f_c'. The peak stress f_c' is the cylinder compressive strength of unconfined concrete. The corresponding strain ε_{c0} at point A is calculated according to the relationship in equation (4):

$$\frac{\sigma}{f_c'} = \frac{A \cdot X + B \cdot X^2}{1 + (A-2)X + (B+1)X^2} \qquad 0 < \varepsilon \leq \varepsilon_{c0} \tag{2}$$

$$X = \frac{\varepsilon}{\varepsilon_{c0}}, \quad A = \frac{E_c \varepsilon_{c0}}{f_c'} \quad B = \frac{(A-1)^2}{0.55} - 1 \tag{3}$$

$$\varepsilon_{c0} = 0.00076 + \sqrt{(0.626 f_c' - 4.33) \cdot 10^{-7}} \tag{4}$$

E_c is the modulus of elasticity of the unconfined concrete calculated as per ACI 318 [31] with the empirical equation (5) where f_c' is in MPa:

$$E_c = 4700\sqrt{f_c'}[MPa] \quad (5)$$

Further, a second branch is a plateau between points A-B, representing an increased peak strain of concrete due to the confinement. The strain at the point B, ε_{cc}, for the concrete model is determined by the following equation (6):

$$e^k = \frac{\varepsilon_{cc}}{\varepsilon_{c0}}, \quad k = (2.9224 - 0.00367f_c')\left(\frac{f_B}{f_c'}\right)^{0.3124+0.002f_c'} \quad (6)$$

The value f_B represents the confining stress at point B where it is assumed that the ultimate column strength is reached. During the elastic stage, no confining stress is registered as the initial lateral expansion of the concrete is smaller than that of the steel tube. It originates from different values of Poisson's ratio of the composite materials. With the increase in axial strain, the lateral expansion of the concrete core gradually becomes more extensive than the expansion of the steel tube. This mechanism highlights the complexity of the interaction in CFST columns. Here equation (7) is provided for circular CFST columns only, where D, t, and f_y are the steel tube's outer diameter, wall thickness and yield strength, respectively.

$$f_B = \frac{\left(1 + 0.027f_y\right) \cdot e^{-0.02\frac{D}{t}}}{1 + 1.6 \cdot 10^{-10} \cdot (f_c')^{4.8}} \quad (7)$$

The third stage is the descending branch defined by the following relationship [32]:

$$\sigma = f_r + (f_c' - f_r)exp\left[-\left(\frac{\varepsilon - \boldsymbol{\varepsilon_{cc}}}{\alpha}\right)^{\beta}\right] \ \varepsilon \geq \varepsilon_{cc} \quad (8)$$

in which f_r is the residual stress, while α and β are parameters determining the shape of the softening branch. The expressions for f_r and α for circular CFST columns are given in (9) and (10). They are calculated as functions of the so-called "confinement factor" ξ_c (11). It is defined as the ratio between the yield strength (f_y) multiplied by the cross-sectional area of the steel tube (A_s) and the concrete compressive strength (f_c') multiplied by the cross-sectional area of the concrete core (A_c). The parameter β in equation (8) has a value of 1.2 for circular CFST columns. Parameters α, β and f_r cannot be directly derived from the tests, and their values are proposed based on the regression analysis as the best match for the test curves used in the study [13].

$$f_r = 0.7\left(1 - e^{-1.38\xi_c}\right)f_c' \leq 0.25f_c' \quad (9)$$

$$\alpha = 0.04 - \frac{0.036}{1 + e^{6.86\xi_c - 3.49}} \quad (10)$$

$$\xi_c = \frac{A_s f_y}{A_c f_c'} \quad (11)$$

Concrete tensile behaviour needs to be defined to complete the necessary inputs for the CDP model in ABAQUS. In the current model, the uniaxial tensile response is assumed to be linear until the tensile strength of concrete is reached, which is taken as $0.1f_c'$. Beyond the failure stress, the linear softening response is defined by the fracture energy G_F [33]:

$$G_F = \left(0.469d_{max}^2 - 0.5d_{max} + 26\right)\left(\frac{f_c'}{10}\right)^{0.7} N/mm \quad (12)$$

where f_c' is in MPa, d_{max} is the maximum coarse aggregate size taken as 20mm.

Once the whole material curve is completed, the concrete plasticity parameters must be defined. For the flow potential eccentricity *e* and viscosity parameter, the default values of 0.1 and 0 are adopted. The ratio of the compressive strength under biaxial loading to uniaxial compressive strength f_{b0}/f_c' is calculated by the expression proposed by Papanikolaou and Kappos [34]:

$$f_{b0}/f_c' = 1.52(f_c')^{-0.075} \quad (13)$$

For the remaining CDP parameters, Tao et al. [14] performed the sensitivity analysis and suggested the following expressions:

– dilation angle ψ should depend on the confinement factor ξ_c:

$$\psi = \begin{Bmatrix} 56.3(1 - \xi_c)\xi_c \leq 0.5 \\ 6.672e^{\frac{7.4}{4.64 + \xi_c}} \ \xi_c > 0.5 \end{Bmatrix} \quad (14)$$

– the ratio of the second stress invariant on the tensile meridian to that on the compressive meridian K_c should depend on f_c' and be calculated as follow:

$$K_c = \frac{5.5}{5 + 2(f_c')^{0.075}} \quad (15)$$

2.2.2.2 Concrete material model by Han et al.[16]

The second concrete material model discussed here is by Han et al. [16]. It is well known for giving good predictions with the CDP model in ABAQUS [16]. It also relies on the idea that improving the concrete strength under triaxial stress states can be introduced into the FE model through the plastic behaviour of the equivalent stress-strain relationship for concrete. The plasticity of the concrete core confined by a steel tube demonstrates an increase in strain corresponding to the maximum stress and strengthening in the descending branch of the curve. Generally, it defines concrete plastic behaviour depending on the confinement factor ξ, equation (16).

$$\xi = \frac{A_s f_y}{A_c f_{ck}} = \alpha \frac{f_y}{f_{ck}} \quad (16)$$

where A_s and A_c are the cross-sectional area of the steel and concrete, respectively; $\alpha(=A_s/A_c)$ is the steel ratio; f_y is the yield strength of the steel; and f_{ck} the characteristic strength of the concrete,which equals $0.67f_{cu}$ for normal strength concrete; $f_{cu}$is the 150 mm cube strength of the concrete.

The following expressions (17-21) define the stress-strain model in Figure 5 proposed for the FE modelling:

$$y = \begin{Bmatrix} 2x - x^2, & (x \leq 1) \\ \frac{x}{\beta_0(x-1)^{\eta} + x}, & (x > 1) \end{Bmatrix}, \quad x = \frac{\varepsilon}{\varepsilon_0} \ , \ y = \frac{\sigma}{\sigma_0} \quad (17)$$

$$\sigma_0 = f_c'\left(\frac{N}{mm^2}\right) \quad (18)$$

$$\varepsilon_c = (1300 + 12f_c')\, x\, 10^{-6} \quad (19)$$

$$\varepsilon_0 = \varepsilon_c + 800\xi^{0.2}\, x\, 10^{-6} \quad (20)$$

where for CFST with circular section:

$$\begin{Bmatrix} \beta_0 = (2.36\,x\,10^{-5})^{[0.25+(\xi-0.5)^7]}(f_c')^{0.5}x\,0.5 \geq 0.12 \\ \eta = 2 \end{Bmatrix} \quad (21)$$

and f_c' is the compressive cylinder strength of the concrete. The initial modulus of elasticity E_c and Poisson's ratio of 0.2 are taken as recommended in ACI Committee 318 [31], equation (22):

$$E_c = 4730\sqrt{f_c'}[MPa] \quad (22)$$

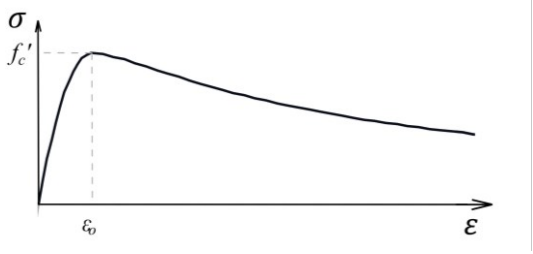

Figure 5. Stress-strain model for confined concrete used in Model 2

The model uses the same fracture energy model as in [16] proposed by Hillerborg [35] for concrete in tension.

Finally, Han suggested constant values for the concrete plasticity parameters in the CDP model. Dilation angle (ψ), flow potential eccentricity (e), the ratio of the second stress invariant on the tensile meridian to that on the compressive meridian (K_c), a ratio of the compressive strength under biaxial loading to uniaxial compressive strength ($\frac{f_{b0}}{f_c'}$), and viscosity parameters are taken as 30º, 0.1, 1.16, 2/3 and 0, respectively.

2.2.2.3 Concrete material model by Ellobody [26]

The third considered concrete material model is an idealised uniaxial response for the compressive stress-strain curve for confined concrete proposed by Ellobody. It originates initially from the model proposed by Mander [36] for confined concrete but is adjusted for application in modelling CFST columns. The main inputs to be determined are the confined concrete compressive strength f_{cc}' and corresponding confined strain ε_{cc} in the equations (23-24) proposed by Mander.

$$f_{cc}' = f_c' + k_1 f_l \quad (23)$$

$$\varepsilon_{cc} = \varepsilon_c\left(1 + k_2\frac{f_l}{f_c'}\right) \quad (24)$$

where f_c is the unconfined concrete cylinder compressive strength. The corresponding unconfined strain $\boldsymbol{\varepsilon_c}$ is taken as 0.003 for plain concrete as the ACI Specification recommends [31]. f_l is the lateral confining pressure imposed by the steel tube and obtained from the empirical equation (25):

$$f_l = \frac{\sigma_\theta t}{D} \quad (25)$$

Where $\boldsymbol{\sigma_\theta}$ is equal to $0.1f_y$ by Mander [36]. The factor k_1 is taken as 4.1, and factor k_2 20.5.

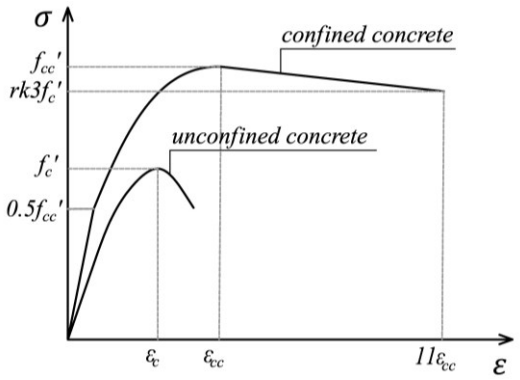

Figure 6. Stress-strain model for confined concrete used in Model 3

The uniaxial stress-strain curve consists of three parts, as shown in Figure 6. The first part considers elastic concrete behaviour until the proportional limit stress, which is taken as $0.5f_{cc}$ as per Hu [37].Recommendations also take the initial Young's modulus of confined concrete E_{cc} from the ACI Specification [31]. Poisson's ratio of confined concrete ν_{cc} is taken as 0.2.

$$E_{cc} = 4700\sqrt{f_{cc}'}[MPa] \quad (26)$$

The second part of the curve between the proportional limit of $0.5f_{cc}$ and confined concrete strength $\boldsymbol{f_{cc}}$ is the nonlinear branch defined by the relation provided in (27).

$$\boldsymbol{\sigma} = \frac{E_{cc}\cdot\varepsilon}{1 + (R + R_E - 2)\cdot\left(\frac{\varepsilon_c}{\varepsilon_{cc}}\right) - (2R-1)\cdot\left(\frac{\varepsilon_c}{\varepsilon_{cc}}\right)^2 + R\cdot\left(\frac{\varepsilon_c}{\varepsilon_{cc}}\right)^3} \quad (27)$$

where R and R_E were computed using the following equations (28-29):

$$R_E = \frac{E_{cc}\cdot\varepsilon_{cc}}{f_{cc}} \quad (28)$$

$$R = \frac{R_E\cdot(R_\sigma - 1)}{(R_\varepsilon - 1)^2} - \frac{1}{R_\varepsilon} \quad (29)$$

In equation (29), R_ε and R_σ are equal to 4,as recommended by [38]. The dilatation angle of 20◦is used in the CDP model, while for the default viscosity parameter, zero value is used. The Poisson coefficient is 0.2 [26].

2.2.2.4 The proposed extended EC2 model

The final considered concrete material model is the EC2 stress-strain relation for the nonlinear structural analysis for short-term uniaxial loading shown in Figure 7. When performing the general nonlinear analysis method for composite columns according to EC4, this is the material model that the engineer is referred to.

The curve in compression is described by the expressions (30-35):

$$\frac{\sigma_c}{f_c'} = \frac{k\eta - \eta^2}{1 + (k-2)\eta} \quad (30)$$

$$k = 1.05\,E_{cm}\cdot\frac{\varepsilon_{c1}}{f_{cm}} \quad (31)$$

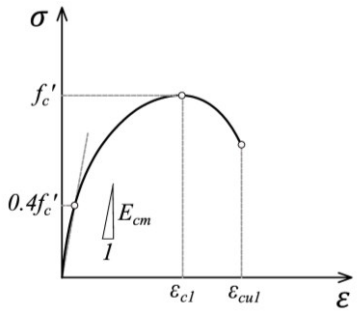

Figure 7. Schematic representation of the EC2 stress-strain relation for nonlinear structural analysis

$$E_{cm} = 22 \cdot 10^3 (f_{cm}/10)^{0.33} \quad (32)$$

$$\eta = \frac{\varepsilon_c}{\varepsilon_{c1}} \quad (33)$$

$$\varepsilon_{c1}[‰] = 0.7 f_{cm}{}^{0.31} \leq 2.8\ ‰ \quad (34)$$

$$\varepsilon_{cu1} = 3.5\ ‰, \qquad f_{cm} \leq 58\ MPa \quad (35)$$

where f_c' is the mean cylinder compressive strength, E_{cm} is the secant modulus of elasticity, ε_{c1} is the strain at peak stress and ε_{cu1} is the nominal ultimate strain.

However, according to EC2, the stress-strain relation in (30) is only valid for $\varepsilon_c \leq \varepsilon_{cu1} = 3.5$ ‰, which is insufficient to simulate the increased ductility and the softening behaviour of the CFST column. Therefore, this paper proposes a simple extension of this curve following the recommendations for the numerical modelling of CFST columns provided in [39].

$$\sigma_{res} = \begin{cases} \sigma_{cu1} & \frac{D}{t} \leq 24 \\ \sigma_{cu1}\left(1.6 - 0.025\frac{D}{t}\right) & 24 < \frac{D}{t} \leq 64 \\ 0 & 64 < \frac{D}{t} \end{cases} \quad (36)$$

The residual stress σ_{res} calculated from expression (36) depend on the D/t ratio and concrete stress value σ_{cu1} at $\varepsilon_{cu1} = 3.5$ ‰. According to [39], the concrete stress decreases with increasing compressive strain to a residual value (σ_{res}) at 15‰ strain. Here, it is proposed that the concrete stress σ_c decreases linearly beyond the strain limit of 3.5‰ to this residual value σ_{res} at 15‰ strain. Further, this stress value remains constant until 20‰ strain, as illustrated in Figure 8.

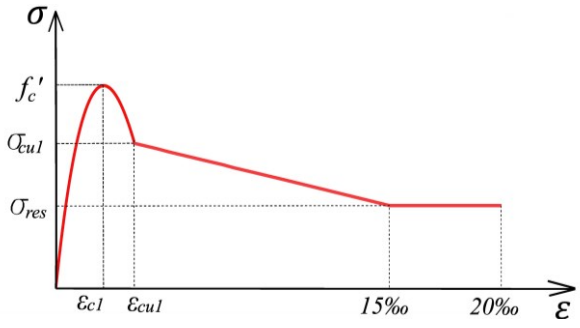

Figure 8. Proposed stress-strain model for confined concrete used in Model 4

Model 4 has the same characteristics for concrete in tension as adopted for Model 2. The plasticity parameters are also taken as for Model 2: 30º, 0.1, 1.16, 2/3 and 0, respectively.

2.2.3 Material modelling of steel tube

Structural steel properties required for ABAQUS are provided within a uniaxial stress-strain relationship $\sigma - \varepsilon$. Key input parameters for defining the curve are yield strength f_y, modulus of elasticity E, and the plasticity parameters that depend on the chosen curve. Researchers have investigated different stress-strain constitutive models for carbon steel, such as elastic-perfectly plastic, bilinear, and multilinear with hardening [40], [41].

This paper considered three different constitutive models for steel, schematically illustrated in Figure 9 for specimen 3HN. The first stress-strain curve is proposed by Tao et al. in [13] and consists of an elastic branch until the yield strain ε_y, a perfectly plastic branch until $15\varepsilon_y$ and hardening until the ultimate strain ε_u. Hardening is defined by strain-hardening exponent *p*.

The second is the five-stage elastic-plastic stress-strain model presented by Han et al. in [16]. It consists of elastic, elastic-plastic, plastic, hardening and fracture defined with $\varepsilon_e = 0.8 f_y/E$, $\varepsilon_{e1} = 1.5\varepsilon_e$, $\varepsilon_{e2} = 10\varepsilon_{e1}$, $\varepsilon_{e3} = 100\varepsilon_{e1}$, respectively, where ε_e is the yield strain and E modulus of elasticity.

The third constitutive model presented is an elastic-perfectly plastic $\sigma - \varepsilon$ relationship for structural steel given in EC3 [27]. Steel material properties used in tests are provided in Table 2. Poisson's ratio is taken as 0.3.

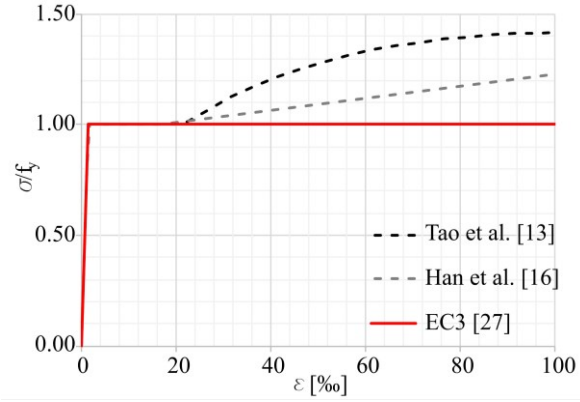

Figure 9. Steel models used illustrated for material properties of specimen 3HN [30]

However, this study showed that the choice of the steel stress-strain model does not significantly impact the numerical results. The same observation was previously reported in the literature [5].

3 Validation of the proposed 3d models

Proposed models have been validated based on test results provided in the literature. Here the validation is presented on eight short circular specimens with test results from various studies for columns with $L/D \leq 3$ to minimise the member slenderness effects. Table 2 lists the material properties of specimens and their references. The specimens are gradually loaded in all selected experiments with increasing axial loading. The loading is simultaneously applied to the whole cross-section.

Table 2. Details of specimens with material properties for concrete and steel

No.	Specimen and reference	Specimen details						Concrete	Steel		
		D	t	L	D/t	L/D	ξ	f_c'	f_y	E	Pois. ratio
		[mm]	[mm]	[mm]	-	-	-	[MPa]	[MPa]	[GPa]	-
1	3HN [30]	150.0	3.20	450.00	46.88	3.0	1.05	28.7	7.4	200.0	0.30
2	CC-0 [11]	139.1	2.79	420.00	49.86	3.0	0.92	41.2	388.5	203.8	0.28
3	cfst8-L35-0-a [22]	140.0	2.74	420.00	51.09	3.0	0.72	40.8	309.0	181.0	0.27
4	cfst12-L35-0-b [22]	140.0	3.90	420.00	35.9	3.0	1.15	40.8	335.3	205.0	0.27
5	310-60-3.6 [24]	114.0	3.60	250.00	31.67	2.2	0.83	60.0	310.0	200.0	0.30
6	310-60-5.6 [24]	114.0	5.60	250.00	20.36	2.2	1.36	60.0	310.0	200.0	0.30
7	310-60-3.1 [24]	167.0	3.10	250.00	53.87	1.5	0.47	60.0	310.0	200.0	0.30
8	C1-178-40-C00 [23]	178.0	6.55	548.33	27.18	3.1	1.91	40.0	403.0	209.6	0.30

Figures 10-19 show the axial load–axial strain ($N-\varepsilon$) relations for specimens from Table 2. Diagrams contain results obtained numerically using presented FE Models 1-4 compared to the results obtained from experiments. When results in the test were originally reported as axial load–axial shortening ($N-\Delta$) relations, they are converted by dividing axial shortening Δ with the column initial length L to obtain ($N-\varepsilon$) relations [9], [13].

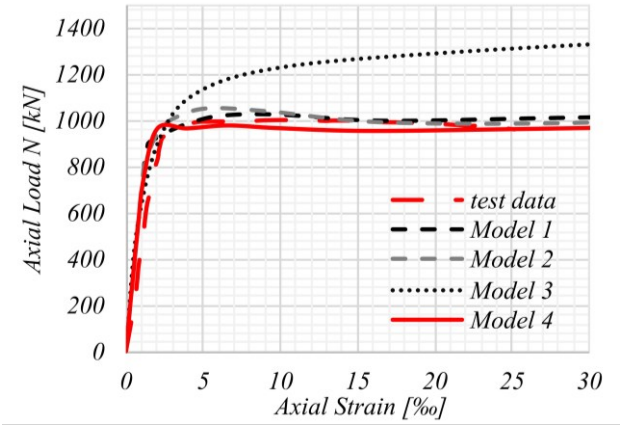

Figure 10. N-ε diagram for specimen 3HN

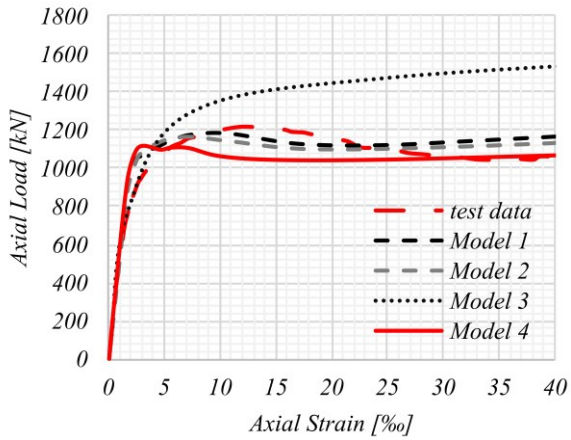

Figure 11. N-ε diagram for specimen CC-0

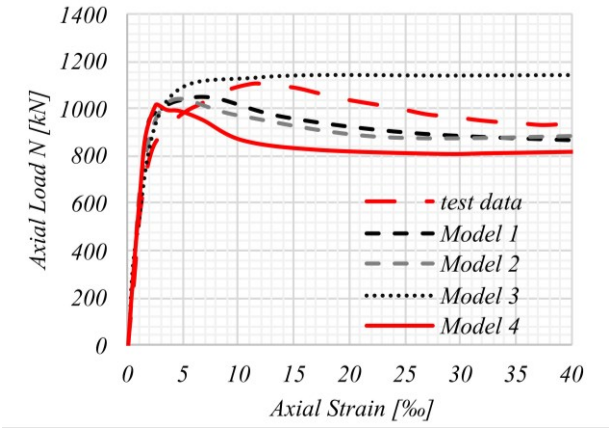

Figure 12. N-ε diagram for specimen cfst8-L35-0-a

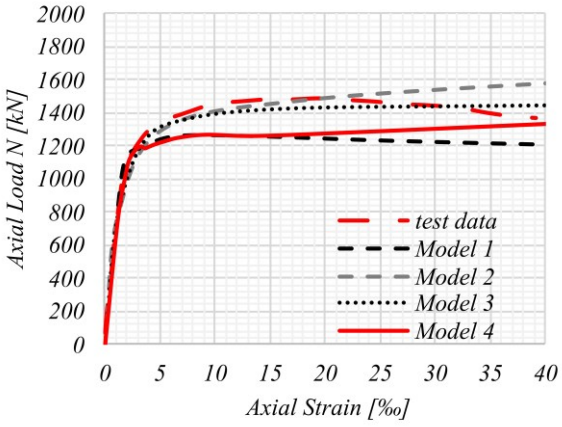

Figure 13. N-ε diagram for specimen cfst12-L35-0-b

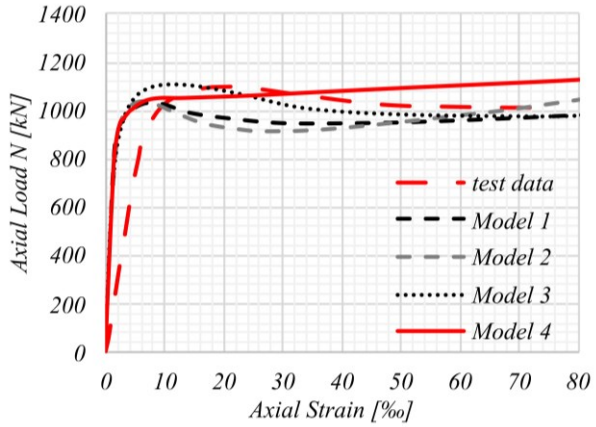

Figure 14. N-ε diagram for specimen 310-60-3.6

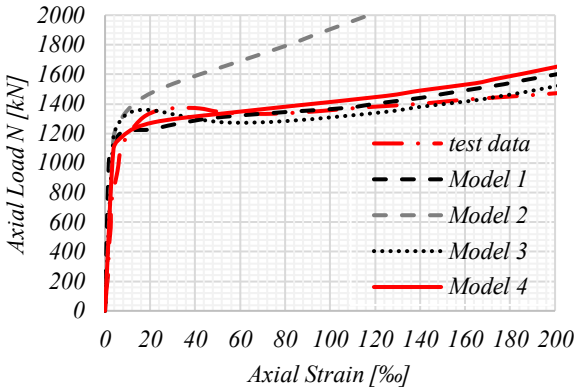

Figure 15. N-ε diagram for specimen 310-60-5.6

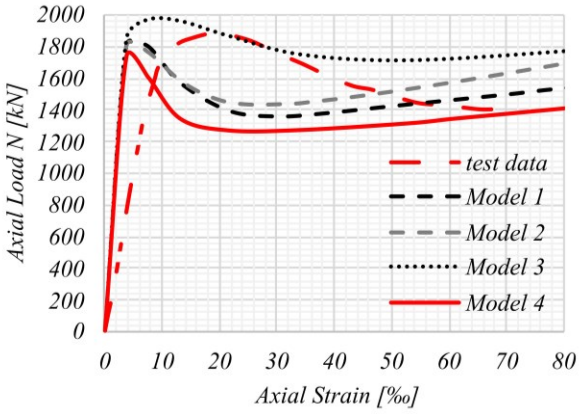

Figure 16. N-ε diagram for specimen 310-60-3.1

Figures 10-17 show that, in general, a satisfactory agreement between the numerical and test results is achieved with all four models regarding the ultimate column capacity. In tests shown in Figures 14, 16, 17, and slightly in Figure 10, the numerical results missed matching the experimental results during the initial elastic stage. This is due to differences in the actual value of the elastic modulus of concrete and the calculated values used in the numerical models. Since the measured values of the elastic modulus of concrete are not reported in all tests, the elastic modulus of concrete is calculated from the corresponding expressions described in Section 2 in all numerical models. Regarding the

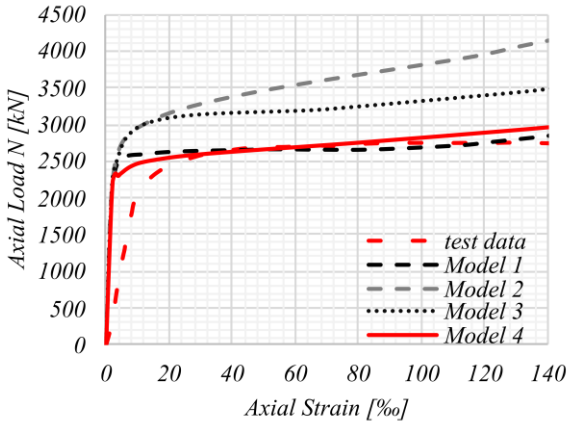

Figure 17. N-ε diagram for specimen C1-178-40-C00

full $N-\varepsilon$ curves, the differences between models are more pronounced. Model 1 has been shown to be the most accurate in this analysis. It successfully simulated CFST column behaviour for most specimens regarding ultimate capacity and the $N-\varepsilon$ response curve. The results obtained by Model 2 have also shown a good correlation with the experimental results for the specimens with a D/t ratio higher than 30. One possible reason for the different behaviour of specimens with a lower D/t ratio is an overestimation of the confinement effect and the strengthening of columns with a ticker steel tube in the post-peak stage. Model 3 gives results that agree well with the experimental results for specimens with concrete strengths higher than 40 MPa. It comes from the Mander concrete material model in Model 3, which considers the increase in concrete ductility and peak strength due to confinement effects. This is not the case for the concrete material models in Models 1 and 2. Finally, the results of Model 4 are in very good agreement with the experimentally obtained results for all tests. These results are similar to those obtained by Model 1. Therefore, the extension of the concrete material model from EC2 enabled Model 4 to capture well the peak and post-peak behaviour of the CFST column.

The shape of the $N-\varepsilon$ response depends on the confinement factor ξ [42][43], equation (16), which varies based on the cross-sectional shape of the column. For different types of CFST's cross-sections, different critical values ξ_0 are defined. Circular CFST columns are estimated to be around 1.01 to 1.21 [43]. When the actual confinement factor is less than ξ_0 the $N-\varepsilon$ response has a "strain softening" shape. When it is equal to ξ_0, the response is "perfectly plastic", while for values of ξ higher than ξ_0, the response is of the "strain hardening" type. The value of ξ for each of the analysed specimens is calculated in Table 2. Clearly, this factor is the smallest for specimen 310-60-3.1 (equal to 0.47); therefore, its response exhibits the most noticeable strain-softening shape. The numerical models also predict this softening branch, but due to previously discussed differences in the initial stiffnesses, there are discrepancies between the numerical and experimental responses.

In addition, it should be noted that nonlinear static analysis in ABAQUS using the CDP model is sensitive to the variation of plasticity parameters. Moreover, it should be underlined that the presented specimens belong to different experimental studies. Test data were carefully reviewed to understand the test setup, instrumentation and results, especially in describing the test, steel and concrete material

properties. However, not all necessary data is reported, and the missing values are calculated from the available expressions.

Finally, as mentioned in the introductory part of the paper, one significant advantage of the detailed $3D$ model is its ability to predict the failure modes correctly. All selected specimens experienced very similar drum-like failure modes with or without local buckling of steel tubes near column ends. It should be emphasised that the concrete core within the steel tube postpones or even completely prevents local buckling of the steel tube. All analysed specimens have a D/t ratio well below the limit value according to EC4 (equal to $90 \cdot 235/f_y$) and can be considered not prone to local buckling. Therefore, local buckling effects were not dominant in these tests. Figure 18 shows the numerically obtained failure modes for all analysed specimens. Here, for each test, the figure on the left side (in green) shows the deformed shape in the last calculation step, while the figure on the right side (in colour) shows the vertical displacements (Z direction) for the middle cut of the corresponding specimen. There is a good correlation between the experimental evidence and numerically obtained failure modes.

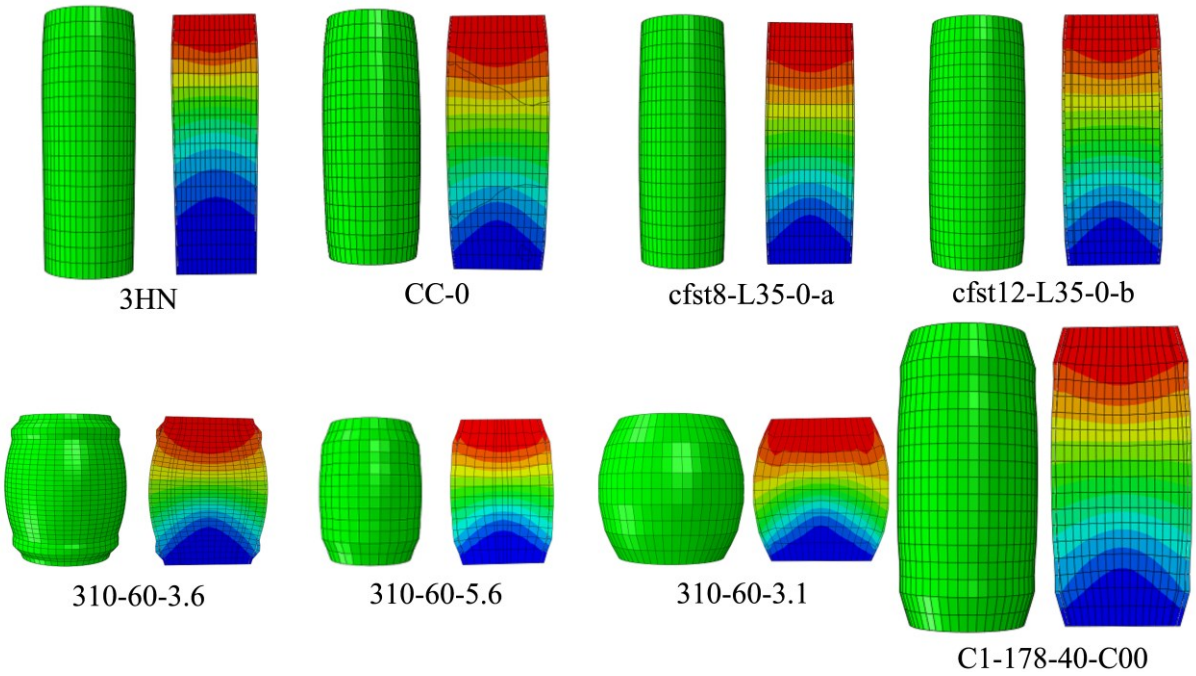

Figure 18. Deformed shapes of circular stub specimens under axial load

4 Ultimate column compression capacity and comparison with EC4 design code calculations

In this section, the numerically obtained column axial compression capacity $N_{u,i}$from Models $i = 1,2,3,4$ for each specimen is compared with the ultimate strength $N_{u,test}$reported in tests. The value $N_{u,i}$ is determined in the following way. For the specimen with a noticeable peak (maximum) value that is achieved for strains lower than 1%, that value is taken as the ultimate capacity $N_{u,i}$. For specimens that have hardening-type behaviour, the ultimate capacity $N_{u,\mathrm{I}}$ is taken to be equal to the force value corresponding to the strain value of 1%,as suggested by[6]. It should be noted that the test values $N_{u,test}$ are taken to be equal to the values reported by the corresponding authors, although, in some tests, these ultimate strengths correspond to unrealistically high strains (e.g., in test C1-178-40-C00, the ultimate strain is 140 ‰). Also, for each specimen, the ratio $N_{u,i}/N_{u,test}$is calculated, and these values are reported in Table 3. The results show that the average ratios are 93%, 98%, 106% and 91%, respectively, for Models 1 to 4. The corresponding standard deviations are 6%, 5%, 11% and 4%, respectively, for Models 1 to 4. These results lead to similar conclusions as previously derived regarding the whole $N-\varepsilon$ response. Here, Model 2 gives the best predictions with an average ratio of 98% and a standard deviation of 5%. Model 1 and the proposed Model 4 have slightly lower average ratios but still give good predictions of the column's ultimate capacity. The results of Model 3 are the least accurate, with an average ratio of 106% for the $N_{u,i}/N_{u,test}$ and the highest standard deviation.

According to EC4, the resistance to axial compression of a doubly symmetrical and uniform composite cross-section N_{EC4} can be determined using a simplified method of design. The plastic resistance to compression of a composite-cross section should be calculated by adding the plastic resistances of its components, steel tube and concrete core. In the case of concentric loading on concrete-filled tubes of circular cross-sections, N_{EC4} may take into account the decrease in steel strength by a factor η_a and the increase in the strength of concrete by a factor η_c due to confinement effects, equations (38-39). This confinement effect can be taken into account only if the relative slenderness $\bar{\lambda}$ defined by equation (40) does not exceed 0.5. The effective buckling length of the column $l_0$was taken as $0.5L$, corresponding to the fixed-ended boundary conditions reported in the tests. The values of the N_{EC4} are calculated with material data reported in tests without applying the partial factors for material properties or any other safety factors in the expression (37).

Table 3. Summary of ultimate axial strength N_u results

Specimen	test data	Model 1		Model 2		Model 3		Model 4		EC4	
	$N_{u,test}$	$N_{u,1}$	$\frac{N_{u,1}}{N_{u,test}}$	$N_{u,2}$	$\frac{N_{u,2}}{N_{u,test}}$	$N_{u,3}$	$\frac{N_{u,3}}{N_{u,test}}$	$N_{u,4}$	$\frac{N_{u,4}}{N_{u,test}}$	N_{EC4}	$\frac{N_{EC4}}{N_{u,test}}$
	[kN]	[kN]	[%]	[kN]	[%]	[kN]	[%]	[kN]	[%]	[kN]	[%]
3HN	1001	1027	103%	1053	105%	1233	123%	980	98%	1175	117%
CC-0	1212	1178	97%	1164	96%	1470	121%	1112	92%	1340	111%
cfst8-L35-0-a	1143	1051	92%	1043	91%	1129	99%	1012	89%	1182	103%
cfst12-L35-0-b	1511	1260	83%	1408	93%	1400	93%	1269	84%	1476	98%
310-60-3.6	1095	1030	94%	1039	95%	1100	100%	1044	95%	1186	108%
310-60-5.6	1365	1220	89%	1402	103%	1303	95%	1235	90%	1464	107%
310-60-3.1	1873	1805	96%	1804	96%	1967	105%	1738	93%	2091	112%
C1-178-40-C00	2781	2579	93%	2905	104%	3050	110%	2465	89%	3134	113%
Mean value			*93%*		*98%*		*106%*		*91%*		*109%*
St dev.			*6%*		*5%*		*11%*		*4%*		*6%*

$$N_{EC4} = \eta_a A_s f_y + A_c f_c' \left(1 + \eta_c \frac{t}{D}\frac{f_y}{f_c'}\right) \quad (37)$$

$$\eta_a = 0.25(3 + 2\bar{\lambda}) \leq 1.0 \quad (38)$$

$$\eta_c = 4.9 - 18.5\bar{\lambda} + 17(\bar{\lambda})^2 \geq 0 \quad (39)$$

$$\bar{\lambda} = \sqrt{\frac{N_{pl}}{N_{cr}}} \quad (40)$$

$$N_{pl} = A_a f_y + A_c f_c' \quad (41)$$

$$N_{cr} = \pi^2 \frac{(EI)_{eff}}{{l_0}^2} \quad (42)$$

$$(EI)_{eff} = E_a I_a + 0.6 E_{cm} I_c \quad (43)$$

where:

$N_{pl,Rk}$ is the characteristic value of the plastic resistance to compression,

N_{cr} is the elastic critical normal force for the relevant buckling mode, calculated with the effective flexural stiffness $(EI)_{eff}$,

I_a, I_c are the moments of inertia of the steel section and the concrete section.

The values of N_{EC4} are compared with the experimental data $N_{u,test}$ in the last column of Table 3. The results show that this ratio's mean value and standard deviation are 109% and 6%, respectively. However, the results are not on the safe side, and EC4 overestimates the ultimate strength capacity of the column when calculated with data from the tests. Figure 19 presents a comparison of $N_{u,4}/N_{u,\text{test}}$ ratios obtained for the proposed Model 4 and EC4 predictions. On the other hand, the predictions of the column's ultimate axial capacity obtained by Model 4 are on the safe side for all specimens.

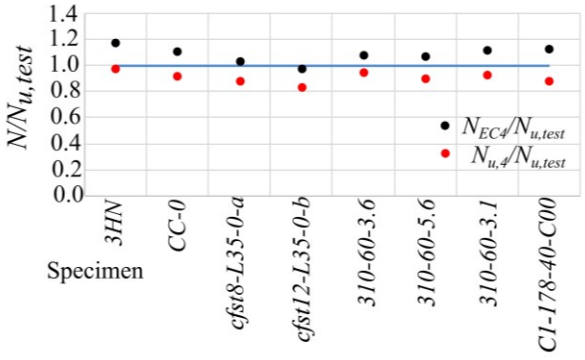

Figure 19. Model 4-to test and EC4 prediction - to test ultimate strength capacity

5 Conclusion

The paper investigates the numerical modelling of CFST columns' behaviour in ABAQUS software. The presented 3D finite element models simulate the behaviour of circular CFST stub columns under axial compression with high accuracy. The selected four models are validated on a set of experimental tests and have been shown to predict well both: the full $N-\varepsilon$ diagrams and the failure modes. Models 1, 2 and 3 are the most commonly applied models for the nonlinear analysis of CFST columns. Model 1 is proven to simulate the actual behaviour very well for all specimens. Model 2 describes the $N-\varepsilon$ relations very well for specimens with a *D/t* ratio higher than 30 due to overestimating the confinement of the ticker steel tube. Model 3 is the most complex of the selected models regarding consideration of the confinement effects. It provides a good prediction of the full $N-\varepsilon$ column response for specimens with concrete strengths higher than 40 MPa.

The proposed Model 4 is a simple model that shows good agreement with test results regarding the full-range $N-\varepsilon$ diagram. This model overcomes the current limitations of the EC4 and EC2 design guides referring to the limitation of the stress-strain relation by EC2 for concrete in compression to 3.5‰ strain and the absence of a suggested relation for concrete in tension. Also, it considers the concrete core confinement effects. Finally, according to the results of this study, the simplified method of the EC4 for the determination of the short column ultimate compression capacity gives ultimate compression values close to the test values. However, for most of the selected specimens, these values are not on the safe side. The ongoing study investigates this issue in detail on a much larger data set.

Acknowledgements

The financial support of the Ministry of Education, Science, and Technological Development, Republic of Serbia, through Project 200092, is acknowledged.

Notation list

D	outer diameter of a circular column
L	length of a column
t	wall thickness of the steel tube
ψ	dilation angle
e	flow potential eccentricity
K_c	ratio of the second stress invariant on the tensile meridian to that on the compressive meridian
f_{b0}/f_c'	ratio of the compressive strength under biaxial loading to uniaxial compressive strength
f_c'	cylinder compressive strength of unconfined concrete
f_{ck}	characteristic strength of the concrete
f_{cu}	cube strength of the concrete
f_{cc}'	confined concrete compressive strength
f_l	lateral confining pressure
ε_c	concrete strain
ε_{c0}	concrete strain at cylinder compressive strength of unconfined concrete
ε_{cc}	concrete strain at peak stress
ε_y	steel yield strain
ε_u	ultimate strain of the steel
E	modulus of elasticity of steel tube
E_c	modulus of elasticity of the unconfined concrete
E_{cc}	modulus of confined concrete
f_B	confining stress
f_y	yield strength of the steel tube
f_r	residual stress
A_s	cross-sectional area of the steel tube
A_c	cross-sectional area of the concrete core
ξ_c	confinement factor
G_F	fracture energy
d_{max}	maximum coarse aggregate size
ξ	confinement factor
E_{cm}	secant modulus of elasticity
ε_{c1}	concrete strain at peak stress
ε_{cu1}	concrete nominal ultimate strain
σ_c	concrete stress
σ_{res}	concrete residual stress
Δ	column shortening
$N_{u,i}$	column axial compression capacity from Models $i = 1,2,3,4$
$N_{u,test}$	column test ultimate strength
N_{EC4}	resistance to axial compression by EC4
η_a, η_c	factors related to the confinement of concrete
$\bar{\lambda}$	column relative slenderness
$N_{pl,Rk}$	characteristic value of the plastic resistance to compression
N_{cr}	elastic critical normal force for the relevant buckling mode
I_a, I_c	moments of inertia of the steel section and the concrete section

References

[1] M. M. L. Radovanovic, J. Z. Nikolic, J. R. Radovanovic, and S. M. Kostic, "Structural Behaviour of Axially Loaded Concrete-Filled Steel Tube Columns during the Top-Down Construction Method," *Appl. Sci.*, vol. 12, no. 8, Apr. 2022, doi: 10.3390/app12083771.

[2] S. M. Kostic, F. C. Filippou, and B. Deretic-Stojanovic, "Generalized plasticity model for inelastic RCFT column response," *Comput. Struct.*, vol. 168, pp. 56–67, May 2016, doi: 10.1016/j.compstruc.2016.02.006.

[3] Y. F. Yang and L. H. Han, "Concrete filled steel tube (CFST) columns subjected to concentrically partial compression," *Thin-Walled Struct.*, vol. 50, no. 1, pp. 147–156, Jan. 2012, doi: 10.1016/J.TWS.2011.09.007.

[4] F. xing Ding, W. jun Wang, D. ren Lu, and X. mei Liu, "Study on the behavior of concrete-filled square double-skin steel tubular stub columns under axial loading," *Structures*, vol. 23, pp. 665–676, Feb. 2020, doi: 10.1016/j.istruc.2019.12.008.

[5] Y. Gunawardena and F. Aslani, "Finite element modelling of concrete-filled spiral-welded mild-steel tube short and long columns," *Structures*, vol. 30, pp. 1020–1041, Apr. 2021, doi: 10.1016/j.istruc.2021.01.074.

[6] Z. Bin Wang, Z. Tao, L. H. Han, B. Uy, D. Lam, and W. H. Kang, "Strength, stiffness and ductility of concrete-filled steel columns under axial compression," *Eng. Struct.*, vol. 135, pp. 209–221, Mar. 2017, doi: 10.1016/j.engstruct.2016.12.049.

[7] C. D. Goode, "1819 tests on concrete-filled steel tube columns compared with Eurocode 4," *Struct Eng*, vol. 8, no. 33, p. 86, 2008.

[8] S. Kostic and B. Deretic-Stojanovic, "Fiber element formulation for inelastic frame analysis," *Gradjevinski Mater. i Konstr.*, vol. 59, no. 2, pp. 3–13, 2016, doi: 10.5937/grmk1602003k.

[9] N. Subedi, T. Obara, and S. Kono, "Noncompact and slender concrete-filled steel tubes under axial compression: Finite-element modeling and evaluation of stress-strain models for fiber-based analysis," *J. Constr. Steel Res.*, vol. 196, Sep. 2022, doi: 10.1016/j.jcsr.2022.107353.

[10] V. I. Patel, Q. Q. Liang, and M. N. S. Hadi, "Nonlinear analysis of axially loaded circular concrete-filled stainless steel tubular short columns," *J. Constr. Steel Res.*, vol. 101, pp. 9–18, 2014, doi: 10.1016/j.jcsr.2014.04.036.

[11] V. W. Y. Tam, Z. Bin Wang, and Z. Tao, "Behaviour of recycled aggregate concrete filled stainless steel stub columns," *Mater. Struct. Constr.*, vol. 47, no. 1–2, pp. 293–310, Jan. 2014, doi: 10.1617/s11527-013-0061-1.

[12] Z. Tao, B. Uy, F. Y. Liao, and L. H. Han, "Nonlinear analysis of concrete-filled square stainless steel stub columns under axial compression," *J. Constr. Steel Res.*, vol. 67, no. 11, pp. 1719–1732, Nov. 2011, doi: 10.1016/j.jcsr.2011.04.012.

[13] Z. Tao, Z. Bin Wang, and Q. Yu, "Finite element modelling of concrete-filled steel stub columns under axial compression," *J. Constr. Steel Res.*, vol. 89, pp. 121–131, 2013, doi: 10.1016/j.jcsr.2013.07.001.

[14] L. H. Han and Y. F. An, "Performance of concrete-encased CFST stub columns under axial compression," *J. Constr. Steel Res.*, vol. 93, pp. 62–76, Feb. 2014, doi: 10.1016/j.jcsr.2013.10.019.

[15] M. H. Lai and J. C. M. Ho, "A theoretical axial stress-strain model for circular concrete-filled-steel-tube columns," *Eng. Struct.*, vol. 125, pp. 124–143, Oct. 2016, doi: 10.1016/j.engstruct.2016.06.048.

[16] L. H. Han, G. H. Yao, and Z. Tao, "Performance of concrete-filled thin-walled steel tubes under pure torsion," *Thin-Walled Struct.*, vol. 45, no. 1, pp. 24–36, Jan. 2007, doi: 10.1016/j.tws.2007.01.008.

[17] N. F. Hany, E. G. Hantouche, and M. H. Harajli, "Finite element modeling of FRP-confined concrete using modified concrete damaged plasticity," *Eng. Struct.*, vol. 125, pp. 1–14, Oct. 2016, doi: 10.1016/j.engstruct.2016.06.047.

[18] European committee for standardization, "EN 1994-1-1: Eurocode 4: Design of composite steel and concrete structures-Part 1-1: General rules and rules for buildings," 2004.

[19] Deretić-Stojanović Biljana, Kostić Svetlana, and Stošić Saša, "Analysis of composite steel and concrete columns," *Build. Mater. Struct.*, vol. 54, no. 1, pp. 62–79, 2011, [Online]. Available: www.dimk.rs

[20] AIJ, *Recommendations for Design and Construction of Concrete Filled Steel Tubular Structures*. Japan: Architectural Institute of Japan, 2008.

[21] *ABAQUS User Manual 6.9. DS SIMULIA Corp., Providence, Rhode Island, USA, 2009*.

[22] Y. Wang, J. Chen, and Y. Geng, "Testing and analysis of axially loaded normal-strength recycled aggregate concrete filled steel tubular stub columns," *Eng. Struct.*, vol. 86, pp. 192–212, Mar. 2015, doi: 10.1016/j.engstruct.2015.01.007.

[23] V. da S. de Azevedo, L. R. O. de Lima, P. C. G. d. S. Vellasco, M. E. d. N. Tavares, and T. M. Chan, "Experimental investigation on recycled aggregate concrete filled steel tubular stub columns under axial compression," *J. Constr. Steel Res.*, vol. 187, Dec. 2021, doi: 10.1016/j.jcsr.2021.106930.

[24] F. Abed, M. Alhamaydeh, and S. Abdalla, "Experimental and numerical investigations of the compressive behavior of concrete filled steel tubes (CFSTs)," *J. Constr. Steel Res.*, vol. 80, pp. 429–439, Jan. 2013, doi: 10.1016/j.jcsr.2012.10.005.

[25] D. Lam, X. H. Dai, L. H. Han, Q. X. Ren, and W. Li, "Behaviour of inclined, tapered and STS square CFST stub columns subjected to axial load," *Thin-Walled Struct.*, vol. 54, pp. 94–105, May 2012, doi: 10.1016/J.TWS.2012.02.010.

[26] E. Ellobody, "Numerical modelling of fibre reinforced concrete-filled stainless steel tubular columns," *Thin-Walled Struct.*, vol. 63, pp. 1–12, 2013, doi: 10.1016/j.tws.2012.10.005.

[27] European committee for standardization, "EN 1993-1-1: Eurocode 3: Design of steel structures - Part 1-1: General rules and rules for buildings," 2005.

[28] European committee for standardization, "EN 1992-1-1: Eurocode 2: Design of concrete structures - Part 1-1: General rules and rules for buildings," 2004.

[29] G. B. Hajjar JF, "A cyclic nonlinear model for concrete-filled tubes formulation.," *J Struct Eng, ASCE*, no. 123(6), pp. 736–44, 1997.

[30] Y. M. M. Tomii, K. Yoshimura, "Experimental studies on concrete filled steel tubular stub columns under concentric loading," in *Proceedings of the International Colloquium on Stability of Structures under Static and Dynamic Loads*, 1977, pp. 718–741.

[31] American Concrete Institute, *Building Code Requirements for Structural Concrete (ACI 318-11) and Commentary*. MI, USA: Farmington Hills, 2011.

[32] B. Binici, "An analytical model for stress–strain behavior of confined concrete," *Eng. Struct.*, vol. 27, no. 7, pp. 1040–1051, Jun. 2005, doi: 10.1016/J.ENGSTRUCT.2005.03.002.

[33] Z. P. Bažant and E. Becq-Giraudon, "Statistical prediction of fracture parameters of concrete and implications for choice of testing standard," *Cem. Concr. Res.*, vol. 32, no. 4, pp. 529–556, Apr. 2002, doi: 10.1016/S0008-8846(01)00723-2.

[34] V. K. Papanikolaou and A. J. Kappos, "Confinement-sensitive plasticity constitutive model for concrete in triaxial compression," *Int. J. Solids Struct.*, vol. 44, no. 21, pp. 7021–7048, Oct. 2007, doi: 10.1016/J.IJSOLSTR.2007.03.022.

[35] A. Hillerborg, M. Modéer, and P.-E. Petersson, "Analysis of crack formation and crack growth in concrete by means of fracture mechanics and finite elements," *Cem. Concr. Res.*, vol. 6, no. 6, pp. 773–781, Nov. 1976, doi: 10.1016/0008-8846(76)90007-7.

[36] J. B. . M. J. P. and R. P. Mander, "Theoretical stress-strain model for confined concrete," *J. Struct. Eng.*, vol. 114, no. 8, pp. 1804–1826, 1988.

[37] H.-T. Hu, C.-S. Huang, M.-H. Wu, and Y.-M. Wu, "Nonlinear Analysis of Axially Loaded Concrete-Filled Tube Columns with Confinement Effect," *J. Struct. Eng.*, vol. 129, no. 10, pp. 1322–1329, Oct. 2003, doi: 10.1061/(ASCE)0733-9445(2003)129:10(1322).

[38] H. Hu and W. C. Schnobrich, "Constitutive Modeling of Concrete by Using Nonassociated Plasticity," *J. Mater. Civ. Eng.*, vol. 1, no. 4, pp. 199–216, 1989, doi: 10.1061/(asce)0899-1561(1989)1:4(199).

[39] J. M. Portolés, M. L. Romero, F. C. Filippou, and J. L. Bonet, "Simulation and design recommendations of eccentrically loaded slender concrete-filled tubular columns," *Eng. Struct.*, vol. 33, no. 5, pp. 1576–1593, May 2011, doi: 10.1016/j.engstruct.2011.01.028.

[40] E. Ellobody, "Nonlinear behaviour of eccentrically loaded FR concrete-filled stainless steel tubular columns," *J. Constr. Steel Res.*, vol. 90, pp. 1–12, 2013, doi: 10.1016/j.jcsr.2013.07.018.

[41] M. M.A. Kadhim, "Numerical modelling of concrete-filled stainless steel slender columns loaded eccentrically," *World J. Eng.*, vol. 17, no. 5, pp. 697–707, Aug. 2020, doi: 10.1108/WJE-09-2019-0268.

[42] L. H. . Z. X. L. . & T. Z. Han, "Tests and mechanics model for concrete-filled SHS stub columns, columns and beam-columns," *Steel Compos. Struct.*, vol. 1, no. 1, pp. 51–74, 2001.

[43] W. Q. Lyu, L. H. Han, and C. Hou, "Axial compressive behaviour and design calculations on recycled aggregate concrete-filled steel tubular (RAC-FST) stub columns," *Eng. Struct.*, vol. 241, Aug. 2021, doi: 10.1016/j.engstruct.2021.112452.

Građevinski materijali i konstrukcije
Building Materials and Structures
journal homepage: www.dimk.rs

https://doi.org/10.5937/GRMK2300002M UDK: 624.078.46
624.012.45

Preliminary report

Local behaviour of the connector with mechanical coupler and rebar anchor under tension load

Ivan Milićević[*1)], Branko Milosavljević[1)], Milan Spremić[1)], Rastislav Mandić[1)], Marko Popović[1)]

[1)] *University of Belgrade, Faculty of Civil Engineering, Bulevar kralja Aleksandra 73, 11000 Belgrade, Serbia*

Article history

Received: 25 January 2023
Received in revised form: 04 April 2023
Accepted: 24 April 2023
Available online: 22 May 2023

Keywords

mechanical couplers,
reinforcement,
demountable connections,
tension loads,
composite structures

ABSTRACT

In the past few decades, demountable connectors have often been used for connections in composite and mixed steel-concrete structures to reduce construction time and costs. Furthermore, the application of demountable connectors enables the reuse of structural elements in these structures, which leads to sustainable design and a circular economy. In this paper, the demountable connector is made out of two parts: (1) mechanical coupler and rebar anchor placed in formwork before casting the concrete element, and (2) steel bolt used for connecting steel to the RC element. Although this connector is increasingly being used in contemporary building structures, its behaviour in composite connections is still insufficiently defined. The paper presents the results of experimental tests and numerical analysis of the connector with a mechanical coupler, focusing on the local behaviour of the tapered threaded connection between the mechanical coupler and rebar anchor.

1 Introduction

The combination of structural steel and reinforced concrete elements in composite and mixed civil engineering structures arose from the desire to reduce costs and shorten construction timelines. The behaviour of such structures significantly depends on the behaviour of the connection between the steel and RC components which is realised by the use of mechanical connecting devices, i.e., connectors. These connectors are most commonly loaded with shear, tension, or combined loads.

Traditionally, headed studs continuously and uniformly welded along the flanges of steel profiles have provided the connections between structural elements made of steel and reinforced concrete (see Figure 1(a)). The reason lies in the quick execution using automatic welding and their adequate and reliable behaviour under shear, tension, and their interaction, which has been proven by numerous experimental and numerical studies [2,3]. In contrast to welded studs, demountable connectors enable relatively simple disassembly and reuse of structural elements and even entire structures after the “first service life”. Over the past few decades, several experimental and numerical studies on the performance of various types of demountable connectors have been performed, the most common of which are shown in Figures 1(b)-1(d). In terms of shear behaviour, it was concluded that these connectors have a comparable load-bearing capacity to welded-headed studs but significantly lower stiffness as well as ductility. It was observed that the stiffness of the connector increased with the addition of one or two embedded nuts. In terms of tensile behaviour, it was concluded that the failure modes and load capacities of demountable-headed connectors are similar to those of welded studs [1].

Over the last few years, different research groups have analysed the application of demountable shear connectors with bolts and mechanical couplers, which are most commonly used for rebar splicing in RC structures. These connector types are shown in Figures 1(e) and 1(f). The connection between the steel and RC element is achieved on the construction site by screwing the short bolt into the coupler, which was previously embedded in the RC element. The connector can be anchored to the RC element by connecting the coupler with another longer bolt [4,5] or by connecting it with the rebar anchor [6,7]. According to research results, the shear behaviour of these connectors was similar to that of bolts with embedded nuts. It was pointed out that under the action of longitudinal shear, regardless of the connector anchoring method, deformation predominantly occurs in the short bolt. At the same time, mechanical couplers provide a flat surface for the RC element at the place of the connector, making disassembly easier compared to other demountable connector solutions.

In the case of tensile force, connectors with mechanical couplers have a more complex behaviour compared to other connectors shown in Figure 1. The reason lies in the fact that connectors with mechanical couplers are, in general, formed by joining three elements of different mechanical and geometric characteristics (see Figures 1(e) and 1(f)). Therefore, their behaviour in tension, and thus under

* Corresponding author:
E-mail address: ivanm@imk.grf.bg.ac.rs

combined load, depends on the behaviour of the "weakest link" in the connector. For example, during the tensile tests conducted on the connectors used by Yang et al. [4] significant deformation occurred in the mechanical couplers. On the other hand, in connectors with mechanical couplers and rebar anchors, the rebar anchor can be the weakest link if high-strength bolts are used [7].

This research aims to analyse the local tensile behaviour of the connector formed by connecting the bolt, mechanical coupler, and rebar anchor (Figure 1(f)). For this purpose, the tensile test was conducted on the connector itself using the tensile testing machine, continuously measuring the load and deformation of the connector at characteristic zones. Based on the load test results, a nonlinear finite element analysis (FEA) analysis of the connector with a mechanical coupler was carried out by the Abaqus software, with an emphasis on modelling the connection between the mechanical coupler and the rebar anchor.

2 Experimental analysis

2.1 Experimental program and material properties

To study the tensile behaviour and determine the corresponding load-bearing capacity of the threaded splice connection between bolt and rebar anchor, tests were performed on a 300 kN capacity Shimadzu tensile testing machine. The connectors were formed by M20 bolts and Ø16 rebar connected to the coupler by ISO coarse metric thread and conical thread, respectively (see Figure 1(f)). The tested mechanical properties of demountable connector components are presented in Table 1.

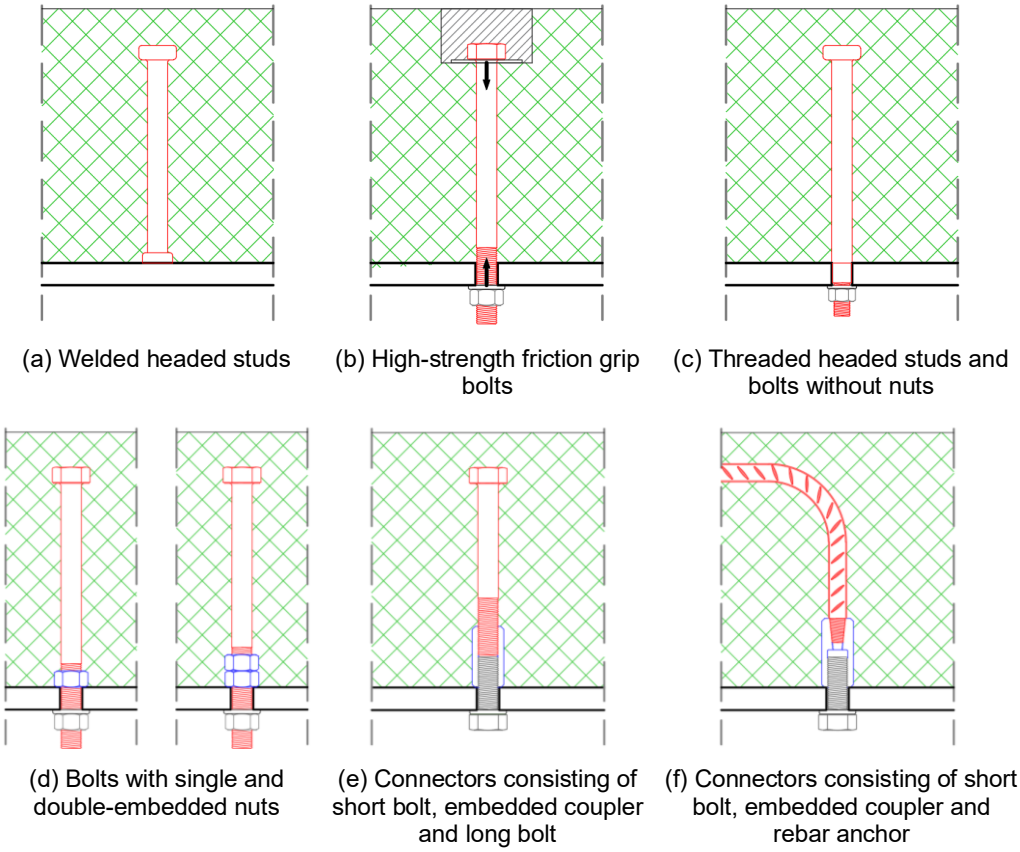

(a) Welded headed studs

(b) High-strength friction grip bolts

(c) Threaded headed studs and bolts without nuts

(d) Bolts with single and double-embedded nuts

(e) Connectors consisting of short bolt, embedded coupler and long bolt

(f) Connectors consisting of short bolt, embedded coupler and rebar anchor

Figure 1. Examples of different types of connectors

Table 1. Tested mechanical properties of demountable connector components

Component	Elastic modulus E (GPa)	Offset yield strength $f_{0,2}$ (MPa)	Tensile strength f_u (MPa)	Ultimate strain ε_u (%)
Bolt M20	204.3	855.2	930.6	16.19
Mech. coupler	206.6	770.1	846.0	6.94
Rebar Ø16	193.3	554.7	668.4	19.65

2.2 Test set-up and measurement procedure

The tensile test layout with measuring point arrangement is presented in Figure 2. In total, two samples were tested. The bolts were preloaded to around 20% of the full preload force, according to [8]. The specimens were loaded in displacement control mode with a 1.0 mm/min stroke rate. Global and local deformation were measured in two ways: (1) measurement at discrete points using inductive displacement transducers, strain gauges, and extensometer, and (2) measurement by Digital Image Correlation, DIC.

In the first case, the rebar elongation was measured by an extensometer with a gauge length l_{ext} = 100 mm. The displacement of specimens along the loading axis (labelled as d), was measured by inductive displacement transducers at 6 points, relative to the fixed position. Rebar-coupler slip values $\delta_{1.1}$ and $\delta_{1.2}$ were estimated as the subtraction of measured values $d_{1.1}$and $d_{1.2}$ and $d_{1.3}$ and $d_{1.4}$, respectively. The mean of rebar slip values $\delta_{1.1}$ and $\delta_{1.2}$ was labelled as δ_1. Similarly, separation between the coupler and bolt grip δ_2 was estimated. This separation was used for estimation of bolt strain ε_b along the 24 mm grip length. Coupler strain ε_{co} was measured by strain gauges at the weakest section – between bolt and rebar, as shown in Figure 1(f).

In the DIC method, digital images of the front side of the connector were captured at different deformation states and post-processed by matching the same points (or pixels) between the two images recorded before and after deformation. The front side of the connector was painted with white paint. Random speckle pattern was achieved with black paint by hand spraying using the small pipe on the spraying can lid. The acquisition of the digital images during the experiment was performed with a full frame Canon 6D (sensor 36x24 mm, resolution 20.2 megapixels) with a Canon EF 24-105 mm f/4L IS II USM telephoto lens. The focal length was fixed at 105 mm with f/8 aperture. The camera was placed on a tripod at 0.96 m from specimen which resulted in an average spatial resolution of 0.06 mm/pixel. The camera was triggered automatically at time increments of 10 s. DIC analysis was done using an open-source 2D MATLAB program – Ncorr [9].

2.3 Results of tensile tests

The appearance of the connector before, during and after the tensile test is shown in Figure 3. Both specimens failed due to the stripping of taper threads on the end of the rebar. As the coupler and bolt deformation were negligible, they could be easily demounted after testing (Figure 3(c)).

Experimental test results are graphically presented in Figure 4. The maximum force of samples 1 and 2 subjected to the tension was $T_{u,1}$ = 128.7 kN and $T_{u,2}$ = 129.9 kN, which is about 4% less than the load capacity of the control rebar. In Figure 4(a) stroke Δ_{st} and rebar elongation within free length Δ_{at} are presented as a function of tensile force T. Rebar elongation Δ_{at} was obtained by scaling the elongations measured by an extensometer. On graphs, four characteristic points can be identified as:„Y“ –yield point, „S“ – beginning of rebar strain hardening, „U“ – the ultimate load of the rebar and connector as a whole and „R“ – connector failure. By observing the graphs, it can be concluded that the displacements Δ_{st} and Δ_{at} differ significantly in the rebar's elastic region due to the wedging of wedge grips into the bar and the bolt fixture. The elastic elongation of the bolt and the mechanical coupler contribute far less to that difference, as confirmed by the small, reversible strains of these two elements (Figure 4(b)).

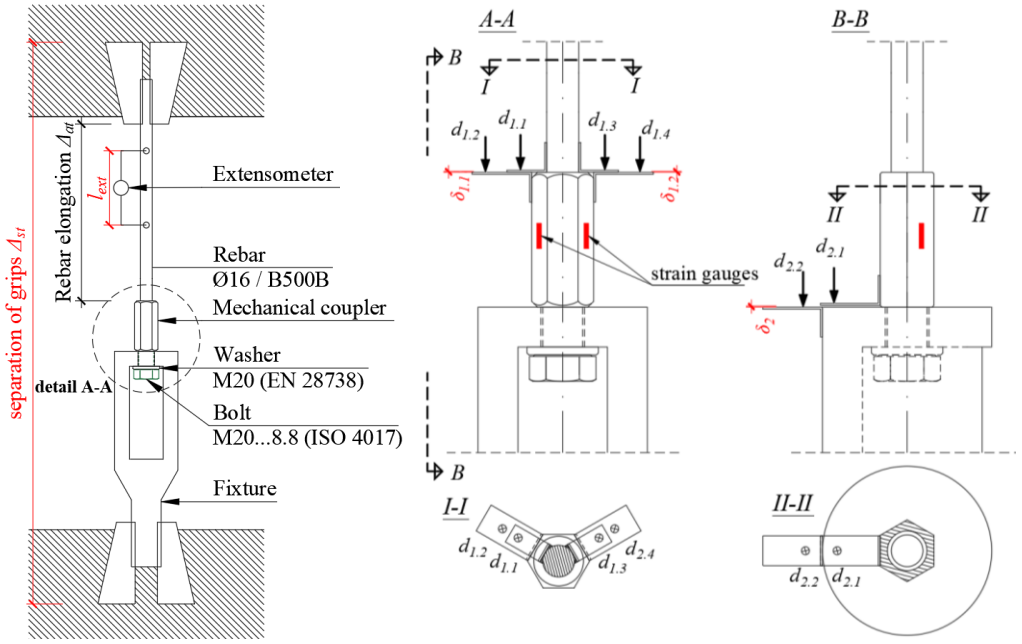

Figure 2.Tensile test layout of threaded splice connection between bolt and rebar – the physical quantities of interest are displayed in red

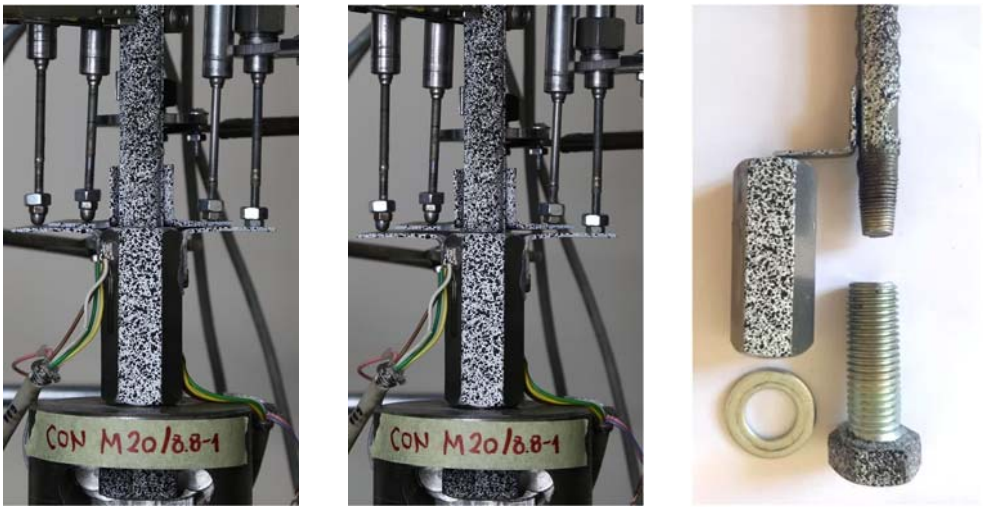

(a) Before loading (b) During loading (part U-R on Figure 4) (c) After the test

Figure 3. Connector appearance before, during and after the tensile test

After that, the difference between Δ_{st} and Δ_{at} is practically negligible until the connector's load-bearing capacity is reached. Test results showed that the behaviour of the connector as a whole corresponds to that of the control rebar (Figure 4(d)). Reaching the ultimate load of the connector coincides with the onset of stripping of the taper thread on the rebar inside the mechanical coupler. The result was the rebar anchor slipping out from the mechanical coupler and the increased measured values δ_1 on the U-R part, as shown in Figure 4(c). In this area, there is no additional increase of rebar anchor strain, which is illustrated by the line U-R' in Figures 4(a) and 4(d).

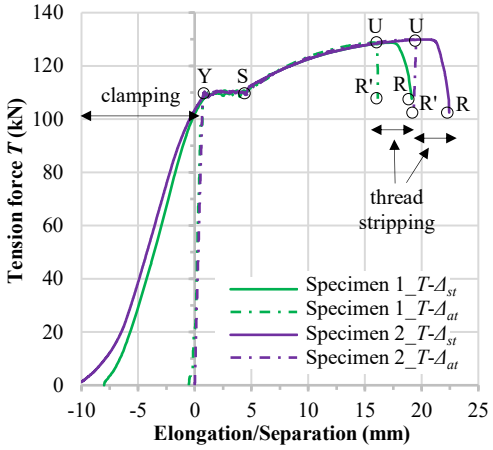

(a) Force-rebar elongation and force-stroke diagrams

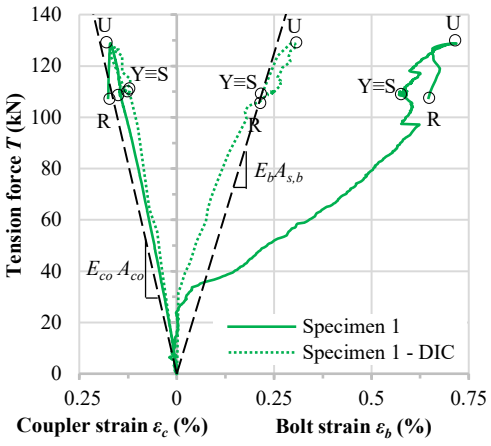

(b) Force-bolt strain and force-coupler strain diagrams

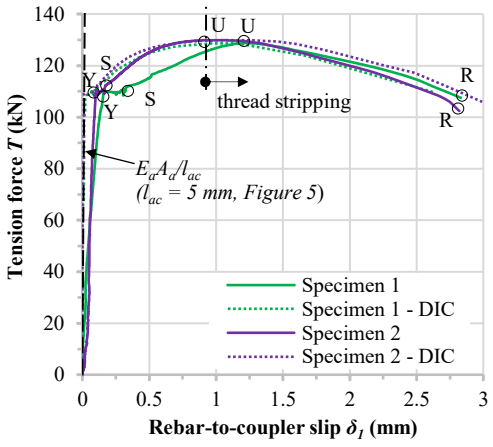

(c) Force-slip diagram for rebar-to-coupler connection

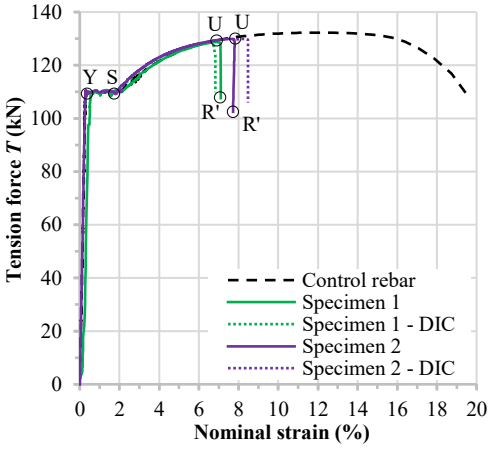

(d) Force-strain diagram for rebar

Figure 4. Tensile test results of the connector with a mechanical coupler

Measurement results of δ_1 and δ_2 in the elastic region deviated to a certain extent from the theoretically calculated values of the corresponding stiffnesses, as can be seen in Figures 4(b) and 4(c). These deviations are especially emphasised in the case of slip δ_2, i.e., bolt strain along the grip length ε_b. This can be attributed to the distance of the displacement transducers from the corresponding connections of the connector components, which can be seen in Figure 2(b). As shown in Figures 4(b) and 4(c), the results of DIC measurements matched much better with the theoretical values since the measurements were made at the surface of the connector.

3 Numerical analysis

3.1 Geometry of numerical model and boundary conditions

Numerical analysis of the threaded splice connector was performed in Abaqus finite element analysis (FEA) software [10] using the three-dimensional (3D) model shown in Figure 5. During the model's development, some geometry simplifications were made as opposed to the real geometry of the connector parts. These simplifications are based on the conclusions from the experimental analysis. Due to the elastic behaviour of the bolt during the test, the bolt thread was not explicitly modelled. A constant circular cross-section equal to the nominal stress area in the threaded part was adopted. In addition, the bolt-coupler connection was modelled as rigid, using the „Tie“ constraint. The contact between the bolt, washer, and fixture is modelled as „Hard contact“ in the normal direction and „Penalty friction“ in the tangential direction with a friction coefficient of 0.14, according to [11]. The rebar anchor and mechanical coupler threads were also excluded because of the complex taper thread geometry on the ribbed rebars (see Fig. 3(c)). The connection between the rebar and mechanical coupler was modelled by an idealised conical contact surface, as shown in Figure 5. The contact length of 25 mm was assigned, which is less than the total length of the rebar inside the coupler. The reason for this was the absence of a complete thread on the upper part of the rebar anchor. The rebar-coupler connection was modelled in two ways: as a rigid connection („Tie“ constraint) and by „Cohesive contact“ formulation, according to [10].

3.1.1 Modelling of rebar-to-coupler contact

For modelling rebar-to-coupler contact, the cohesive contact formulation was used. According to [10], cohesive contact between two surfaces was defined by the relation between the nominal traction stress t as a function of the separation (slip) of the surfaces δ, as shown in Figure 5. The behaviour of this connection includes four characteristic parts: *0-i* – elastic part, *i* – damage initiation, *i-f* – damage development and *f* – connection failure. The uncoupled stress-separation relationship defines the elastic behaviour of the contact:

$$t = \begin{Bmatrix} t_n \\ t_s \\ t_t \end{Bmatrix} = \begin{bmatrix} K_n & 0 & 0 \\ 0 & K_s & 0 \\ 0 & 0 & K_t \end{bmatrix} \begin{Bmatrix} \delta_n \\ \delta_s \\ \delta_t \end{Bmatrix} \tag{1}$$

whereby:

t_n, t_s, t_t normal, tangential and longitudinal nominal traction stress,
δ_n, δ_s, δ_t normal, tangential and longitudinal separation,
K_n, K_s, K_t normal, tangential and longitudinal stiffness.

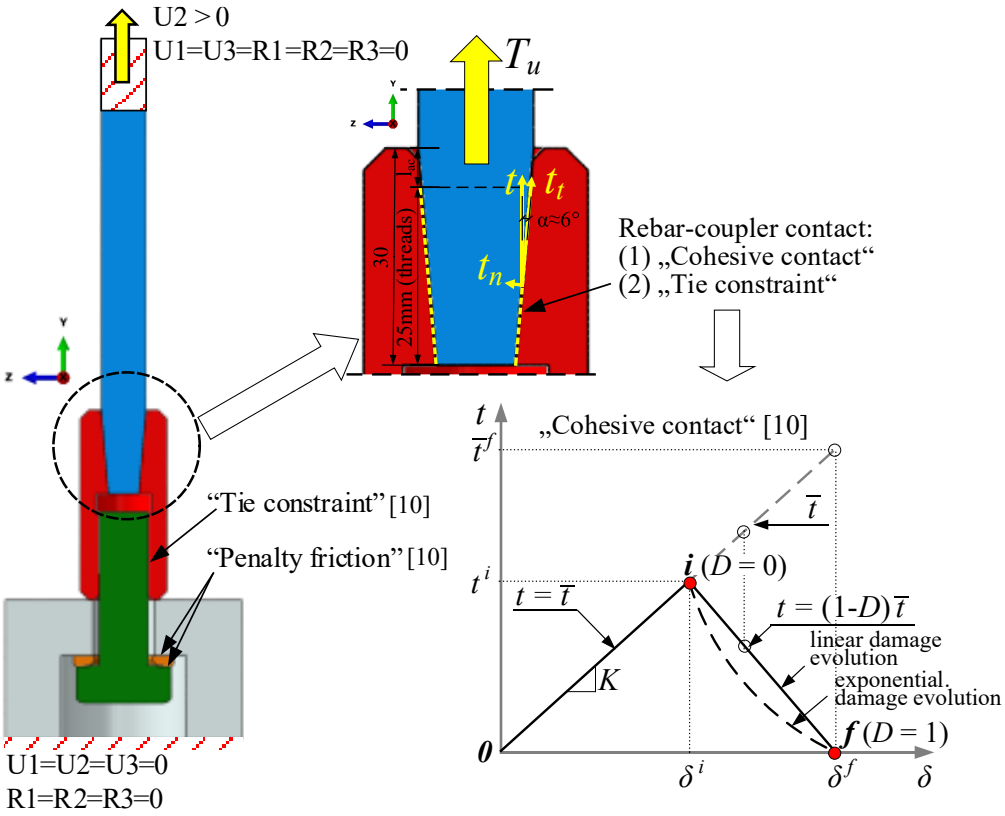

Figure 5. Numerical model geometry and boundary conditions of the connector with a mechanical coupler

Degradation and failure of the contact between two surfaces are defined by the damage initiation criterion, the damage evolution function (law), and the maximum separation. Damage initiation criteria can be defined by the corresponding maximum stress (t^i) or maximum separation (δ^i) from Equation (1). In general, the damage development function can have an arbitrary form. As an example, linear and exponential damage evolution functions are shown in Figure 5. Regardless of shape, the damage evolution function depends on the scalar quantity named damage parameter D, which represents the main input parameter during the definition of degradation and failure of contact in Abaqus software [10]. The damage parameter has a value of $D = 0$ at the maximum stress and a value of $D = 1$ at the maximum separation of the connection. As can be concluded from equation (1), all three components have different behaviours in the elastic region. However, after fulfilling the damage initiation criteria for any of the components (directions) of the connection, damage occurs in all three directions in line with the same damage evolution law.

In this study, the properties of the cohesive contact between the rebar and coupler were defined based on the experimentally determined force-slip relation (T-δ_1), as shown in Figure 4(c). Considering the small inclination of the conical thread generatrix (see Figure 5), the main parameters for defining the behaviour of the contact are the longitudinal stress $t_t$and the longitudinal separation δ_t. The value of $K_s = K_n = K_t = 10000$ MPa/mm was determined iteratively and adopted for connection elastic stiffness to match the test result obtained by DIC method. The initiation criteria was defined by maximum longitudinal stress $t_t^I = 128$ MPa. The value of this stress is approximately equal to the value obtained by dividing the connector load capacity T_u by the contact area and by the projection on the generatrix, as shown in Figure 5. The linear damage evolution with the maximum longitudinal traction $\delta_t^f = 2.0$ mm was considered and adopted based on the test results (part U-R). For the other two directions, the same connection properties were used. Figure 6 shows the adopted cohesive contact characteristics.

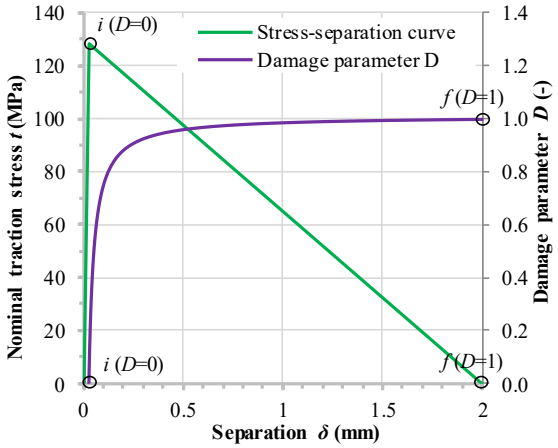

Figure 6. Cohesive contact for modelling rebar-to-coupler connection

3.2 Material models

The Poisson's ratio of 0.3 and a density of 7850 kg/m^3 were set for all steel materials. The material model of the bolt, coupler, and rebar anchor was adopted following the properties shown in Table 1. For the bolt, mechanical coupler, fixture, and washer the modulus of elasticity E_0 = 210 GPa was adopted. Taking into consideration negligible permanent deformation of couplers and bolts during loading, a bilinear elastoplastic stress-strain relation was adopted, while completely elastic behaviour was adopted for the fixture and washer. For reinforcement, the modulus of elasticity E_0 = 200 GPa was adopted. The behaviour of the rebar anchor was modelled based on the stress-strain curve of the control rebar without taking into account the descending branch. Figure 7 shows the adopted stress-strain relationships for the bolt, mechanical coupler, and rebar anchor.

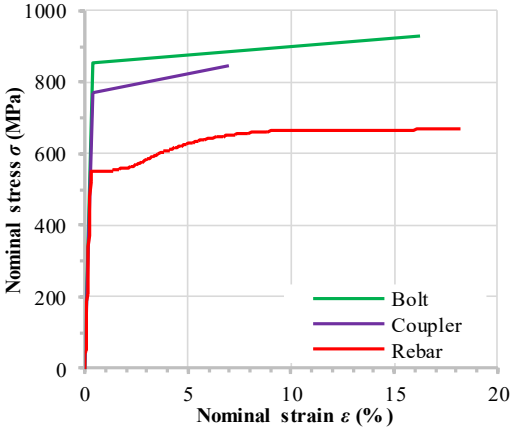

Figure 7. Stress-strain curves for bolt, mechanical coupler and rebar anchor

3.3 Finite element mesh and analysis procedure

Tetrahedral finite elements (C3D4) were adopted for all connector components. The bolt, washer, mechanical coupler, and rebar anchor were modelled with 1.5 mm finite elements, while the bolt grip was modelled with 3 mm finite elements. A sensitivity analysis of FEA model's global behaviour was performed by using the 1 mm, 1.5 mm, 2 mm and 3 mm finite elements representing the connector.

For nonlinear quasi-static anaysis, the Abaqus/Explicit solver was used [10]. The displacement U2 was applied at the top of the specimen (Figure 5) at a time interval of 100 s.The mass scaling method with a desired time increment of 0.002s was used to increase calculation speed.

3.4 Result of FE analysis

Nonlinear FEA results of the threaded splice connector subjected to tension are shown in Figure 8. Considering the failure mode identified during the connector tensile test, a comparison was made between the rebar force-slip and force-strain curves. Modelling the rebar-coupler contact with a rigid connection („Tie" constraint) describes relatively well the connector behaviour until the yield point (Y) of the rebar anchor, as shown in Figures 8(a) and 8(b). After the rebar yield point, there are clear differences between the experimental and FEA results. In the latter, the connector failure was caused by rebar tensile failure (see Figure 8(b), part U→R). As can be seen from the figures, a good match between the test results and FEA results of the model with cohesive contact was achieved in the rebar-to-coupler slip branch up to 0.7 mm (up to the maximum load). At larger values of slip δ_1, contact damage occurs in accordance with the adopted linear damage evolution (part U-R), which is characterised by a faster drop in tensile force compared to

the experimentally obtained results. Although a better model behaviour on the descending branch of the force-slip curve can be obtained by defining a more accurate damage evolutionlaw (trilinear, parabolic, etc.), the presented model well describes the global behaviour of the connection. In the case of the FEA model with cohesive contact, rebar pull-out failure mode occurred due to contact failure. Also, as can be seen from the graphs, the behaviour of the connection had low sensitivity to changes in the size of finite elements.

Figures 8(c) and 8(d) show a comparison of von Mises stress distribution in the connection of a mechanical coupler and a rebar anchor at various levels of tension load, based on FEA models with „Tie“ constraint and a „Cohesive contact“ model, respectively. The tensile force levels corresponding to the yielding point of the rebar anchor and the load capacity of the connector were analysed. It can be concluded that with a rigid connection, the tensile force is dominantly transmitted in the upper part of the mechanical coupler, regardless of the load level. On the other hand, by modelling the connection with cohesive contact, rebar-coupler force transmission is more uniform up to the rebar yield point. After that, the thread damage occurs in the higher part of the rebar, and the force transmission zone moves towards the lower part, i.e., the free end of the rebar. This fact is supported by the distribution of von Mises stress at the maximum tensile force, presented in Figure 8(d). Similar to the experimental analysis, the failure of the connector was caused by the loss of contact between the coupler and the lower part (end) of the rebar.

4 Conclusions

In this paper, the tensile behaviour of a demountable connector consisting of a bolt, mechanical coupler, and rebar anchor was analysed. Tensile test results showed that the behaviour of the rebar, as the weakest component, has a significant influence on the behaviour of such a connector as a whole. The tensile load capacity of the tested samples was approximately equal to that of the control rebar (T_u = 129.3 kN). Both samples failed due to rebar pull-out from the mechanical coupler, as a result of the conical thread stripping on the rebar anchor.

The connector's nonlinear three-dimensional finite element model was created and calibrated using the results of experimental tests. Particular focus was placed on modelling the connection between the mechanical coupler and rebar anchor. It was shown that the complex behaviour of this connection, up to the connector load capacity, can be adequately represented by applying the cohesive contact model in Abaqus software [10], whose application and parameters are described in detail.

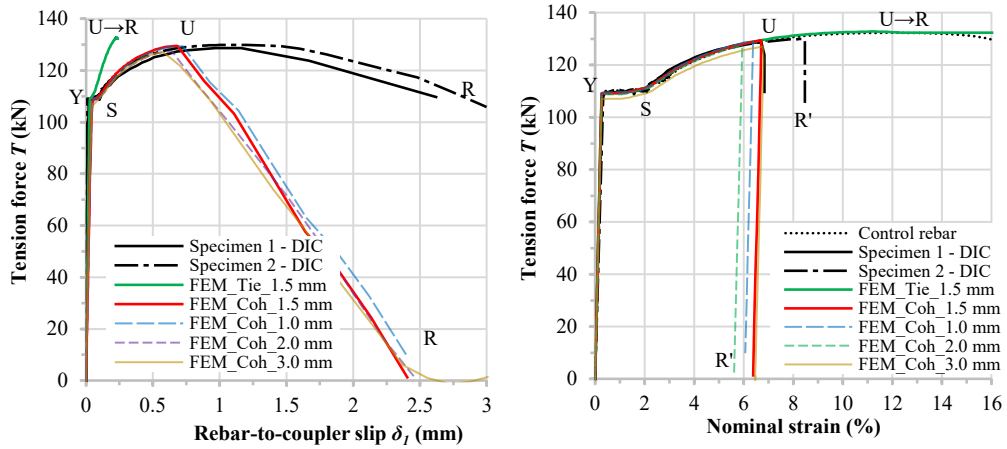

(a) Force-slip diagram

(b) Rebar force-strain diagram

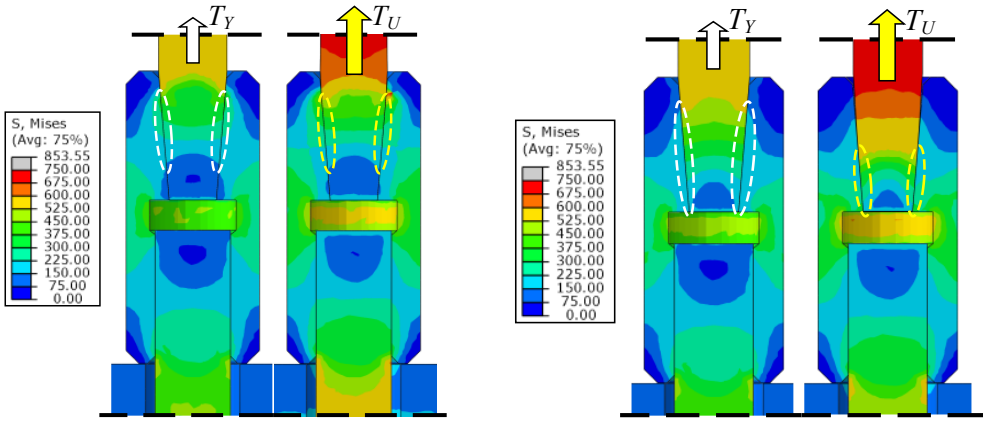

(c) Connector stresses in case coupler-rebar connection modelled with „Tie“ constraint

(d) Connector stresses in case of coupler-rebar connection modelled with „Cohesive contact“

Figure 8. Tensile FEA results of the connector with mechanical coupler

Acknowledgement

The authors would like to express their gratitude to the Ministry of Education, Science, and Technological Development of the Republic of Serbia for the financial support within Project 200092.

References

[1] EN1992-4, Eurocode 2: Design of concrete structures - Design of fastenings for use in concrete. Brussels: CEN, 2018.

[2] L. Pallarés and J. F. Hajjar, "Headed steel stud anchors in composite structures, Part II: Tension and interaction," J. Constr. Steel Res., vol. 66, no. 2, pp. 213–228, 2010, doi: 10.1016/j.jcsr.2009.08.008

[3] L. Pallarés and J. F. Hajjar, "Headed steel stud anchors in composite structures, Part I: Shear," J. Constr. Steel Res., vol. 66, no. 2, pp. 198–212, 2010, doi: 10.1016/j.jcsr.2009.08.009

[4] F. Yang, Y. Liu, Z. Jiang, and H. Xin, "Shear performance of a novel demountable steel-concrete bolted connector under static push-out tests," Eng. Struct., vol. 160, no. December 2017, pp. 133–146, 2018, doi: 10.1016/j.engstruct.2018.01.005

[5] Kozma, C. Odenbreit, M. V. Braun, M. Veljkovic, and M. P. Nijgh, "Push-out tests on demountable shear connectors of steel-concrete composite structures," Structures, vol. 21, no. Asccs, pp. 45–54, 2019, doi: 10.1016/j.istruc.2019.05.011

[6] B. Milosavljević, I. Milićević, M. Pavlović, and M. Spremić, "Static behaviour of bolted shear connectors with mechanical coupler embedded in concrete," Steel Compos. Struct., vol. 29, no. 2, pp. 257–272, 2018, doi: 10.12989/scs.2018.29.2.257.

[7] I. Milićević, B. Milosavljević, M. Pavlović, and M. Spremić, "Bolted connectors with mechanical coupler embedded in concrete: Shear resistance under static load," Steel Compos. Struct., vol. 36, no. 3, pp. 321–337, 2020, doi: 10.12989/scs.2020.36.3.321.

[8] EN1993-1-8: Eurocode 3: Design of steel structures. Part 1-8: Design of joints. Brussels, Belgium: European Committee for Standardization (CEN); 2005

[9] Blaber, J., Adair, B., Antoniou, A., 2015. Ncorr: Open-Source 2D Digital ImageCorrelationMatlab Software. Exp. Mech. 55, 1105–1122.

[10] ABAQUS User Manual. Version 6.12. Providence, RI, USA: DS SIMULIA Corp; 2012.

[11] ECCS Publication No38 - European Recommendations for Bolted Connections in structural steelwork. Brussels, Belgium: ECCS; 1985

Građevinski materijali i konstrukcije
Building Materials and Structures
journal homepage: www.dimk.rs

https://doi.org/10.5937/GRMK2300003M UDK: 624.04:005.521

Review paper

Risk management in civil engineering

Snežana Mašović [*1)], Nenad Pecić[1)], Saša Stošić[1)], Rade Hajdin[1,2)], Nikola Tanasić[3)]

[1)] *University of Belgrade, Faculty of Civil Engineering, Bulevar kralja Aleksandra 73, 11000 Belgrade, Serbia*
[2)] *Infrastructure Management Consultants, Zürich, Switzerland*
[3)] *Infrastructure Management Consultants GmbH Mannheim, Germany*

Article history
Received: 11 January 2023
Received in revised form: 10 April 2023
Accepted: 24 April 2023
Available online: 22 May 2023

Keywords
risk management,
reliability,
design,
construction,
maintenance,
assessment

ABSTRACT

Risk is involved in the whole lifecycle of a structure: design, construction, utilization, and demolition. There is a close connection between reliability and risk. Contemporary building codes introduce consideration of reliability in structural design. Here, the concept of risk takes into account the level of consequences of a failure. Structural engineers, who are used to deterministic calculation procedures, are often unfamiliar with the uncertainties associated with risk analysis. An overview of the basic principles of risk management in civil engineering is presented in this paper.

1 The concept of risk

Risk can be seen as a concept invented by humans to help them understand and deal with the dangers and uncertainties of life [1]. In general, the concept of risk is considered in ISO 31000:2009 [2, 3], where risk is defined as “the effect of uncertainty on objectives”. ICE/ISO 31010 [4] summarizes a number of techniques that can be used to improve the understanding of risk and how uncertainty is taken into account. The document also provides references to other documents where particular techniques are described in more detail.

Risk analysis supports decision making in various activities. In 2010, the European Commission published a Working Document - "Guidelines for Risk Assessment and Mapping for Disaster Management", which sets a general framework for disaster prevention and proposes measures to minimize the impact of disasters. The guidelines take into account existing EU legislation and Eurocodes. The document contains research results in the field of risk assessment and risk mapping of major natural and man-made disasters, based on existing good practice in Member States at the time. In 2019, a report [5] was published, based on the aforementioned guidelines, with the aim of providing scientific support to EU Member States in the preparation of a National Risk Assessment. The document provides tools and methods for risk assessments related to specific hazards and assets: drought, earthquake, flood, terrorist attacks, biological disasters, critical infrastructure, chemical accidents, nuclear accidents and Natech accidents (Natural Hazards Triggering Technology Accidents).

Structural engineers predominantly use deterministic calculation procedures and feel uncomfortable with the fact that risk analysis in practice can mean different things depending on the professionals doing the analysis and the client's requirements [6]. In this regard, the book [7], intended for both engineers and students, provides clear definitions and instructions for conducting risk analysis and is a useful text for structural.

Risk R is often estimated by the expected value E(L) of the consequences L (i.e., losses):

$$R = E(L) = \sum_i p(L_i) \cdot C(L_i) \quad (1)$$

Here L_i represents a particular loss i related to something valuable to humans, $p(L_i)$ is the probability of L_i, and $C(L_i)$ is the measure of that loss (commonly expressed in monetary units). The event of loss is a random variable (for example, the number of affected people), and it is conditional on the event designated as the failure. The failure is “non-conformance to some defined performance criterion”, [8]. There may be a number of failure modes F_j corresponding to the established performance criteria.

The probability $p(L_i)$ is obtained by conditioning on the failure modes:

$$p(L_i) = \sum_j p(F_j) \cdot p(L_i | F_j) \quad (2)$$

where $p(F_j)$ is the probability of a failure mode F_j, and $p(L_i | F_j)$ is the related conditional probability.

* Corresponding author:
E-mail address: smasovic@grf.bg.ac.rs

Each failure mode is a result of an event H_k - hazard (a single initiating event). Introducing conditional probabilities $p(F_j|H_k)$, expression (1) is extended to:

$$R = E(L) = \sum_k p(H_k) \cdot \sum_j p(F_j|H_k) \cdot \sum_i p(L_i|F_j) \cdot C(L_i) \tag{3}$$

where $p(H_k)$ is the probability of hazard H_k occurrence.

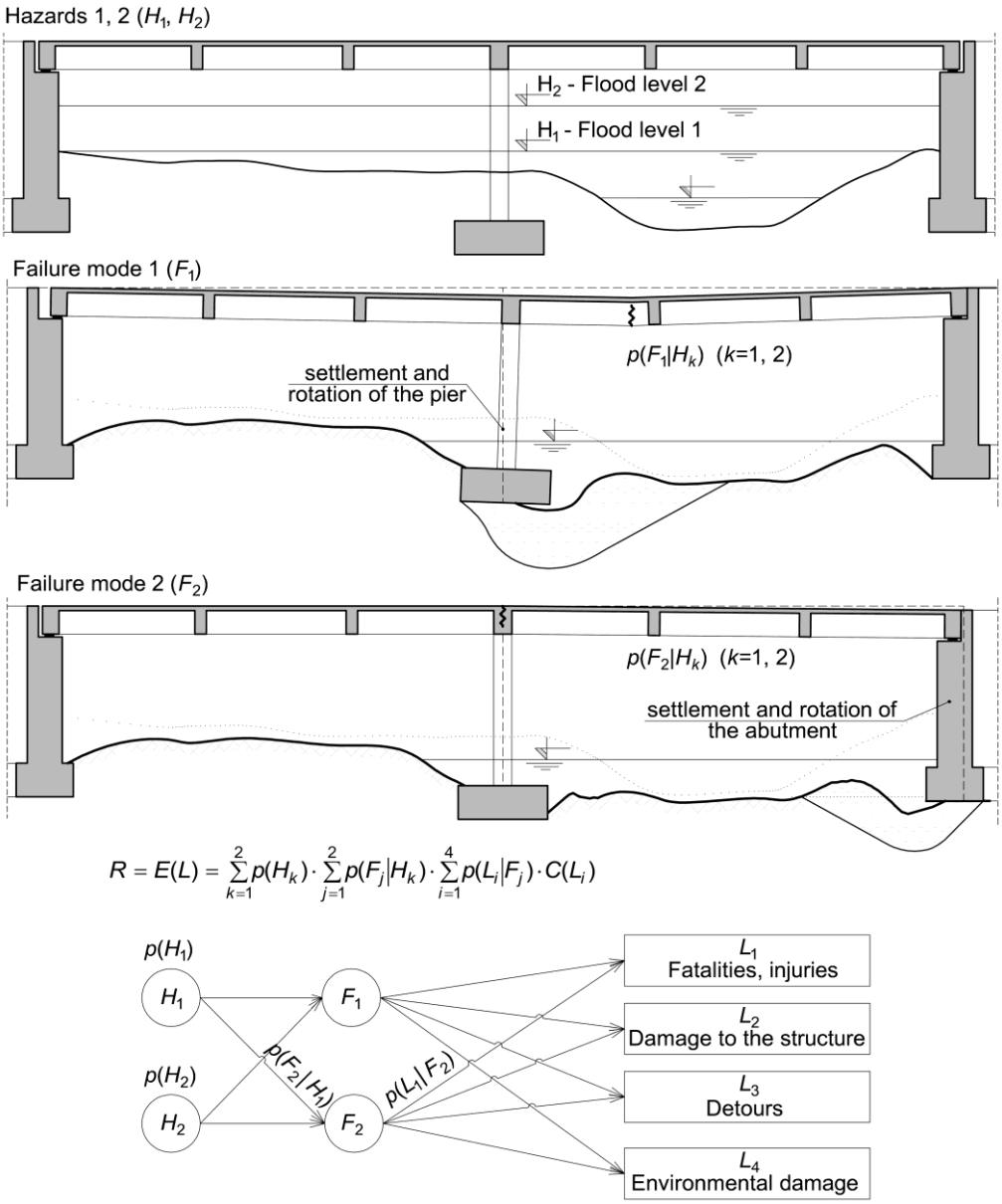

Figure 1. Example of the risk assessment

An example of the risk assessment is illustrated in Figure 1 [9]. A bridge structure is exposed to two hazardous situations that may cause two failure modes (related to local scour at substructures), leading to four types of losses.

Civil engineers are constantly facing risk in their practice (in conceptual design, construction, and maintenance), which is due to diverse uncertainties related to loads, design models, material properties, construction procedures, and environmental impacts. Risk cannot be avoided, given the uncertainties of future events, but it can be reduced by risk mitigation measures. Rational measures require adequate risk assessment. Risk assessment provides a basis for rational decision-making in the context of uncertain and/or incomplete information [10].

2 Framework for risk management

ISO 31000 [2, 3] provides general framework for risk management. General principles on risk assessment of systems involving structures are presented in ISO 13824 [11]. The risk management process, applicable in civil engineering, is presented in Figure 2.

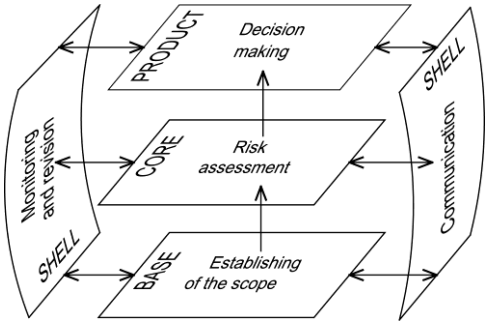

Figure 2. Framework for risk management (adapted from [2])

2.1 Establishment of the scope

The essential step within risk management is the establishment of the scope (context). It comprises:

- definition of the system (Figure 3);
- setting the time frame;
- setting the level of risk analysis (qualitative, semi-quantitative, quantitative, or probabilistic);
- identification of stakeholders (e.g., investor, designer, contractor, owner, user, society, etc.) and their responsibilities;
- setting the acceptance criteria.

The system to be considered is the totality of all objects, events, consequences, assumptions, agreements, and constraints that are necessary for a particular risk assessment. Within the system, the definitions of all elements are provided, and all relevant facts are collated (information, data, expertise, models, etc. [12].

The definition of the system is essential to establishing exposure, vulnerability and robustness. Due to the properties of the considered system, specific sequences of events (scenarios) arise that cause direct and indirect consequences [13].

Direct consequences refer to the losses related to individual elements of the system and their vulnerability. Vulnerability ($V_{j,k}$) can be interpreted as the conditional probability of a specific failure mode as a result of a specific hazard:

$$V_{j,k} = p(F_j|H_k) \tag{4}$$

Several systems with different levels of complexity are presented in Figure 3 with examples of direct/indirect losses. Narrowing the boundaries of the system (1 → 4) enables detailed modelling of system properties. The use of detailed models followed by expansion of the system boundaries (4 → 1) results in a significant increase in the complexity. The complexity is also significantly affected by the selected time frame and the level of risk analysis (see section 2.2). Within risk management, "the level of complexity should be tailored to the decision at hand and the quality of data that supports the decision analysis" [14].

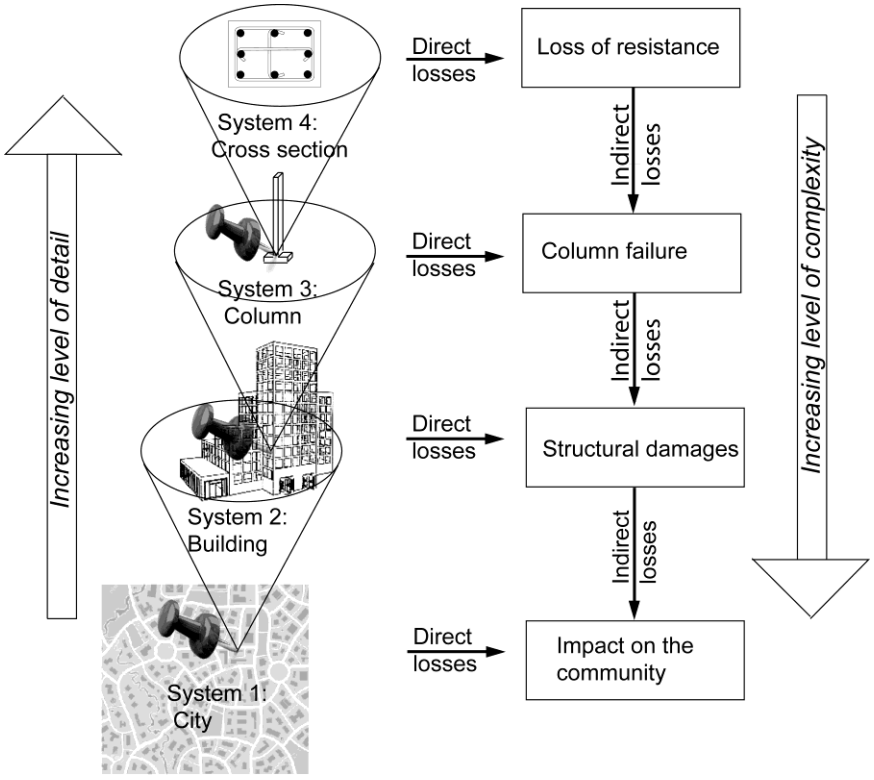

Figure 3. Systems with direct/indirect losses and the level of complexity

A system can exhibit various failure modes. They can be related as a series, while some of them may comprise the simultaneous (parallel) occurrence of certain failure events. An example of possible structural failure modes for a restrained beam is shown in Figure 4.

Indirect consequences refer to losses beyond the direct consequences and are usually associated with the loss of system functionalities. A structural system is said to be robust if the structure will not lose its functionality at a rate or extent that is not proportional to the cause of structural damage [13]. Robustness represents the ability to withstand the propagation of losses throughout the system, and is a function of system properties like redundancy, ductility and load redistribution, but it also depends on failure consequences [15].

Consequences are categorized in classes which relate to cost bearer (internal, e.g. owner, and external, e.g. users or society) and by tangibility (tangible, e.g. material loss, and intangible, e.g. fatalities). Categories are obtained combining classes of losses that are presented in Figure 5 (category "direct-external-intangible" is marked for example).

Risk acceptance criteria denote acceptable limits to the probabilities of certain consequences of an undesirable event and are expressed in terms of annual frequencies. Risk acceptance criteria are generally determined by the specialists but may reflect the risk attitude of a particular decision-maker. "These criteria are normally determined by the authorities to reflect the level of risk considered to be acceptable by people and society", [16]. Rational risk acceptance criteria should be based on socioeconomic considerations.

The problem with making decisions about risk acceptance is that the group that pays for safety measures frequently differs from the group that benefits from them. Those who do not directly pay for the safety measures want very strict rules, and vice versa [17]..

Societal risk criteria are presented as curves on *F-N* plots (usually log-log scales) that show the relationship between the annual frequency *F* of accidents with *N* and more fatalities. These curves have been developed for various industrial fields. The mathematical expression for an *F-N* criterion curve contains the risk aversion factor α, and may be expressed as:

$$F = k \cdot N^{-\alpha} \tag{5}$$

where *k* is the constant and the risk aversion factor $\alpha = 1 \div 2$, [14-16]. Value $\alpha = 1$ denotes a risk-neutral attitude. An example of F-N curve is shown in Figure 6.

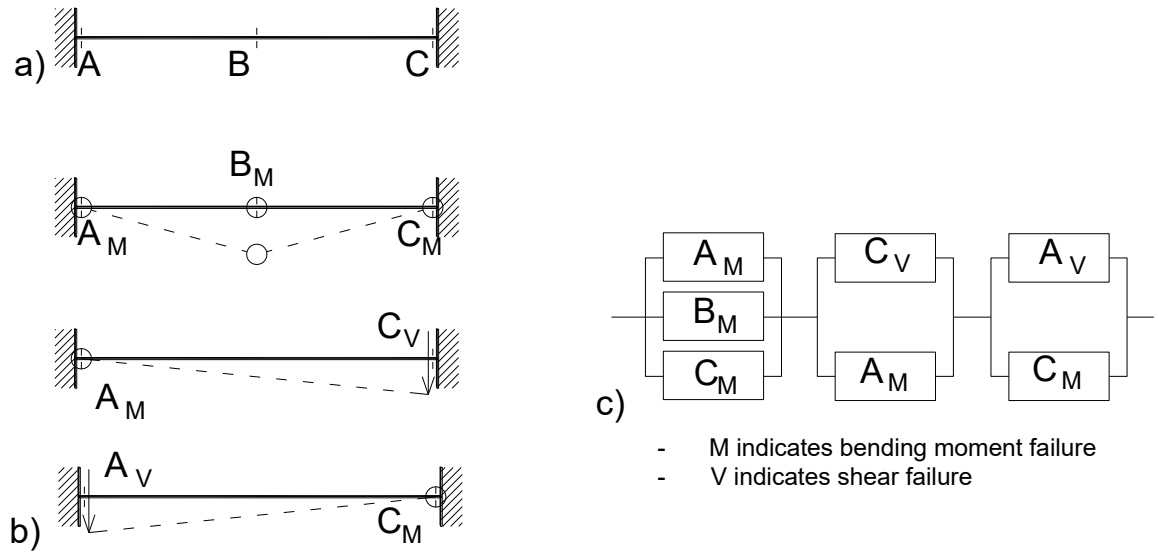

Figure 4. Illustration of some structural failure modes: a) structural system, b) corresponding failure modes and c) block diagram for systems reliability analysis

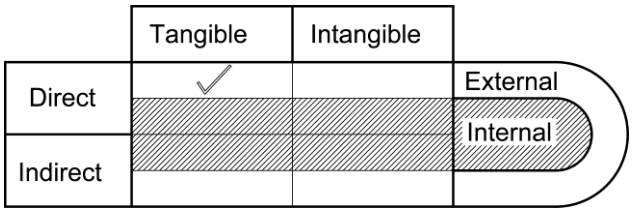

Figure 5. Categorization of losses

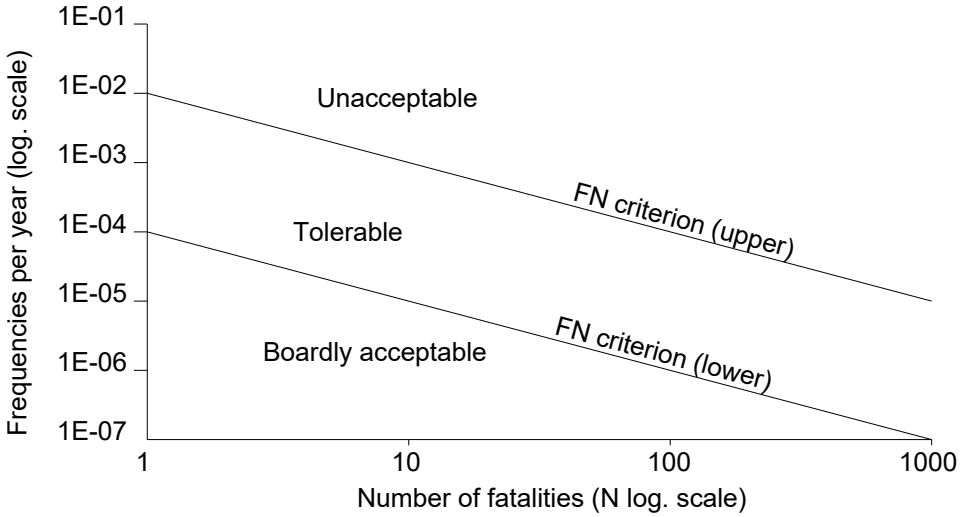

Figure 6. Example of F-N criterion lines (adapted from [7])

2.2 Risk assessment

Risk assessment involves three steps: identification, analysis, and evaluation of risks. Identification of relevant hazards and consequent losses is performed within the established context (Section 2.1). Risk analysis is carried out by an appropriate method in accordance with a defined level. A risk matrix is usually used for a qualitative or preliminary analysis. The modified risk matrix, involving pre-defined failure mode probabilities, is used for semi-quantitative analysis [21]. For quantitative and probabilistic risk analyses, the event tree, the fault tree, or the Bayesian network [4, 7, 8] are commonly applied. The last step of a risk assessment is evaluation, which is necessary for a decision about the risk treatment.

Identification of hazards (i.e., initiating events) and hazard scenarios, followed by identification of the type and extent of related consequences (losses), is an essential prerequisite for the risk analysis. Hazard scenarios establish the chain of events leading to specific losses.

The hazards may originate from various causes:

- natural (e.g., earthquake, flood, landslide);
- human activities (e.g., impact of vehicles, overload, fire);
- malicious attacks (e.g., bomb explosions, vandalism);
- human errors (e.g., design or construction errors, misuse);
- negligence (e.g., lack of inspection or maintenance).

Hazard identification procedures may vary from the simple use of a list of threats or extensive tables for a formal identification process to a detailed expert study as an interdisciplinary process. Selected hazards should be documented as a part of the risk assessment, and explanations should be provided for the omitted ones.

Design codes and recommendations address in detail only some of the abovementioned hazards (e.g., earthquake, fire, impact, etc.). Human errors and negligence are also acknowledged, but besides general requirements for quality control and supervision, the codes usually do not provide detailed instructions. Inaccuracy in design models and uncertainty in input data are partially covered by safety factors.

These factors are calibrated based on target values of the reliability index β which is the ratio of the expected value to the standard deviation of the performance function [10, 22-25].

Consequences (losses) may be related to various domains:

- human safety (e.g., fatalities, injuries, damage to important facilities);
- property (e.g., damage to structures, contents, and surroundings);
- economics (e.g., loss of income, cost of detours or delays);
- environmental (e.g., pollution, environmental damage);
- social (e.g., loss of reputation, increase in public fears).

The method of *risk analysis* is selected in accordance with a defined level: qualitative, semi-quantitative, quantitative, or probabilistic.

A qualitative risk assessment is the starting point for any risk analysis, providing a risk ranking and identification of credible event scenarios for further, detailed analysis. It is based on the comprehensive experience or studies of experts and does not involve mathematical calculations. Results are commonly expressed in a risk matrix Figure 7.

In Fig. 7, consequences are classified as “low”, “medium” and “high”, similarly to CC1, CC2 and CC3 in Annex B of EN1990 [21]. The time frame has to be specified within the selected context. For example, the occurrence of a scenario that is “occasional” in 50 years might be “remote” in a single year. The classification presented in Fig. 7 is the starting point for decision making. If the risk is “intolerable”, risk mitigation measures are mandatory, or the planned activity is to be cancelled. In the case that the risk is “broadly accepted”, no action is required. Between these regions, there is the wide zone referred to as ALARP (“As Low As Reasonably Practical”). The words “Reasonably practical” refer to the costs of risk mitigation measures. Only general risk mitigation measures (i.e., verified in common practice) can be suggested by the qualitative risk assessment.

In the simplest quantitative risk assessment, the occurrence rate of the initiating event, conditional probabilities, and the corresponding value of losses, are the point estimates. The effects of the uncertainties in inputs and their interdependency should be assessed in sensitivity analyses. A quantitative approach with point estimates can

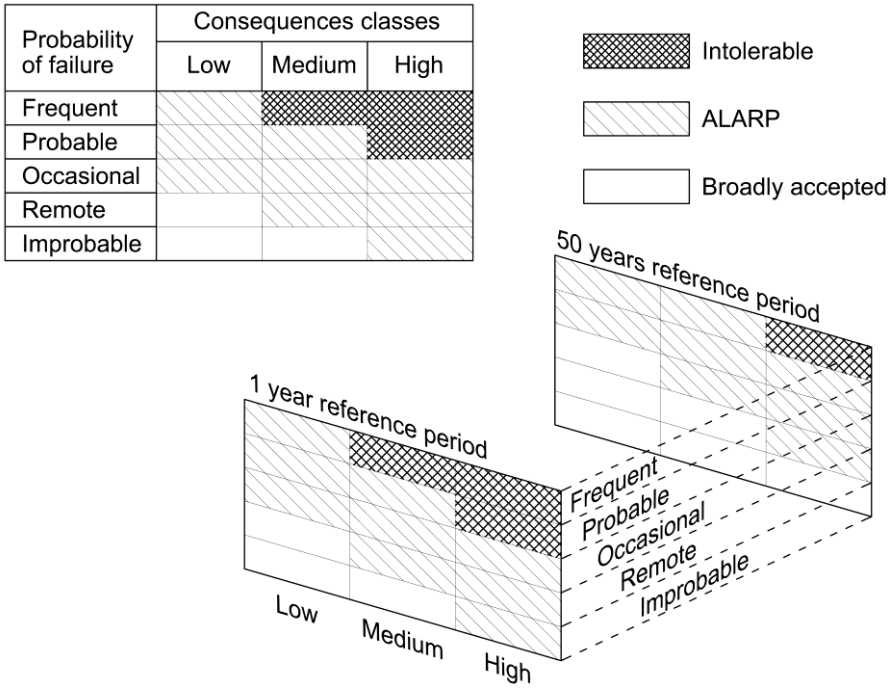

Figure 7. Example of risk matrix and impact of the reference period

be used in cases where uncertainties have no significant influence on decision-making. Probabilistic risk assessment is used when the sensitivity analyses indicate that uncertainties in the input estimates cannot be neglected. The events (including losses) are treated as random variables.

Available historical data can be used for the selection of probability distributions and the estimation of distribution parameters, but a high amount of reliable data is required. Reliability analyses of elements and systems are the next steps in the probabilistic risk assessment. The most complex risk assessment involves time-dependent reliability analysis of various limit states and time-dependent modelling of losses related to the spectrum of consequences.

Switching from qualitative to quantitative risk assessment is suitable only where it is reasonable and feasible. Reasonable means that the cost of doing a quantitative analysis is not high compared to the value of solving the problem. Feasible refers to the availability of computing tools, information, and data.

The simplest way of evaluating *risk* is qualitative: high, medium, or low risk (risk matrix, Fig. 7). A more comprehensive result of the risk analysis provides the spectrum of losses with estimated probabilities in the prescribed time frame.

2.3 Decision making

There are four basic options to deal with risk: acceptance, transfer, avoidance, and risk reduction (i.e. mitigation). If all of the prescribed performance goals (e.g., Dutch risk- driven concept named RAMSSHE€P comprises Reliability, Availability, Maintainability, Safety, Security, Health, Environment, Economics (€) and Politics [26-28]) are fulfilled, then the risk is accepted. Risk transfer is a measure that involves the contractual shifting of a particular loss from one stakeholder to another (e.g., insurance company). Avoidance is the act of staying away from a risky situation. Acceptance, transfer, and avoidance are already decisions.

The combination of decision theory and risk assessment enables consideration of alternatives to reduce risk. Basically, risk mitigation measures aim to reduce the probabilities of a scenario and/or the probabilities of losses. The spectrum of measures ranges from knowledge improvement to changes in system characteristics. Knowledge about statistical characteristics (i.e., adequate probability distribution and its parameters) of hazards and/or the state of the system is updated by research and/or inspections (i.e., risk mitigation through improvement of knowledge).

Risk mitigation through changes in the system´s characteristics may be achieved by:

- limiting the use of the structure (avoiding overload and reducing the probabilities of losses);
- strengthening the components of the structure (reducing vulnerability) and/or
- increasing the redundancy of the structural system (increasing robustness).

Every risk mitigation measure incurs costs. Optimization should be supported by data concerning efficiency of measures and related costs. Within the framework of optimization, losses can be expressed in monetary units. In this context, the monetisation of fatalities is a particularly delicate issue. There are several approaches: Societal Value of Statistical Life (SVSL), Societal Willingness to Pay (SWTP), Implied Cost of Averting a Fatality (ICAF), Societal Life Saving Cost (SLSC), compensation to be paid for death by accident…[29-32] . A systematic review is given in [33].

2.4 Communication, monitoring, and revision

Communication, monitoring, and revision are ever-present activities in risk management. Communication and discussion are continuous and iterative processes that are conducted to provide, share, or exchange information about risk between the decision-maker and other stakeholders. Communication procedures are of essential importance

when high probabilities of large social losses are anticipated, in order to prevent or reduce such consequences.

Monitoring and revision imply constant feedback of information from the considered system in order to evaluate the efficiency of the risk mitigation measures and propose modifications if necessary.

3 Structural reliability and risk mitigation measures

Contemporary design standards and codes follow the principle that the more severe the consequences, the lower the failure probabilities should be accepted. Risk-informed decisions are incorporated into the codes.

3.1 Structural design codes

Statistical analysis of load and material data resulted in the concept of partial safety factors. Safety factors for individual failure modes of structural components are calibrated using an appropriate failure probability related to the accepted risk. It is usually suggested that structures should be designed with sufficient robustness (e.g., by strengthening key elements, selecting ductile materials, or providing sufficient redundancy) [16]. The reliability of a robust structural system is expected to be at least equal to the reliability of system components.

The main tool proposed in Annex B of EN 1990, [21, 22] for the management of structural reliability is modification of partial factors depending upon:

- consequences of a failure;
- design supervision differentiation;
- quality control and inspection during execution.

The purpose of reliability differentiation is the socio-economic optimization of the resources required for a construction project, taking into account all expected consequences of failure and the cost of construction [21].

3.2 Risk over the life cycle of the structure

The comprehensive decision process covers all aspects of the life cycle of structures:

- planning (conceptual design);
- design;
- construction;
- service (including inspection, maintenance, and repair or rehabilitation) and
- demolishing.

A decision-maker can apply risk mitigation measures that are inherent to a particular phase of the life cycle to reduce risk. However, the best effect is achieved when it is applied at the strategic level and during conceptual design. Different hazards, losses, or risk mitigation measures are specific for each phase of the life cycle [34].

3.2.1 Risk in design

“Good engineering practice involves looking beyond minimum prescriptive code requirements and considering the risk from low-probability, high-consequence events, regardless of whether the event is an ‘accidental’ or ‘normal’ load.” [35]

In the design phase, it is necessary to consider all subsequent phases in the life cycle of the structure.

These phases are implicitly considered in design codes through the chosen reference period for the design loads and general guidelines: ‘The structure will be adequately maintained’ and ‘The structure will be used in accordance with the design assumptions’, [21]. This implies that the designer should recommend a maintenance regime and emphasize the loads anticipated in the design to the owner. The owner or user should provide appropriate maintenance and prevent overloading or misuse of the structure.

A number of studies of failures in structural engineering have shown that most of the failures producing economic consequences originated in the planning phase, while the failures and errors leading to fatalities and injuries are connected to the construction phase [32].

Designers and practitioners should recognize safety hazards during the design phase. The review paper [36] refers to the various possibilities of considering the safety of workers during the construction or maintenance of civil engineering works in the context of registered accidents at work.

Planning in the early phases of a project is the best way to control risk in design and construction. That includes:

- preliminary investigations for conceptual design (reducing the uncertainties related to site conditions, environment, ground condition, etc.);
- expected utilization of the structure and anticipated loads;
- anticipated construction method;
- supervision requirements, and
- quality control requirements.

3.2.2 Risk during construction

Risk analysis is incorporated into well-established project management. Risk management is currently considered a mandatory and integral part of successful project management [37], which must be continuously implemented during the entire execution of the project [38].

Within the framework of project management, the project life cycle ends when the final structure is handed over to the owner.

The construction phase is a complex activity that is frequently the most critical phase in project management due to the uncertainties that might lead to additional design and planning activities during project implementation, with negative effects on costs or schedule. Besides, the construction could be adversely affected by environmental changes, natural disasters, and/or unforeseen geological conditions. It is estimated that a large percentage of projects (more than 70 %) fail to be realized on time, within budget or with the expected level of quality [39].

A review of the literature on construction project risk management reveals that force majeure risks and those related to workers are rarely studied, according to [38]. However, many cases of failure involving injuries and fatalities were recorded during construction: “It is estimated that there are around 60,000 construction fatalities occurred worldwide each year (ILO 2006)” [40] The construction sector employs about 6-10% of the workforce in industrialized countries, but 20-40% of fatal accidents at work occur in this sector. This trend is even worse in developing countries [41]. A recent review paper [42] provides a systematic overview and detailed analysis of the content of published studies related to risk identification in construction over the last three decades.

Temporary works, e.g., scaffolding or shoring for excavations, often receive less attention than permanent works. Loading on temporary structures may be inadequately foreseen. Furthermore, most structures are more susceptible to instability in the assembly stage than

when completed. A combined effort of designers, constructors, and adequate supervision, including quality control, is required to ensure that proper sequencing of construction works is achieved while material weakness, temporary structural instability, or overload are avoided [34]. These actions, together with compliance with health and safety regulations during construction work, are risk mitigation measures in the construction phase.

3.2.3 Risk during the service life of a structure

The service phase is the longest period in the life cycle of a structure.

During the service life, structural failures usually do not occur due to ageing processes since they may be, to some extent, controlled by maintenance. More frequently, the effects of extreme events (earthquake, flood, extreme wind, landslide, etc.), or their combination, result in partial failures or total collapse. Intensities and occurrence probabilities of extreme events, as well as direct and indirect losses, mostly depend on the geographic location of the structure. There is abundant literature on risk estimation due to extreme events, usually involving case studies [14, 18, 35, 43-55]. Multiple hazards were considered in [56-60].

If the functionality of the structure is reduced, indirect losses may in some cases, exceed the value of the structure. To avoid such losses, inspections, maintenance, and, if necessary, repair or rehabilitation actions are to be carried out during the service life of the structure. Inspections can be of various types: visual, direct measurement, non-destructive testing, response measurements, or even a proof load. They are aimed at detecting damages, but the probability of damage detection depends on the type of inspection and the type of damage or hazard that has caused the damage. For example, damages caused by accidental actions or natural disasters will probably be detected, while corrosion of an inaccessible component may not be. The methodology for maintenance management and risk management is the same.

Risk-based inspection planning implies frequent and/or more reliable inspection of elements that have a high failure probability and elements whose failure may cause excessive consequences. It is assumed that if damage is indicated, particular action will be taken either to reduce the consequences (e.g., evacuate the structure or restrict its use) or to reduce the probability of failure (e.g., make repairs). “Reliability analysis, coupled with economic decision theory, has been recognized as one of the most effective tools for assessment of optimal inspection and maintenance plans” [61]. An overview of several procedures for the reliability assessment of existing structures may be found in [62].

The prioritization of inspection and maintenance activities can be based on quantitative risk analysis. Probabilistic, time-dependent analysis can be used to evaluate and optimize inspection and maintenance costs. Different maintenance strategies may be compared using a risk-based approach. Uncertainties about cost-related items may also be included. Bayesian updating offers a suitable framework for incorporating available information into risk-based maintenance. The mentioned approaches are elaborated in the literature [61, 63-78]..

4 Conclusion

The risk approach can be used to rank the structural design alternatives, construction alternatives, maintenance procedures, or prioritize interventions on existing structures. An advanced risk approach can be used for decision-making regarding design and construction activities, for inspection, monitoring, or maintenance to prevent structural deterioration, and for disaster preparedness.

Risk management is not one man's job and requires a multidisciplinary approach. It is also a continuous process and usually requires a vast amount of reliable cost and performance-related data, statistical operations, and, in some cases, considerable computer simulation capabilities.

Contemporary design codes enable management of risk in the design phase. The best effect on cost savings is achieved when risk management is applied during conceptional design. During construction supervision, adequate quality control and compliance with health and safety regulations are common risk mitigation measures. After construction and for existing structures, risk-based maintenance should be applied. Guidelines for risk-based assessment of existing structures are envisaged in the further development of the Eurocodes.

Acknowledgments

This investigation is supported by the Serbian Ministry of Education, Science, and Technological Development through the 36002 project (Computational Intelligence Techniques in Transportation and Communication Planning and Traffic Control) and COST action TU1406 - Quality specifications for roadway bridges, standardization at a European level (BridgeSpec).

References

[1] Slovic, P., Weber, E.U.: Perception of Risk Posed by Extreme Events, *Center for Decision Sciences (CDS) Working Paper*, Columbia University, 2002. Available at SSRN: https://ssrn.com/abstract=2293086

[2] ISO 31000:2009, Risk management - Principles and guidelines.

[3] ISO 31000:2018, Risk management – Guidelines Second edition 2018-02

[4] ISO/IEC 31010, Risk management — Risk assessment techniques Edition2, 2019-06

[5] Poljansek, K., Casajus Valles, A., Marin Ferrer, M. et al: Recommendations for National Risk Assessment for Disaster Risk Management in EU, *JRC Science for Policy report by the Joint Research Centre (JRC), the European Commission’s science and knowledge service, Publications Office of the European Union, 2019 European Union, 2019, pp.* 166

[6] Faber, M.H., Stewart, M.G.: Risk assessment for civil engineering facilities: critical overview and discussion, *Reliability Engineering and System Safety*, 80, (2003),pp. 173–184. https://doi.org/10.1016/S0951-8320(03)00027-9 .

[7] Marvin Rausand, *Stein Haugen* : Risk Assessment Theory, Methods, and Applications *Second Edition 2020 John Wiley & Sons, Inc, pp. 770.* DOI:10.1002/9781119377351

[8] Smith, D.J.: *Reliability, Maintainability and Risk: Practical Methods for Engineers*, *eight edition*, Elsevier, Oxford, 2011.

[9] Mašović, S.,Tanasić, N.: Rizik u građevinskom konstrukterstvu, *Simpozijum Društva građevinskih konstruktera Srbije*, Zlatibor, pp. 1105-1114, 2016.

[10] Faber, M.H.: Risk and Safety in Civil, Surveying and Environmental Engineering, *Lecture notes*, http://webarchiv.ethz.ch/ibk/emeritus/fa/education/ws_safety/Safety07/Script_secure.pdf 14.12.2017.

[11] ISO 13824:2009, Bases for design of structures - General principles on risk assessment of systems involving structures.

[12] Faber, M.H. et al.: *Methodik zur vergleichenden Risikobeurteilung*, Schweizerischer Verband der Strassen- und Verkehrsfachleute, Zürich, 2009.

[13] Joint Committee on Structural Safety: *Risk Assessment in Engineering*, edited by M.H. Faber, 2008, http://www.jcss.byg.dtu.dk/Publications/Risk_Assessment_in_Engineering, 14.12.2017.

[14] Ellingwood, B.R, Wen, Y.K.: Risk–benefit-based design decisions for low-probability/high consequence earthquake events in Mid-America, *Progress in Structural Engineering and Materials*, 7, (2005) pp. 56-70. DOI: 10.1002/pse.191.

[15] COST Action TU0601Technical Report: *Structural Robustness Design for Practising Engineers*, Editor T.D.G. Canisius, http://www.cost-tu0601.ethz.ch/Documents/Final%20Report/COST_TU0601_structural_robustness_design_practising_engineers_Version1_2-11Sept11.pdf, 14.12.2017.

[16] EN 1991-1-7: 2006, *Eurocode 1: Actions on structures - Part 1-7: General actions - Accidental actions.*

[17] CIB Report: *Risk Assessment and Risk Communication in Civil Engineering,* Pub. 259, Edited by A. Vrouwenvelder et al., CIB General Secretariat, 2001, https://www.irbnet.de/daten/iconda/CIB14314.pdf, 05.04.2023.

[18] Stewart, M.G., Mueller, J.: Homeland security: a case study in risk aversion for public decision-making, *International Journal of Risk Assessment and Management*, 15, (2011), 5/6, pp. 367-386.

[19] Cha, E.J., Ellingwood, B.R.: Seismic risk mitigation of building structures: The role of risk aversion, *Structural Safety* 40 (2013), pp.11–19, https://doi.org/10.1016/j.strusafe. 2012.06.004.

[20] Schubert, M., Faber, M.H., Baker, J.W.: Decision making subject to aversion of low frequency high consequence events, *Special Workshop on Risk Acceptance and Risk Communication*, 2007, Stanford University, https://web.stanford.edu/~bakerjw/Publications/Faber%20et%20al%20(2007)%20risk%20aversion%20workshop%20paper.pdf, 05.04.2023.

[21] Gulvanessian, H., Calgaro, J.-A., Holicky, M.: *Designers' Guide To Eurocode: Basis Of Structural Design*: *EN 1990*, second edition, ICE Publishing, London, 2012.

[22] EN 1990:2002+A1: *Eurocode – Basis of structural design*, 2002.

[23] fib. (2016). *Bulletin 80, partial factor methods for existing concrete structures* Recommendation. Lausanne, Switzerland: Fédération internationale du béton (129 pages, ISBN 978-2-88394-120-5, December 2016)

[24] Faber, M.H. & Sørensen, J.D. 2003. *"Reliability Based Code Calibration - The JCSS Approach"*. Proceedings of the 9th International Conference on Applications of statistics and Probability. San Francisco. 9th International Conference on Applications of Statistics and Probability in Civil Engineering 06/07/2003 → 09/07/2003 pp. 927-935

[25] *Probabilistic model code part I – part III* https://www.jcss-lc.org/jcss-probabilistic-model-code/, 05.04.2023.

[26] Linneberg, P., Masovic, S., Hajdin, R.: Quality Control Plans for Girder and Frame Bridges, *39th IABSE Symposium – Engineering the Future*, Vancouver, 2017, pp. 2659-2666, ISBN 978-3-85748-153-6.

[27] COST Action TU1406 WG1 Technical Report: *Performance Indicators for Roadway Bridges*, edited by A. Strauss, A. Mandić Ivanković, ISBN: 978-3-900932-41-1, http://www.tu1406.eu/wp-content/uploads/2016/10/COST_TU1406_WG1_TECH_REPORT.pdf, 19.12.2017

[28] COST Action TU1406 WG2 Technical Report: *Performance Goals for Roadway Bridges*, edited by I. Stipanovic et al., ISBN: 978-3-900932-41-1, http://www.tu1406.eu/wp-content/uploads/2017/11/tu1406_wg2.pdf, 19.12.2017

[29] Pandey, M.D., Nathwani, J.S.: Life quality index for the estimation of societal willingness-to-pay for safety, *Structural Safety*, 26 (2004), pp.181–199, doi.org/10.1016/j.strusafe.2003.05.001.

[30] Rackwitz, R.: The Philosophy Behind the Life Quality Index and Empirical Verification, Basic Documents on Risk Assessment in Engineering, 2008, https://www.jcss-lc.org/publications/raie/06_risk_backgrounddoc_lqi_philosophy.pdf, 05.04.2023.

[31] Fischer, K., Virguez, E., Sánchez-Silva, M., Faber, M.H.: On the assessment of marginal life saving costs for risk acceptance criteria, *Structural Safety*, 44 (2013), pp. 37–46, doi.org/10.1016/j.strusafe.2013.05.001

[32] Faber, M.H.: Risk and Safety in Engineering, Lecture Notes, 2009, http://webarchiv.ethz.ch/ibk/emeritus/fa/education/ws_safety/Non_printable_script.pdf 19.12.2017.

[33] Panagiotis K. Marhavilas, Dimitrios E. Koulouriotis: Risk-Acceptance Criteria in Occupational Health and Safety Risk-Assessment - The State-of-the-Art through a Systematic Literature Review. *Safety* 2021, 7, 77. https://doi.org/10.3390/safety7040077

[34] Technical Report: *Risk in structural engineering*, Task group chairman C. Bolton, The Institution of Structural Engineers, London, 2013

[35] Ellingwood, B.R.: Mitigating Risk from Abnormal Loads and Progressive Collapse, *Journal of Performance of Constructed Facilities*, 20 (2006), 4, pp. 315-323, doi.org/10.1061/(ASCE)0887-3828(2006)20:4(315).

[36] Dylan Hardison, Matthew Hallowell: Construction hazard prevention through design: Review of perspectives, evidence, and future objective research agenda *Safety Science 120 (2019),* pp.*517–526*, https://doi.org/10.1016/j.ssci.2019.08.001

[37] Burcar Dunović, I., Radujković, M., Vukomanović, M.: Risk register developement and implementation for construction projects, *Građevinar - Journal of Croatian Society of Civil Engineers*, 65, (2013), 1, pp. 23-35, http://casopis-gradjevinar.hr/assets/Uploads/JCE_65_2013_1_4_722_EN.pdf, 05.04.2023.

[38] COST Action TU1003 Working group final report: *Risk in the Front End of Megaprojects*, Editor I. Burcar Dunović, University of Leeds, 2015, ISBN 978-0-9576805-8-6,

http://www.mega-project.eu/assets/exp/docs/Risk_in_the_Front_End_of_Megaprojects.pdf, 19.12.2017.
[39] Westland, J.: *Project Management Life Cycle: A complete step-by-step methodology for initiating planning, executing and closing a project successfully*, Kogan Page, London, 2006.
[40] Wang, J., Zou, P.X.W., Li, P.P.: Critical factors and paths influencing construction workers' safety risk tolerances, *Accident Analysis and Prevention*, 93 (2016), pp. 267-279, https://dx.doi.org/10.1016/j.aap.20 15.11.027.
[41] Raheem, A.A., Hinze. J.W.: Disparity between construction safety standards: A global analysis, *Safety Science*, 70 (2014), pp. 276–287, https://doi.org/10.1016/j.ssci.2014.06.012.
[42] Nasir *B. Siraj,; and Aminah Robinson Fayek,*: Risk Identification and Common Risks in Construction: Literature Review and Content Analysis, *Journal of Construction Engineering and Management, 2019, 145(9): 03119004-1-13,* DOI: 10.1061/(ASCE)CO.1943-7862.0001685
[43] Faber, M.H., Kübler, O., Fontana, M., Knobloch, M.: *Failure Consequences and Reliability Acceptance Criteria for Exceptional Building Structures - A Study taking Basis in the Failure of the World Trade Center Twin Towers*, Institute of Structural Engineering Swiss Federal Institute of Technology, Zürich, 2004, https://doi.org/10.3929/ethz-a-004807495.
[44] Tesfamariam, S., Sánchez-Silva, M., Rajeev, P.: Effect of Topology Irregularities and Construction Quality on Life-Cycle Cost of Reinforced Concrete Buildings, *Journal of Earthquake Engineering*, 17 (2013), 4, pp. 590-610, https://doi.org/10.1080/13632469.2012.762955.
[45] Kunnath, S.K., 2007. Application of the PEER PBEE Methodology to the I-880 Viaduct, PEER Report 2006/10, 2006., http://peer.berkeley.edu/publications/peer_reports/reports_2006/web_PEER610_KUNNATH.pdf, 05.04.2023.
[46] Bayraktarli, Y.Y., Ulfkjaer, J.-P., Yazgan, U., Faber M.H.: On the Application of Bayesian Probabilistic Networks for Earthquake Risk Management, Safety and reliability of engineering systems and structures, Proceedings *of the Ninth International Conference on Structural Safety and Reliability ICOSSAR '05*, Rome, pp. 3505-3512, 2005.
[47] Grêt-Regamey, A., Straub, D.: Spatially explicit avalanche risk assessment linking Bayesian networks to a GIS, *Natural Hazards and Earth System Sciences*, 6 (2006), pp. 911–926, https://doi.org/10.5194/nhess-6-911-2006.
[48] Padgett, J. at al.: Bridge Damage and Repair Costs from Hurricane Katrina, *Journal of Bridge Engineering*, 13 (2008), 1, pp. 6-14, https://doi.org/10.1061/(ASCE)1084-0702(2008)13:1(6).
[49] Sykora, M., Holicky, M., Maňas, P.: General approach to risk optimization of road bridges exposed to accidental situations, *WIT Transactions on The Built Environment*, 134 (2013), pp. 11-20, https://www.witpress.com/Secure/elibrary/papers/SAFE13/SAFE13002FU1.pdf, 05.04.2023.
[50] Tanasić, N., Ilić, V., Hajdin, R.: Vulnerability assessment of bridges exposed to scour, *Transportation Research Record: Journal of the Transportation Research Board*, 2360 (2013), pp. 36-44 https://doi.org/10.3141/2360-05
[51] anasic, N., Hajdin, R.: Management of bridges with shallow foundations exposed to local scour, *Structure and Infrastructure Engineering*, (2017, online), https://doi.org/10.1080/15732479.2017.1406960.
[52] Mohsin Abbas, Khalid Elbaz, Shui-Long Shen, Jun Chen: Earthquake effects on civil engineering structures and perspective mitigation solutions: a review, *Arabian Journal of Geosciences (2021) 14: 1350* https://doi.org/10.1007/s12517-021-07664-5
[53] Y. Zhang, W.G.Weng: A Bayesian Network Model for Seismic Risk Analysis, *Risk Analysis,* Volume41, Issue10 *October 2021 Pages 1809-1822* https://doi.org/10.1111/risa.13690
[54] Reza Fathi-Fazl,; Zoubir Lounis, Zhen Cai,: Multicriteria and Multilevel Framework for Seismic Risk Management of Existing Buildings in Canada, *Journal of Performance of Constructed Facilities 2020, 34(2): 04020004-1-9,.* https://doi.org/10.1061/(ASCE)CF.1943-5509.0001393
[55] Davit Shahnazaryan, · Gerard J. O'Reilly: Integrating expected loss and collapse risk in performance-based seismic design of structures, *Bulletin of Earthquake Engineering (2021) 19:pp, 987–1025,* https://doi.org/10.1007/s10518-020-01003-x
[56] Wen, Y. K.: Minimum lifecycle cost design under multiple hazards, *Reliability Engineering and System Safety*, 73 (2001), pp. 223–231. https://doi.org/10.1016/S0951-8320(01)00047-3
[57] Decò, A., Frangopol, D.M.: Risk assessment of highway bridges under multiple hazards, *Journal of Risk Research*, 14 (2011), 9, pp. 1057–1089, https://doi.org/10.1080/13669877.2011.571789.
[58] Kameshwar, S., Padgett, J. E.: Multi-hazard risk assessment of highway bridges subjected to earthquake and hurricane hazards, *Engineering Structures*, 78 (2014), pp. 154–166, https://doi.org/10.1016/j.engstruct.2014.05.016.
[59] Ilaria Venanzi, Oren Lavan, Laura Ierimonti & Stefano Fabrizi, Multi-hazard loss analysis of tall buildings under wind and seismic loads, *Structure and Infrastructure Engineering* Volume 14, 2018 - Issue 10 pp. 1295-1311, https://doi.org/10.1080/15732479.2018.1442482
[60] Mitsuyoshi Akiyama, Dan M. Frangopol & Hiroki Ishibashi: Toward life-cycle reliability-, risk- and resilience- based design and assessment of bridges and bridge networks under independent and interacting hazards: emphasis on earthquake,tsunami and corrosion, *Structure and Infrastructure Engineering* Volume 16, 2020 - Issue 1, pp. 26-50 *https://doi.org/10.1080/15732479.2019.1604770*
[61] Barone, G., Frangopol, D.M.: Hazard-Based Optimum Lifetime Inspection and Repair Planning for Deteriorating Structures, *Journal of Structural Engineering*, 139 (2013), 12, *https://doi.org/10.1061/(ASCE)ST.1943-541X.0000810*.
[62] Šavor, Z., Šavor Novak, M.: Procedures for reliability assessment of existing bridges, *Građevinar - Journal of Croatian Society of Civil Engineers*, 67 (2015), 6, pp. 557-572, https://doi.org/10.14256/JCE.1190.2014.
[63] Arunraj, N.S., Maiti, J.: Risk-based maintenance - Techniques and applications, *Journal of Hazardous*

Materials,142 (2007), pp. 653–661, DOI:10.1016/j.jhazmat.2006.06.069

[64] Stewart, M.G., Rosowsky, D.V., Val, D.V.: Reliability-based bridge assessment using risk-ranking decision analysis, *Structural Safety*, 23 (2001), 4, pp. 397–405, https://doi.org/10.1016/S0167-4730(02)00010-3.

[65] Kong, J.S., Frangopol, D.M.: Life-Cycle Reliability-Based Maintenance Cost Optimization of Deteriorating Structures with Emphasis on Bridges, *Journal of Structural Engineering*, 129 (2003), 6, pp. 818-828, https://doi.org/10.1061/(ASCE)0733-9445(2003)129:6(818).

[66] Adey, B., Hajdin, R., Bruhwiler, E.: Risk-based approach to the determination of optimal interventions for bridges affected by multiple hazards, *Engineering Structures*, 25 (2003) 7, pp. 903–912, https://doi.org/10.1016/S0141-0296(03)00024-5.

[67] Kallen, M.-J., van Noortwijk, J.M.: Optimal Inspection and Replacement Decisions for Multiple Failure Modes, Proceedings of *The 7th International Conference on Probabilistic Safety Assessment and Management (PSAM7-ESREL'04)*, Berlin, pp. 2435-2440, 2004. DOI: 10.1007/978-0-85729-410-4_391

[68] Straub, D., Faber, M.H.: Risk based inspection planning for structural systems, *Structural Safety*, 27 (2005), 4, pp. 335–355, https://doi.org/10.1016/j.strusafe.2005.04.001.

[69] Junca, M., Sanchez-Silva, M.: Optimal maintenance policy for permanently monitored infrastructure subjected to extreme events, *Probabilistic Engineering Mechanics*, 33 (2013), pp. 1–8, https://doi.org/10.1016/j.probengmech.2013.01.008.

[70] Mašović, S., Hajdin, R.: Optimalna politika održavanja drumskih mostova u Srbiji, *Put i saobraćaj*, LXI (2015), 2, pp. 12-22. https://grafar.grf.bg.ac.rs/handle/123456789/1035, 05.04.2023.

[71] Barone, G., Frangopol, D.M.: Reliability, risk and lifetime distributions as performance indicators for life-cycle maintenance of deteriorating structures, *Reliability Engineering and System Safety*, 123 (2014), pp. 21–37, https://doi.org/10.1016/j.ress.2013.09.013.

[72] Neves, L.A.C., Frangopol, D.M., Cruz, P.J.S.: Probabilistic Lifetime-Oriented Multi objective Optimization of Bridge Maintenance: Single Maintenance Type, *Journal of Structural Engineering*, 132, (2006), 6, pp. 991-1005, https://doi.org/10.1061/(ASCE)0733-9445(2006)132:6(991).

[73] Mašović, S., Hajdin, R.: Modelling of bridge elements deterioration for Serbian bridge inventory, *Structure and Infrastructure Engineering*, 10 (2014), 8, pp. 976-987, https://doi.org/10.1080/15732479.2013.774426.

[74] Qin, J., Faber, M.H.: Risk management of large RC structures within a spatial information system, *Computer- Aided Civil and Infrastructure Engineering*, 27 (2012), 6, pp. 385–405, https://doi.org/10.1111/j.1467-8667.2012.00757.x DOI: 10.1111/j.1467-8667.2012.00757.x.

[75] Mašović, S., Stošić, S., Hajdin, R.: Application of Semi Markov decision process in bridge management, *IABSE Conference Geneva 2015: Structural Engineering: Providing Solutions to Global Challenges*, Geneva, pp. 1017 – 1025, 2015, https://doi.org/10.2749/222137815818358204.

[76] Luque, J., Straub, D.: Reliability analysis and updating of deteriorating systems with dynamic Bayesian networks, *Structural Safety*, 62 (2016), pp. 34–46, https://doi.org/10.1016/j.strusafe.2016.03.004.

[77] Ilić, V., *Tanasić*, N., Hajdin,R.: Procena indirektnih troškova usled prekida putne veze zbog smanjenja funkcionalnih performansi mosta, *Put i saobraćaj*, LX (2014), 4, pp. 61-69. https://grafar.grf.bg.ac.rs/bitstream/handle/123456789/557/555.pdf?sequence=1&isAllowed=y, 05.04.2023.

[78] Dongjin Kim, Yongjun Lee, Min-jae Lee: Development of Risk-Based Bridge Maintenance Prioritization Methodology, KSCE Journal of Civil Engineering volume 22, pp. 3718–3725 (2018) https://doi.org/10.1007/s12205-018-2058-

Građevinski materijali i konstrukcije
Building Materials and Structures
journal homepage: www.dimk.rs

https://doi.org/10.5937/GRMK2300005M UDK: 620.193.2:666.972.1

Review paper

Carbonation of limestone powder concrete: state-of-the-art overview

Matija Marinković[*1)], Andrija Radović[2)], Vedran Carević[1)]

[1)] *University of Belgrade, Faculty of Civil Engineering, Bulevar kralja Aleksandra 73, 11000 Belgrade, Serbia*
[2)] *University of Priština in Kosovska Mitrovica, Faculty of Technical Sciences, Knjaza Miloša 7, 38220, Kosovska Mitrovica, Serbia*

Article history
Received: 07 April 2023
Received in revised form: 04 May 2023
Accepted: 15 May 2023
Available online: 09 June 2023

Keywords
concrete,
limestone powder,
carbonation resistance,
experimental results,
prediction models

ABSTRACT

Recently, research into finding long-term solutions to CO_2 mitigation in the cement and concrete sectors was initiated since commonly used supplementary cementitious materials are not globally available in sufficient amounts. One of the possible solutions to that problem is to develop concrete with a higher percentage of limestone in the powder phase. This work presents a critical overview of the state-of-the-art in the field of the carbonation resistance of limestone powder concrete. Experimental research performed so far has shown that if the simple replacement of cement with limestone powder is applied in the standard mix design, a maximum of 10-15% of cement (clinker) could be replaced to maintain similar carbonation resistance. It has also been proven that the dilution effect of weakly inert limestone powder can be compensated for with several measures in the mix design of concrete. By adjusting the cement, limestone, and water content and their particle size distribution, it is feasible to design concrete formulations with up to 50% limestone in the powder phase that are comparable to referent Portland cement concrete in terms of rheological and mechanical performance and carbonation resistance. This is an environmentally significant reduction in the clinker content, but it comes at the cost of a larger superplasticizer content. Prediction models for the carbonation resistance of the limestone powder concrete are poorly developed. Amongst them, the *fib* MC 2010 prediction model is considered relatively simple and robust; however, it has not yet been proven that the model is applicable to concrete with a higher content of limestone powder (>15-20% of the powder phase). The future research should be oriented towards further optimization of the concrete mix design and implementing this model on the middle- and high-content limestone concrete carbonation.

1 Introduction

Concrete is the most widely used construction material today. The global production of concrete is extremely high – roughly 33 billion tons of concrete are produced globally each year, or over 4.7 tons per person annually [1]. Humanity 'consumes' only water, more than concrete. No alternative to concrete as a major global construction material currently exists that can be applied at sufficient scale. Other materials can be substituted in some applications, but not for such broad applications as current concrete use.

The production of concrete is responsible for 8-9% of global anthropogenic greenhouse gas (GHG) emissions [2]. Cement, aggregates, water, mineral, and chemical admixtures are used to manufacture concrete. Cement (clinker) is, however, the primary driver of GHG emissions from concrete production: emissions from cement production make up 90-95% of total GHG emissions from concrete production [2, 3]. Decarbonization of the sector is therefore an important part of the CO_2 mitigation pathways towards global temperature rise targets.

The obvious solution to this problem is to reduce the amount of clinker in the cement that is used in concrete production and other applications. To do so, part of the clinker is usually replaced by so-called supplementary cementitious materials (SCMs) with low embodied CO_2. The most common SCMs are reactive by-products (wastes) from other industries or inert minerals, such as:

– fly ash (FA), the residue of the coal combustion in power plants, which has pozzolanic properties if finely ground – in the presence of water reacts with calcium hydroxide to form compounds possessing cementitious properties,

– ground granulated blast furnace slag (GGBS), a by-product of iron and steel production in blast furnaces, which has latent hydraulic activity – reacts with water to form calcium silicate hydrates (C-S-H),

– fillers, inert or weakly reactive fine particulate materials, the most commonly used is limestone powder.

The clinker content in concrete can also be reduced by particle packing mix design methods [4, 5, 6]. The idea is to minimize the void space to be filled with cement paste by selecting appropriate amounts of aggregate of different particle sizes in order to optimize packing. These methods enable better concrete properties with a smaller amount of cement paste.

* Corresponding author:
E-mail address: matija.marinkovic.1@gmail.com

Generally speaking, reactive SCMs like GGBS and FA have a lesser impact on the concrete´s mechanical and durability-related properties compared to inert or weakly reactive mineral admixtures such as limestone powder [7-10]. This is a consequence of their pozzolanic or latent hydraulic activity, which enables them to have not only the filler effect but also a binder role in the concrete mix. Therefore, a larger part of the clinker can be replaced with reactive SCMs without significantly jeopardizing the concrete´s performance at both the material and structural levels. In other words, they are more efficient in reducing the clinker content in the concrete mix if no other measure in concrete mix design or technology is undertaken.

However, due to the high global production of concrete, long-term solutions for CO_2 mitigation require that alternatives for clinker replacement be abundantly available everywhere in the world. According to an UN report [11], there is not much future in replacing clinker with common SCMs such as GGBS and FA because of their limited global availability. The estimate is that quality sources of GGBS and FA will be limited globally to only about 15–25% of cement production by 2050 and are unlikely to increase. This amount is hardly enough for the production of composite cement (CEM II), which contains up to 35% SCMs and is highly utilized in structural concrete. For that reason, alternative SCM systems that use calcined clays, ground limestone, or other minerals and their combinations should be developed, along with particle packing mix design methods. Since minerals are available everywhere in practically unlimited quantities and many of them can be used for such purposes, this could be a more permanent solution to CO_2 mitigation problems in all cement-based building and construction materials. To pursue that direction, it is necessary to explore and develop possible measures to overcome the negative dilution effect of inert mineral admixtures in concrete, i.e., to increase their efficiency as SCMs.

The objective of this work is to systemize and critically analyze the research performed in the field of concrete with middle-to-high limestone powder content, specifically research regarding the carbonation resistance of such concretes. Based on this critical review, directions for future research in the area are pointed out.

2 Current standards and applications

The use of limestone as a partial replacement for clinker was introduced into cement standards during the 1980s mostly for economic reasons. Currently, most national and international standards allow a certain amount of limestone in the limited range of cement compositions shown in Figure 1 [12]. For instance, the European EN 197-1 cement standard [13] allows up to 35% of limestone substitution in cements within CEM II type.These are CEM II/A (< 20% of limestone) and CEM II/B (between 20% and 35% limestone). Depending on the total organic carbon content (TOC) they are classified as L (TOC<0.5% of the weight of limestone) and LL type (TOC<0.2% of the weight of limestone) [14]. Limestone is introduced into cement by grinding it together with clinker, which normally results in cements with a lower strength class than the original pure clinker cement, despite the limited reaction of limestone powder. Therefore, CEM II/B cements typically belong to the lowest-grade strength class (32.5 MPa), while CEM II/A is mostly of the 42.5 MPa class.

The actual application of limestone in cement is significantly lower than the allowable limits in the standards. According to the statistics given in WBCSD [15], the average limestone amount in cement is globally below 7%, and that has been observed only in the last decade (Figure 2).

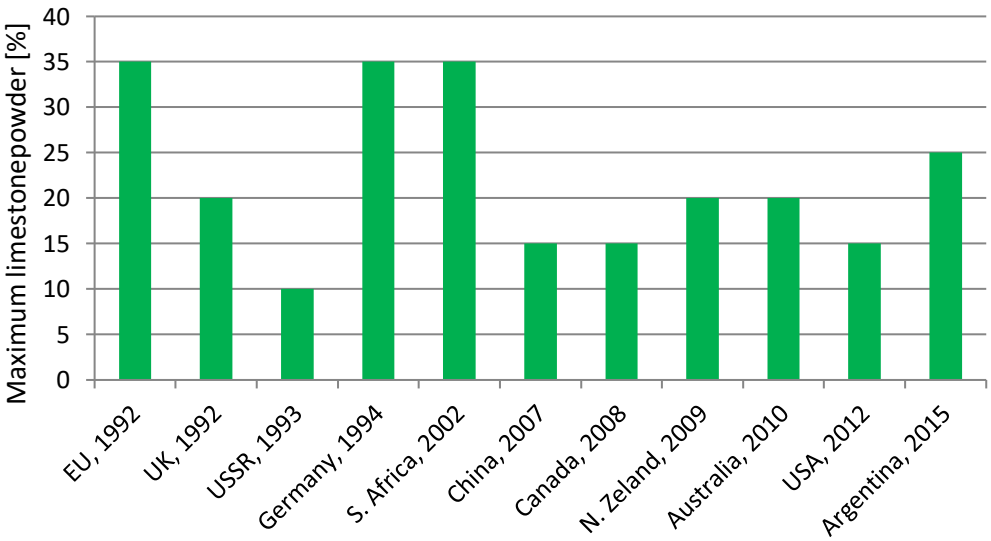

Figure 1. Maximum limestone powder (%) in cements according to standards (figures present the year of the first publication of the standard), adapted from [12]

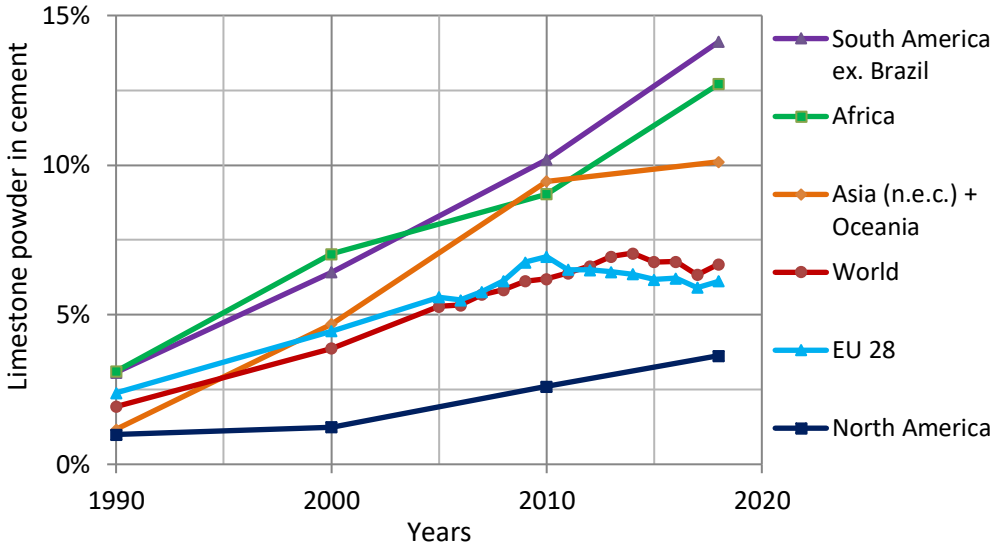

Figure 2. Limestone powder content in cement, data from WBCSD [15]

3 Effects of limestone powder in concrete

Binder is defined as a mineral that hydrates. In modern limestone cements, the clinker part represents the binder. Limestone powder, on the other hand, is almost inert – it partially reacts with aluminates, producing carbo-aluminate and carbo-silicate hydrates [12]. This reaction is weak and produces a low volume of hydrates, meaning that limestone powder physically dilutes the binder phase in concrete. This physical dilution of the binder is the major effect of substituting clinker with limestone powder. It results in a higher porosity of the binder paste and consequently leads to a lower quality of concrete regarding mechanical and durability-related properties that are directly connected to porosity, such as resistance to carbonation, for instance.

Secondly, higher early-age strength is obtained due to an increase in cement hydration rate as a combined effect of dilution and nucleation - the formation of nucleation sites in hydrating cement particles[16]. Besides, early production of carbo-aluminates contributes to the strength of concrete. However, this effect is lost with time – later strength is reduced due to the dilution effect.

Finally, improved particle packing is attainable due to the filler effect of the limestone powder. Finer limestone powder can fill the space between cement particles and improve the packing density of the paste and the interfacial transition zone (ITZ) between paste and aggregates [7]. The magnitude of all these effects depends on the content, fineness, and morphology of the limestone powder.

Currently, several strategies to compensate for the dilution effect of limestone powder are being investigated:

– optimizing the composition of the paste and lowering the water content,

– paste replacement instead of cement replacement,

– particle packing improving,both at the paste and the whole mix (including aggregates) level.

The first is the most efficient one; however, it causes problems with the rheological behavior of concrete. Reduced water content reduces porosity but also reduces the workability of concrete. The second one is based on the function that cement paste has in filling the voids between the aggregate particles. The paste volume must be sufficient to fill up the voids; otherwise, air will be entrapped in the concrete mix, causing reductions in strength and durability. So the idea is that by adding the limestone powder, the cement paste volume can be reduced by an amount equal to the limestone powder volume while maintaining the total “powder” paste volume needed to fill up the voids. This is equivalent to adding limestone powder to replace an equal volume of cement paste [17]. According to authors [17], such addition of limestone powder as a cement paste replacement without changing the mix proportions of the cement paste should have no adverse effect on the concrete properties but would reduce the cement clinker consumption. Finally, methods to improve particle packing are, in one way or another, included in the previously mentioned strategies.

Therefore, the major research challenge in low-cement (clinker) concrete mix design is how to combine these measures to obtain the maximum possible compensation for the dilution effect while providing the required rheological behaviour. Since the water content required for adequate workability is usually above the content needed for full clinker hydration, the key strategy to improve the performance of low-cement concrete is to keep this excess water to a minimum. In order to obtain this goal, the composition of the paste is optimized regarding the content of water and the content and particle size distribution of clinker and limestone (Figure 3).

According to John et al. [12], the proper combination of a ‘dilution powder’ that has approximately the same particle size as the clinker, an ‘ultra-fine powder’ that reduces the interparticle volume of pores, and a superplasticizer that prevents particle agglomeration to disrupt mobility allows for a significant reduction in water content compared to standard mixtures, as experimentally proved in [18]. An additional reduction in cement content can be realized based on the optimization of aggregate grading and in the increase in total volume of the “powder” paste [17]. However, increasing packing density usually requires more mixing energy. On the other hand, the type and amount of superplasticizer must be chosen carefully to prevent problems with its stability over time and possible retardation of hydration.

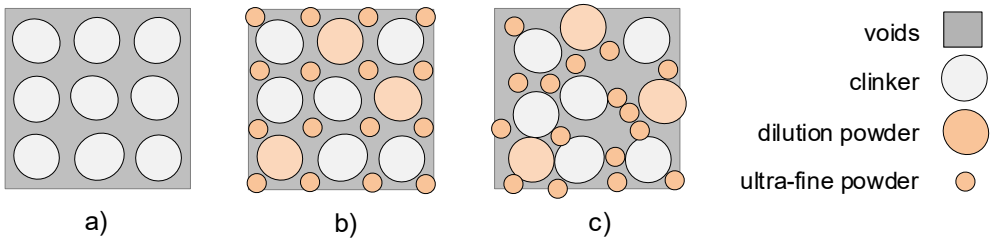

Figure 3. Optimization of the paste composition: a) clinker particles only – high porosity; b) clinker is partially replaced with 'dilution' and 'ultra-fine' powder and superplasticizer added – improved packing, lower porosity, and lower water demand, and c) without superplasticizer, agglomeration disrupts mobility and destroys packing – higher water demand, adapted from [12]

3.1 Effect on the carbonation resistance of concrete

The calcination process, necessary in cement production, is a chemical reaction in which limestone (which mainly contains calcium carbonate) is converted to calcium oxide and carbon dioxide at high temperatures ($CaCO_3$ + heat → $CaO + CO_2$). When exposed to air, concrete structures will over time reabsorb CO_2 from the atmosphere in a process called carbonation. It is a physicochemical reaction reversed to calcination in which atmospheric CO_2 diffuses into concrete to react with hydration products (calcium hydroxide and other calcium-rich hydrated oxides) and form calcium carbonate again ($Ca(OH)_2+CO_2 \rightarrow CaCO_3+H_2O$). For this reaction to happen, it is necessary that CO_2 be dissolved in the pore solution. Carbonation causes a reduction in the alkalinity of the pore solution in the concrete (mainly because of the loss of $Ca(OH)_2$). However, a highly alkaline environment inside concrete is essential to form the passive film of ferrous oxide at the surface of steel reinforcement, protecting steel from active corrosion. When the carbonation front propagates,the initially formed passive film is gradually destroyed, and consequently, the steel reinforcement becomes more vulnerable to electrochemical corrosion in the presence of moisture and oxygen. On the other hand, carbonation decreases to a certain extent the total porosity due to the precipitation of $CaCO_3$ on the pore walls, slowing down the carbonation process in that way. Carbonation is generally considered one of the major causes of the deterioration of reinforced concrete structures. Jones et al. [19] state that 2/3 of all structural concrete is exposed to environmental conditions that favour carbonation-induced corrosion.

Since carbonation is a diffusion-controlled process, the relationship between the carbonation depth d_c and time t can generally be described as $d_c = k \cdot \sqrt{t}$. The carbonation rate coefficient k is directly proportional to mass transport properties or the permeability (p), which is related to the porosity of the concrete (total volume of the pores, their size, and interconnectivity), and it is inversely proportional to the alkaline reserve (a):

$$k \propto \frac{p}{a} \quad (1)$$

The alkaline reserve depends on the chemical composition and the number of hydrated phases. Therefore, if cement is replaced with limestone while holding all other variables constant, the carbonation rate coefficient k increases (carbonation is accelerated) because a decreases. The content of $Ca(OH)_2$ is reduced by dilution of limestone, leading to less carbonatable constituents for carbonation reactions in a low-cement paste [8]. In addition, highly porous mixtures allow faster diffusion of CO_2. The dilution effect is somewhat compensated by the filler and nucleation effects of the limestone powder [20].

The chance to keep the carbonation rate similar to that of concrete with only clinker paste is to reduce the permeability of the limestone concrete and reduce the effective diffusivity of CO_2 in that way. The permeability generally depends on the porosity of hardened cement paste and the proportion and density of ITZ, i.e., mainly on the quality and volume of the paste and the separation between particles. By adjusting the cement, limestone, and water content and their particle size distribution, it should be feasible to design concrete formulations that comply not only with rheological and mechanical performance specifications but also with the required carbonation resistance.

4 Experimental results on the carbonation of limestone powder concrete

In a large part of previous research, the effect of limestone powder on the concrete properties was investigated on concrete made with limestone CEMII/A and CEMII/B cements and keeping the same water content as in the referent pure clinker (Portland cement) concrete [21, 22]. Therefore, concrete mixes contained up to 35% of fine limestone powder as a cement replacement. Since limestone is far easier to grind than clinker, joint grinding produces limestone particles that are finer than clinker particles. It was shown, however, in the previous research that this increased fineness of the limestone powder compared to the clinker fineness, is not efficient enough if the intention is to significantly reduce the clinker content in concrete.

Different authors used different terms for the ratio between the content of water and the content of cement (clinker) + limestone powder. In this text, the original terms (as reported in reviewed articles) are used, and an exact explanation of these terms is given in each case of the presented experimental campaigns.

Elgalhud et al. [21] in their recent study have analysed a large number of experimental results on carbonation of concrete made with Portland-limestone cement, where the vast majority of results were obtained on concretes made with limestone CEMII/A (6-20% of limestone) and CEMII/B cements (21-35% of limestone). Analyzed test results point to the conclusion that replacement of clinker with limestone powder significantly increased the carbonation depth of concrete; the higher the replacement percentage, the greater the increase. Under natural exposure conditions, for 35% limestone powder content, and at equal strength of limestone and pure clinker cement concrete, an average increase of 32% was calculated. In the same case, but at an equal water-to-cement ratio (where cement is understood as cement+limestone) an average increase of 75% was

reported. They have also reported from analyzed test results that accelerated carbonation gave rise to higher carbonation compared with natural exposure: up to 58% on an equal concrete strength basis and 85% on an equal water-to-cement ratio basis. The commonly used accelerated exposure in tests consisted of a CO_2 concentration of up to 5%, a duration of less than 30 days, a temperature of 20-30°C, and a humidity of 61–80%, whereas the natural indoor exposure had a duration of up to 5 years.

Lollini et al. [23] investigated the effect of the percentage of replacement of Portland cement CEM I 52.5 with ground limestone, the water-to-binder ratio, and the cement content on the carbonation resistance. They have experimentally tested concrete mixes with 0, 15, and 30% replacement of Portland cement with limestone powder, three different water-to-binder ratios (binder understood as cement+limestone) equal to 0.61, 0.46, and 0.42, and four different binder contents equal to 250, 300, 350, and 400 kg/m^3 of concrete. Besides, the effect of curing time (1, 7, and 28 days) was also investigated. The median particle size (i.e., the particle sizes corresponding to 50% cumulative passing) of about 7.5 μm for both Portland cement and limestone was reported, indicating similar fineness, although the Blaine surface area was 534 m^2/kg and 610 m^2/kg for Portland cement and limestone powder, respectively. The carbonation resistance was tested on 100 mm cube specimens under accelerated conditions: 20°C, 65% RH (relative humidity), and a 2% CO_2 for different times of exposure. The minimum and maximum carbonation depths were measured with the phenolphthalein test on 20 mm diameter cores taken perpendicularly to the mould surface, and the average value between the two was determined. The accelerated carbonation coefficient K_{ACC} was evaluated according to the relationship $d_c = K_{ACC} \cdot \sqrt{t}$ where d_c is the average carbonation depth at time t. At 30% replacement, K_{ACC}, i.e., carbonation depth was larger for limestone concrete for all water-to-binder ratios and all binder contents. At 15% replacement, K_{ACC} was similar, slightly higher, or slightly smaller compared to that of Portland cement concrete for all water-to-binder ratios and all binder contents. According to the authors, when concretes with equal compressive strength were compared, they showed the same carbonation resistance regardless of the amount of Portland cement replaced with limestone indicating that, provided the compressive strength requirement is guaranteed, the resistance to carbonation is also achieved. However, it is not clear what results support such a conclusion since for all 30% limestone concrete mixes, compressive strengths lower than the lowest strength of Portland cement concrete were reported.

Khokhar et al. [24] tested two concrete mixtures with 40% and 80% (by volume) replacement of Portland cement CEM I 52.5 with limestone powder, keeping the same water content (same powder paste volume). Blaine values were 405 m^2/kg and 397 m^2/kg for cement (0/100μm) and limestone powder (0/100μm), respectively. The specimens with dimensions of 7 x 7 x 28.4 cm were stored at 20°C and 50% RH for 18 months under natural conditions, and carbonation depths were assessed with the phenolphthalein test. Compared to reference Portland cement concrete, the concrete incorporating limestone powder showed significantly lower resistance to carbonation - four to eight times larger carbonation depth for 40% and 80% replacement, respectively. According to the authors, a possible reason is the dominating effect of the reduction in calcium hydroxide over pore refinement.

Collepardi et al. [25] tested concrete mixtures with 15% and 25% replacement of Portland cement CEM I 52.5 and four different water-to-cementitious ratios equal to 0.4, 0.5, 0.6, and 0.7 (cementitious in this work means cement+limestone). Blaine fineness of cement and limestone powder was 530 m^2/kg and 550 m^2/kg, respectively. Concretes (shape and size of samples not reported) were exposed to natural conditions at 20°C and 60% RH for a year after 28 days of curing at 20°C and 95% RH. Carbonation depths were assessed with the phenolphthalein test as usual. Similarly to Lollini et al. [23], they obtained that at the same water-to-cementitious ratio, the carbonation depth of limestone concrete was larger compared to Portland cement concrete, the increase being larger with a larger replacement level. At the same compressive strength in the range of 40 – 45 MPa (on a 150 mm cube at 28 days), differences were much smaller. For instance, measured carbonation depths after 360 days were 4.8mm, 4.7mm, and 6.9mm for Portland cement concrete, 15% limestone concrete, and 25% limestone concrete, respectively. However, similar compressive strengths were in fact obtained with similar water-to-cement ratios, and since the water content was practically kept constant, the cement content also had to be similar. In other words, no reduction in cement content was obtained with this methodology if similar carbonation resistance is expected.

Another example of tests performed on Portland cement and limestone concrete mixes with different replacement ratios but constant water content was found in Meddah et al. [26]. The percentage replacement was 15, 25, 35, and 45% (by weight), and for each percentage, the water-to-cement ratio (cement understood as cement+limestone) varied from 0.79 to 0.45. Blaine fineness of Portland cement CEM I 42.5and limestone powder was 381 m^2/kg and 638 m^2/kg, respectively. So, in this experiment, limestone powder was significantly finer than clinker. Accelerated carbonation testing was performed on cubes of 100 mm size that were wet cured during the first 28 days. The specimens were then pre-conditioned by drying in the laboratory for 14 days and exposed to 4% CO_2 at 20 ± 2°C and 55 ± 5% RH in the carbonation chamber. The carbonation depths were measured by applying a phenolphthalein test. Measured carbonation depths were reported for water-to-cement ratiosequal to 0.52 and 0.65. At a water-to-cement ratio equal to 0.65, carbonation depths varied from 15 mm for Portland cement to 42 mm for 45% limestone concrete. At a water-to-cement ratio equal to 0.52, increase was smaller, and carbonation depths varied from 12 mm for Portland cement to 27 mm for 45% limestone concrete. The larger the replacement percentage, the greater the increase in carbonation depth. For 15% replacement, the increase was relatively small (about 3 mm at 0.52 and about 6 mm at 0.65 water-to-cement ratio), which led these authors (as well as many others) to conclude that 15% replacement of clinker with limestone powder is acceptable regarding carbonation resistance. At any replacement ratio, it was necessary to decrease the water-to-cement ratio to decrease the carbonation depth. If the water content is kept constant, this means that the content of clinker must be increased. Again, it was shown that such a mix design philosophy couldn't reduce the cement (clinker) content in the concrete, so the environmental goal could not be achieved.

It is obvious from the presented experimental results that desirable carbonation resistance cannot be achieved with higher replacement percentages (>15-20% by weight) unless something is changed in the mix design. All the previous experimental work based on the simple

replacement of cement with limestone powder and standard mix design showed that a maximum 10-15% of cement (clinker) could be replaced to maintain similar carbonation resistance [23-27].

As mentioned in Chapter 3, one possible measure is to reduce the water-to-cement (clinker) ratio. This procedure suggests the use of a high-performance superplasticizer. Furthermore, the optimization of the packing density is advantageous. The particle size distribution and the fineness of limestone powder play a key role in that sense. According to Palm et al. [28], parts of the limestone should be ground finer than clinker to serve as nucleation sites and therefore enhance the progress of hydration. Other parts of the limestone should be ground coarser than clinker to provide a broader particle size distribution and, therefore, a better packing density and a lower water demand [28]. This allows the reduction of the water demand and therefore the simultaneous minimization of the clinker content in the cement, as mentioned in Chapter 3.

This strategy of lowering the water-to-cement ratio in concrete mix design was thoroughly investigated and developed by a group of authors at the Technical University in Darmstadt, Germany [18, 28]. Some of their tested concrete mixture proportions and experimental results reported in [18] are presented in Table 1. Exact values of table-test flow were not reported, but it was stated in the article that the target value of table-test flow diameter of 550 mm was fulfilled in all mixtures.

The Blaine value of the limestone powder was 310 m^2/kg while this value was not reported for the used Portland cements. Carbonation resistance was tested under accelerated conditions. After 28 days of curing (7 days in water and 21 days at RH 65% and a temperature of 20°C), concrete samples (prisms 100×100×500 mm) were exposed to 2% CO_2, RH65% and a temperature of 20°C in the carbonation chamber. Carbonation depths were measured using the phenolphthale test.

It can be observed from Table 1 that not only the lowering of the water content was applied in the concrete mix design but also the measure of increasing the total powder paste volume, since the content of applied limestone powder was much larger than the content that corresponded to simple cement replacement. It can also be observed that limestone concretes had similar strength and carbonation resistance to Portland cement concrete with a water-to-cement ratio of 0.75 and a cement content of 240 kg/m^3. Although these concretes can be characterized as low-strength concretes, a reduction in clinker content of 37.5% was achieved. This is a significant reduction from an environmental point of view.

The same authors [18] also tested the influence of the limestone powder fineness, with the idea of enabling a further reduction in the water content. So they substituted successively the 'ordinary' limestone powder (limestone 1 in Table 2) with the Blaine value of 310 m^2/kg and d_{50}=15.4μm with very fine limestone powder with the Blaine value of 1600 m^2/kg and d_{50}=1.8μm (limestone 2 in Table 2).

Substitution of the ordinary with very fine limestone powder from 0-100% resulted in a compressive strength increase from 32 to 46 MPa. However, the lowest concrete viscosity and consequently the lowest demand for superplasticizer were obtained with a replacement ratio of 30%. These tests showed that particle size distribution and the fineness of the powder significantly affect the packing density, workability, and strength of concrete. The carbonation depths of the concrete mixes in Table 2 were not reported.

Table 1. Mixture proportions and measured carbonation depths [18]

	cement	fly ash	limestone	water	aggregate	SP	w/c*	f_c**, 28 days	d_c
concrete	kg/m^3	kg/m^3	kg/m^3	kg/m^3	kg/m^3	kg/m^3	/	MPa	mm
CEMI 52.5	270	10	-	165	1890	2.8	0.61	53.9	2.9
CEMI 42.5	270	10	-	165	1896	1.9	0.61	40.8	2.8
CEMI 32.5	270	10	-	165	1896	3.0	0.61	34.7	5.6
CEMI 52.5	240	-	-	180	1887	-	0.75	33.6	6.1
CEMI 32.5	240	-	-	180	1887	1.3	0.75	24.0	11.1
C150L289w145	150***	-	289	145	1781	5.1	0.97	27.6	12.3
C150L289w125	150***	-	289	125	1829	6.5	0.83	37.8	8.4

* water-to-cement ratio (cement refers to the amount of Portland cement)
** 150 mm cubes
*** CEMI 52.5

Table 2. Effect of the limestone powder fineness [18]

	CEM1 52.5	limestone 1	limestone 2	water	SP	w/c*	f_c**, 28 days
concrete	kg/m^3	kg/m^3	kg/m^3	kg/m^3	kg/m^3	/	MPa
C150L289/0	150	289	0	142	2.5	0.96	32.0
C150L246/43	150	246	43	142	2.5	0.96	36.8
C150L202/87	150	202	87	142	1.8	0.96	40.3
C150L159/130	150	159	130	142	2.2	0.96	40.1
C150L116/173	150	116	173	142	3.0	0.96	44.2
C150L72/217	150	72	217	142	3.0	0.96	46.3
C150L0/289	150	0	289	142	3.1	0.96	45.7

*) water-to-cement ratio (cement refers to the amount of Portland cement)
**) 150 mm cubes

The effect of particle size distribution and the fineness of the limestone powder was also investigated in Palm et al. [28]. This effect was investigated on concretes with 50% (by weight) replacement of cement (clinker) with three different limestone powders, LL1, LL2-1 and LL2-2 (Table 3). Limestone cement CEMII/A-LL 32.5 was adopted as the referent concrete. The terms cement and designation *c* in the w/c ratio in this work refer to the amount of CEMII/A-LL, and to the amount of cement+limestone in concretes with 50% replacement, respectively (designation of these concretes is CEM in Table 3).

Blaine values of limestone powders were: 420 kg/m^2 for LL1, 1050 kg/m^{2}for LL2-1 and 270 kg/m^{2}for LL2-2. The Blaine value of CEMII/A-LL was 365 kg/m^2. It should also be noted that the clinker part in CEM concretes was in fact CEMI 52.5 with a Blaine value of 551 kg/m^2. Each tested concrete mix was prepared with only one type of limestone powder.

Carbonation resistance was tested on 100×100×500 mm prisms under accelerated conditions: (2%CO_2, temperature equal to 20 ± 2°C and RH equal to 65 ± 5%) for 28 days. Before testing in the carbonation chamber, concrete samples were cured for 6 days in water and for 21 days at a RH of 65% and a temperature of 20°C. Carbonation depths were measured using the phenolphthalein test.

Let us choose CEMII/A-LL 32.5 with w/c equal to 0.5 as a reference middle-strength concrete with reasonably good carbonation resistance. It can be seen from Table 3 that concrete with 50% clinker replaced with limestone powder LL1 and w/c equal to 0.45 has significantly lower compressive strength and carbonation resistance. However, if the w/c is reduced to 0.35, all concretes with 50% limestone powder, regardless of the limestone type, have comparable or even higher strength and resistance to carbonation. The clinker part in CEMII/A-LL 32.5 ranges between 80 and 94%, in this case between 256 and 300 kg/m^3. Since the clinker part in CEM concretes with w/c equal to 0.35 was equal to 190 kg/m^3, the reduction in clinker content ranges between 25 and 37%, which is important from an environmental point of view. The cost is a significantly higher amount of superplasticizer: 2.6-11.9 kg/m^3, depending on the limestone powder fineness, instead of 1.6 kg/m^3.

Zhang et al. [7] have also experimentally shown that this approach in the mix design - lowering the water content – can have a positive effect on the carbonation resistance of limestone concrete, as well as on other properties. They tested two concrete mixes with the same amount of Portland cement CEM I 42.5 (240 kg/m^3) and limestone powder (160 kg/m^3) but different water contents equal to 160 kg/m^3 and 136 kg/m^3. Therefore, the replacement percentage was 40% in both mixes, while the water-to-binder ratios were equal to 0.4 and 0.33, respectively (binder is understood as cement+limestone). Since the water-to-binder ratios were low, relatively high amounts of superplasticizer were applied (6.36 and 8.18 kg/m^3, respectively), although measured slumps were not reported. Actual Blaine fineness was also not reported, but from the figure showing the particle size distribution, it can be concluded that limestone powder was significantly finer than cement. The carbonation tests on 100 mm cubes (after 3 and 28 days of standard curing) were conducted with a constant temperature and humidity (20±1°C, 60%±10% RH) in natural conditions for 1 year. For both periods of curing, measured carbonation depths were significantly lower for the mix with lower water content, i.e., a lower water-to-cement ratio: at 3 days of curing, carbonation depths were 9.8 mm and 6.7 mm, and at 28 days of curing, 4.5 mm and 2.7 mm for the mix with higher and lower water content, respectively. Since the total (cement and limestone) powder content was the same in both mixes, lower water content resulted in a lower water-to-cement ratio, which resulted in lower porosity and permeability of the concrete. No reference concrete with Portland cement was tested.

The strategy of "paste replacement", promoted by Chen et al. [17], is presented in the following text, although the authors did not investigate the carbonation resistance itself but compressive strength, water permeability, and sorptivity, as well as permeable porosity. However, these concrete properties are connected to carbonation resistance and therefore can indicate the effectiveness of this strategy. The authors tested three groups of concrete mixtures in which the volume of limestone powder was 0, 4, or 8% of the concrete volume. Within each group, three water-to-cement ratios (the term cement refers to the amount of used Portland cement, CEM I 52.5) were tested: 0.4, 0.5, and 0.6. In all concrete mixtures, the powder paste volume (cement paste + limestone powder), expressed as a percentage of the concrete volume, was kept constant at 34%. The mean particle sizes (d_{50}) of Portland cement and limestone powder were equal to 11.4 μm and 14.5 μm, respectively (similar fineness).

Mixture proportions and some of the experimental results are presented in Table 4. From these results, it can be concluded that the addition of limestone powder as a cement paste replacement, at a constant water-to-cement ratio increased the compressive strength and reduced the water penetration depth and permeable porosity. According to the authors, this indicated that the added limestone powder, which had a similar fineness as cement, was capable of filling into pores in concrete to reduce the porosity. The cost is, as before, the larger required amount of superplasticizer, which was almost doubled for the 8% addition of limestone powder.

Table 3. Mixture proportions and measured carbonation depths [28]

	cement*	w/c	SP	table flow	f_c**, 28 days	d_c
concrete	kg/m^3	/	kg/m^3	mm	MPa	mm
CEMII/A-LL 32.5	280	0.6	0	485	26.3	8.9
CEMII/A-LL 32.5	320	0.5	1.6	565	38.8	6.3
CEM(50% LL1)	335	0.45	NA	NA	26.7	11.5
CEM(50% LL1)	380	0.35	2.6	620	49.1	6.3
CEM(50% LL2-1)	380	0.35	5.7	515	52.1	3.9
CEM(50% LL2-2)	380	0.35	11.9	550	36.8	6.1

*) amount of CEMII/A in CEMII concretes, and amount of CEMI 52.5+limestone powder in CEM concretes
**) 150x300mm cylinder

Table 4. Mixture proportions and experimental results [17]

	cement	limestone powder	water	cement paste, vol.	SP, by mass of powder	slump	f_c **	Penetration depth	Permeable porosity***
concrete	kg/m^3	kg/m^3	kg/m^3	%	%	mm	MPa	mm	%
C-0.4-0*	470	0	188	34	0.98	225	74.8	31.0	10.1
C-0.4-4	415	106	166	30	1.23	245	80.5	19.5	8.4
C-0.4-8	359	211	144	26	1.94	255	85.1	18.5	7.8
C-0.5-0	413	0	207	34	0.89	230	56.0	56.0	14.3
C-0.5-4	364	106	182	30	0.98	235	62.0	26.5	10.4
C-0.5-8	315	211	158	26	1.57	255	68.7	23.0	8.8
C-0.6-0	368	0	221	34	0.48	210	44.3	75.0	16.2
C-0.6-4	325	106	195	30	0.79	230	49.2	36.0	12.5
C-0.6-8	281	211	169	26	1.05	230	51.5	29.0	10.9

*) C-w/c-%of limestone powder
**) 150 mm cubes at 28 days
***) the volume of pores that can be filled by water, expressed as a percentage of the concrete volume

Figure 4 presents the relationship between the carbonation depth and mean compressive strength of concrete, for Portland cement concrete (OPC) and limestone powder concrete (LS) with 15-65% (by weight) of limestone in the powder phase, calculated on a larger database. In total, 45 experimental results on the carbonation depth measured under accelerated conditions were taken from [18, 23, 25, 26, 28-32]. Since the concentration of CO_2 and the exposure time were different in the analysed research, the results on measured carbonation depth were converted to a CO_2 concentration equal to 2% and an exposure time equal to 28 days. As already mentioned in Chapter 3.1, the carbonation process can generally be described with the following equation:

$$d_c = k \cdot \sqrt{t} = K \cdot \sqrt{CO_2} \cdot \sqrt{t} \quad (2)$$

where carbonation rate coefficient k can be expressed as $K \cdot \sqrt{CO_2}$, K being a coefficient that depends on the concrete properties, curing, and environmental conditions, and CO_2 being a concentration of CO_2 in %. Considering the fact that the coefficient K does not depend on the CO_2 concentration, the previous equation allows us to compare the two carbonation depths ($d_{c,1}$ and $d_{c,2}$) from different test conditions (CO_2 concentrations ($[CO_2]_1$ and $[CO_2]_2$) and exposure times (t_1 and t_2)) for the same concrete type in the form:

$$\frac{d_{c,1}}{d_{c,2}} = \frac{\sqrt{[CO_2]_1}}{\sqrt{[CO_2]_2}} \cdot \frac{\sqrt{t_1}}{\sqrt{t_2}} \quad (3)$$

For $[CO_2]_1$ =2% and t_1 = 28 days, it follows:

$$d_{c,1} = d_{c,2} \cdot \frac{\sqrt{2}}{\sqrt{[CO_2]_2}} \cdot \frac{\sqrt{28}}{\sqrt{t_2}} \quad (4)$$

Reported compressive strengths of concrete were converted to the strength of a 150 mm cube and were considered as the mean compressive strength f_{cm}.

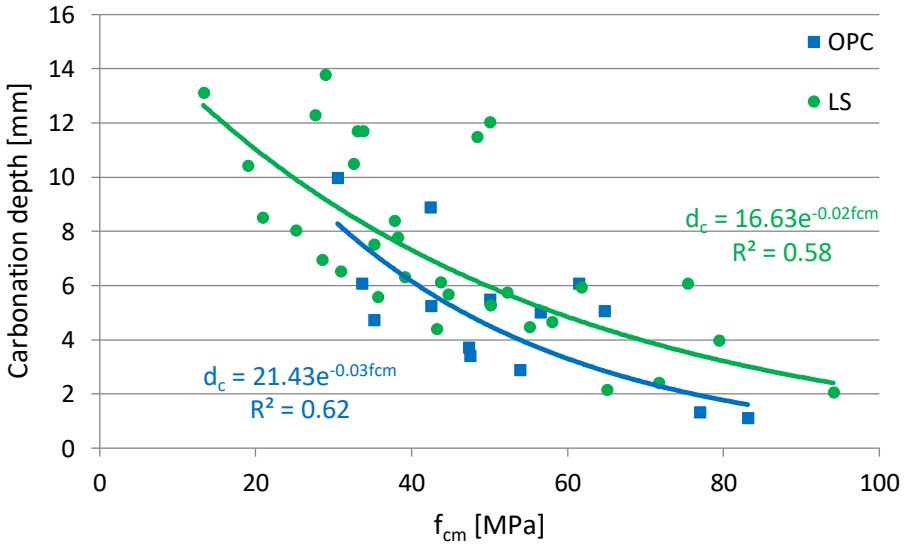

Figure 4. Relationship between the carbonation depth and mean compressive strength of concrete for Portland cement concrete (OPC) and limestone powder concrete (LS) with 15-65% (by weight) limestone in the powder phase

Figure 4 shows, as expected, that limestone powder concrete has a lower resistance to carbonation compared to OPC concrete. Experimental results were best fitted with exponential functions; however, the scatter is large for both types of concrete. In order to find out whether there is a limit in the limestone content where carbonation resistance similar to that of the OPC can be expected, the limestone concretes were divided into 3 groups with different limestone contents, as shown in Figure 5.

If we compare the carbonation depth of analyzed concrete mixes at equal strength, concrete with 15-25% limestone powder in the total powder phase performed even better than Portland cement concrete. With increasing limestone content, the resistance to carbonation decreased. Concrete with 26-35% limestone powder in the total powder phase had slightly lower carbonation resistance, while concrete with 45-65% limestone powder in the total powder phase showed significantly lower carbonation resistance; carbonation depth was on average doubled compared to Portland cement and 15-25% limestone concrete. Again, the experimental results were best fitted with exponential functions. It should be kept in mind that these relationships were obtained from a limited amount of experimental data, which may be the reason for the relatively high scatter of results. What is interesting, however, is that the scatter obtained for Portland cement concrete was higher than the scatter obtained for 15-25% and 26-35% limestone concrete. It can also be observed from Figure 5 that the results obtained by Palm et al. [28] are more of an exception than a general rule, pointing to a need for further experimental investigation into concrete mix design optimization.

5 Prediction models

The basic factors that influence the carbonation of cementitious materials are mixture proportions and related material quality, stress state (whether compression or tension [33], existence of cracks [34, 35]), environmental exposure (relative humidity, temperature, concentration of CO_2, and eventual coupling with other exposures such as chloride ingress [36]), and curing conditions.

Generally, mathematical models of the carbonation process are established by understanding the basic influential factors and quantitatively correlating these parameters with carbonation depth. Essentially, these are empirical models, and the vast majority of them are based on Fick's first law: the carbonation process is considered a diffusion of CO_2 through capillary pores under a concentration gradient (2):

$$d_c = k \cdot \sqrt{t} \tag{5}$$

The kinetics of carbonation, however, also depend on the kinetics of the hydration process and pore structure modification over time, which are mostly related to the type of SCM. Some researchers therefore proposed a value of exponent n different from 0.5 in the equation (2), modifying the relationship between d_c and time while keeping the carbonation rate coefficient k constant [37, 38]:

$$d_c = k \cdot t^n \tag{6}$$

So far, many prediction models of different complexity have been developed for Portland cement concrete and concrete with blended cements with FA and GGBS [39] or recycled aggregate concrete [37]. These models do not take into account other deterioration processes that can act simultaneously with carbonation or the effects of stress states and cracks. However, only a few models that can be applied to the concrete with limestone powder were found in the literature.

Wang [40] developed the hydration model that includes the dilution effect and the nucleation effect of limestone powder during the hydration of cement. From this model, he was able to calculate the carbonatable material contents and porosity, and considering the environmental conditions, the CO_2 diffusivity and carbonation depth of concrete. Starting from this model and the model proposed by Papadakis [41], Wang recently [16] proposed the following model for the carbonation depth of concrete with limestone powder:

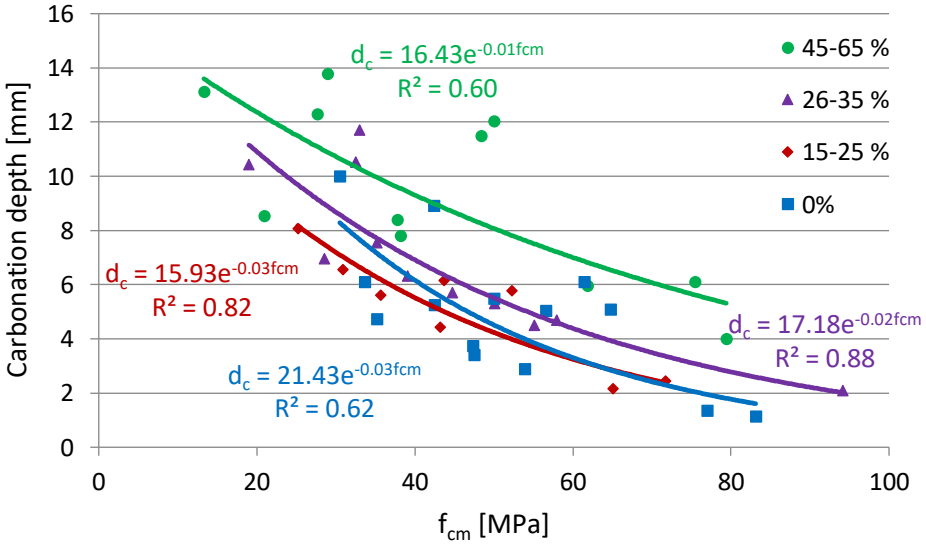

Figure 5. Relationship between the carbonation depth and mean compressive strength of concrete for Portland cement concrete (0%) and limestone powder concrete with different percentages of limestone in the powder phase

$$d_c = \sqrt{\frac{2D \cdot (CO_2)}{0.33 \cdot CH + 0.214 \cdot CSH}} \cdot \sqrt{t} \quad (7)$$

where

d_c is the carbonation depth
D is the CO_2 diffusivity
(CO_2) is the concentration of CO_2 in the exposure environment
CH is the mass of calcium hydroxide hydrate
CSH is the mass of calcium silicate hydrate

The CO_2 diffusivity depends on the concrete porosity and exposure conditions and author purposed the following equation:

$$D = 6.1 \cdot 10^{-6} \cdot \left(\frac{\varepsilon}{\frac{C}{\rho_C} + \frac{LS}{\rho_{LS}} + \frac{W}{\rho_W}} \right)^3 \cdot \cdot (1 - RH)^{2.2} \cdot \exp\left[\beta \left(\frac{1}{T_{ref}} - \frac{1}{T} \right) \right] \quad (8)$$

where

$$\varepsilon = \frac{W}{\rho_W} - \frac{0.25 \cdot C \cdot \alpha}{\rho_{CW}} - \frac{1.62 \cdot LS \cdot \alpha_{LS}}{\rho_{CW}} - \Delta\varepsilon_C \quad (9)$$

is the porosity of carbonated concrete

W, C, and LS are the contents of water, cement and limestone powder, respectively
ρ_C, ρ_{LS},ρ_W, and ρ_{CW} are the densities of cement, limestone powder, mixing water, and chemical combined water, respectively
α, α_{LS} are the degrees of the reactions of cement and limestone powder, respectively
RH is the relative humidity of the environment
$\beta = 4270$ is the activation energy of the CO_2 diffusion
$T_{ref} = 293K$ is the reference temperature
T is the environmental temperature

The equations for the calculation of the amounts of carbonatable compounds, CH and CSH, and degrees of cement and limestone powder reactions, α and α_{LS} were provided in the paper [16]. This rather complex model takes into account the reduction of concrete porosity due to the hydration of cement, the reaction of limestone powder, and carbonation (second, third, and fourth terms in equation (9), respectively). The reduction due to carbonation $\Delta\varepsilon_C$ can be evaluated using the change in the solid volume of reactants and products of carbonation [41]. The model was tested on limestone concretes with a 10% and 20% replacement ratio, and a good correlation with the experimental results was obtained.

Shah and Bishnoi [8] developed the empirical equation to predict carbonation depth in Portland cement and various blended cement concretes. They used the concrete strength and water-to-cement ratio instead of porosity in computing diffusion coefficient D, arguing that the properties of ITZ also have an impact on carbonation resistance. On the other hand, their model did not take into account the changes occurring in the microstructure due to carbonation that could alter the diffusion characteristics significantly. The model was tested against the experimental results obtained on several binary and ternary blend compositions (FA, limestone, and two types of clay at 45% joint replacement), and a reasonable correlation was obtained.

Beside Papadakis' models for carbonation of Portland cement and blended cement concrete [42, 41], Yang's model [43] is also often referred to. However, the correction factors for the substitution of cement with SCMs are given for FA, GGBS and silica fume and not for the limestone powder in this model.

It is obvious that such mathematical models are extremely time- and cost-consuming for every-day engineering practice and that simpler models are needed. One such simpler and more robust model, which considers the concrete quality, curing conditions, and environmental conditions, is given in the *fib* Model Code 2010 [44]. The Model Code 2010 equation has already been applied in practice for the assessment of carbonation depth d_c with time t:

$$d_c = k \cdot W(t) \cdot \sqrt{t} \quad (10)$$

where

$$k = \sqrt{2 \cdot k_e \cdot k_c \cdot R_{NAC,0}^{-1} \cdot C_s} \quad (11)$$

is the carbonation rate coefficient

k_e is the environmental function [-]
k_c is the execution transfer parameter [-]
$R_{NAC,0}^{-1}$ is the inverse effective carbonation resistance of concrete under natural conditions [(mm^2/years)/(kg/m^3)]
C_s is the CO_2 concentration in the air [kg/m^3]
$W(t)$ weather function [-]

The inverse effective carbonation resistance of concrete under natural conditions $R_{NAC,0}^{-1}$ is a property of concrete that depends mostly on the water-to-cement ratio and binder type. The đetermination of this concrete property would, however, take years. For that reason, Code purposefully applied the inverse effective carbonation resistance measured under accelerated carbonation conditions $R_{ACC,0}^{-1}$ and established the relationship between them:

$$R_{NAC,0}^{-1} = k_t \cdot R_{ACC,0}^{-1} + \varepsilon_t \quad (12)$$

where

$R_{ACC,0}^{-1}$ is the inverse effective carbonation resistance of dry concrete, determined at a certain time $t_0$using the accelerated carbonation test ACC[(mm^2/years)/(kg/m^3)]
$R_{NAC,0}^{-1}$ is the inverse effective carbonation resistance of dry concrete (65%RH) at a certain time t_0 using the normal (natural conditions) carbonation test NAC [(mm^2/years)/(kg/m^3)]
k_t is the regression parameter for the test effect of the ACC test [-]
ε_t is the error term for inaccuracies which occur conditionally when using the ACC test method [(mm^2/years)/(kg/m^3)]

For further instructions, MC 2010 refers to *fib* Model Code for service life design [45] in which all the required parameters are given. $R_{ACC,0}^{-1}$ is to be determined experimentally and conditions for the ACC test are defined: 100/100/500 mm prisms are to be exposed to CO_2 2% vol., temperature equal to 20°C and RH equal to 65% for 28 days. If no test data is available, fib Model Code for service life design offers $R_{ACC,0}^{-1}$ values for several cement types (CEM I, CEM I+FA and CEM III) and several water-to-cement ratios. So, the model should be valid for all binder types and water-to-cement ratios, only the $R_{ACC,0}^{-1}$ has to be measured.

However, some researchers have proven that for some binder types, for instance, binders with high amounts of FA, this doesn't have to be true [37]. There is, of course, the question of the capability of the ACC tests to represent the real natural conditions. Some researchers have pointed out that the kinetics of carbonation can be significantly changed under accelerated conditions, especially for high (>4%) CO_2 concentrations [37, 46, 47]. Moreover, this effect is different for different types of SCM, probably depending on their different reactivity, whether being inert or having pozzolanic activity. Lollini and Redaelli in their recent study [9] showed, however, that the ACC conditions in [45] were chosen well, at least for the outdoor sheltered conditions. They compared the measured carbonation rate coefficient of concretes with various types of SCM, including concretes with up to 30% limestone powder, under natural (outdoor sheltered for 12 years) and accelerated conditions according to [45] and obtained reasonable agreement. They also concluded that the type of binder had the greatest effect on the quality of the modelling of NAC with ACC conditions.

Although relatively simple, the application of this model requires an experimental determination of $R_{ACC,0}^{-1}$. In that way, this property gets the same importance as the compressive strength of concrete in practical applications: it has to be experimentally determined. Aside from the time needed for the ACC test, proper laboratory equipment (carbonation chamber) is also required. Finding alternatives, for instance, by connecting empirically $R_{ACC,0}^{-1}$ to the compressive strength of concrete, would significantly improve the practicability of the model.

6 Conclusion

From the analysis of the experimental and theoretical work in the area of the carbonation resistance of concrete with limestone powder, the following conclusions are drawn:

– replacing the clinker with up to 15% limestone powder practically does not affect the resistance to carbonation,

– replacing the clinker with a higher content of limestone powder significantly reduces the carbonation resistance, if no other measure in the concrete mix design and technology is undertaken; the decrease is larger with a larger replacement ratio,

– several measures in the concrete mix design were experimentally proven to be effective in compensating the dilution effect of limestone powder: lowering the water content, increasing the powder paste volume, and improving the particle packing by combing the powders with different fineness,

– concrete with 50% of limestone in the powder phase can be designed to have satisfactory carbonation resistance (in comparison to the pure-clinker concrete), enabling the environmentally significant reduction of clinker; however, this comes at the cost of a significantly larger superplasticizer content,

– several complex mathematical prediction models of the carbonation resistance of limestone concrete, based on Fick's first law, can currently be found in the literature,

– it is not yet proven that the *fib* MC 2010 prediction model is applicable to concrete with a higher content of limestone powder (>15-20% of the powder phase).

The *fib* MC 2010 prediction model for concrete carbonation is relatively simple and robust and therefore recommendable for practical applications. The future research should be oriented towards advancements in mix design optimization and implementing this model on middle- and high-content limestone concrete carbonation. Further, in order to avoid the experimental determination of the ACC inverse effective carbonation resistance, finding the empirical relationship to the compressive strength of concrete would significantly improve the practicability of the model.

In general, research on the new SCMs, such as calcined clay or calcined sand, is recommended. It is necessary to find and investigate long-term solutions to CO_2 mitigation that can replace commonly used FA and GGBS, keeping in mind that these SCMs are not globally available in sufficient amounts.

Acknowledgement

This work was performed within the Master´s thesis of Matija Marinković, student of the Master Studies at the Faculty of Civil Engineering, University of Belgrade. We gratefully acknowledge the support of the teaching staff at the Department of Materials and Structures, especially the group for Concrete Structures.

References

[1] ISO/TC 071 (2016). Strategic Business Plan ISO/TC 071 (ISO Technical Committee for concrete, reinforced concrete and prestressed concrete). https://www.iso.org/

[2] S.A. Miller, A. Horvath, P.J.M.Monteiro, (2016) Readily implementable techniques can cut annual CO_2 emissions from the production of concrete by over 20%, Environmental Research Letters 11, 074029.doi:10.1088/1748-9326/11/7/074029

[3] S.Marinkovic, M. Malesev, I. Ignjatovic(2014) Life cycle assessment (LCA) of concrete made using recycled concrete or natural aggregates. In (eds.) Pacheco-Torgal, F., Cabeza, L.F., Labrincha, J., de Magalhaes, A.: Eco-efficient construction and building materials, Woodhead Publishing Limited, Cambridge, 2014.

[4] Sonja A.A.M. Fennis, Joost C. Walraven (2012) Using particle packing technology for sustainable concrete mixture design, HERON Vol. 57 No. 2, 73-101.

[5] SushreeSunayana, Sudhirkumar V. Barai (2017) Recycled aggregate concrete incorporating fly ash: Comparative study on particle packing and conventional method, Construction and Building Materials 156, 376–386. http://dx.doi.org/10.1016/j.conbuildmat.2017.08.132

[6] Ksenija Tešić, Snežana Marinković, Aleksandar Savić (2021) Influence of cement replacement with limestone filler on the properties of concrete, Building Materials and Structures 64, 165-170. doi: 10.5937/GRMK2103165T

[7] Zengqi Zhang, Qiang Wang, Honghui Chen (2016) Properties of high-volume limestone powder concrete under standard curing and steam-curing conditions, Powder Technology 301, 16–25. http://dx.doi.org/10.1016/j.powtec.2016.05.054

[8] Vineet Shah, Shashank Bishnoi (2018) Carbonation resistance of cements containing supplementarycementitious materials and its relation to various parameters of concrete, Construction and Building Materials 178, 219–232. https://doi.org/10.1016/j.conbuildmat.2018.05.162

[9] Federica Lollini, Elena Redaelli (2021) Carbonation of blended cement concretes after 12 years of natural exposure, Construction and Building Materials 276, 122122. https://doi.org/10.1016/j.conbuildmat.2020.122122

[10] Eliana Soldado, Ana Antunes, Hugo Costa, Ricardo do Carmo, Eduardo Júlio (2021) Durability of mortar matrices of low-cement concrete with specific additions, Construction and Building Materials 309, 125060. https://doi.org/10.1016/j.conbuildmat.2021.125060

[11] UN Environment (2017) Eco-efficient cements: Potential economically viable solutions for a low-CO_2 cement based materials industry. United Nations Environment Programme, Paris 2017.

[12] Vanderley M. John, Bruno L. Damineli, Marco Quattrone, Rafael G. Pileggi (2018)Fillers in cementitious materials — Experience, recent advances and future potential. Cement and Concrete Research 114, 65–78. http://dx.doi.org/10.1016/j.cemconres.2017.09.013

[13] EN 197-1, Cement - Part 1: Composition,specifications and conformity criteria for commoncements Eur. Comm. Stand. Brussels. (2011).

[14] Andrija Radović, Snežana Marinković, Aleksandar Savić(2021) Compressive strength of green concrete with low cement and high filler content, Building Materials and Structures 64, 93-108. doi: 10.5937/GRMK2102093R

[15] WBCSD Cement Sustainability Initiative, GNR Project Reporting CO_2, World Bus.Counc. Sustain. Dev.(2018). https://gccassociation.org/gnr/. Accessed 7.4.2021.

[16] Xiao-Yong Wang (2020) Optimal mix design of low-CO_2 blended concrete with limestone powder, Construction and Building Materials 263, 12100. https://doi.org/10.1016/j.conbuildmat.2020.121006

[17] J.J. Chen, A.K.H. Kwan, Y. Jiang (2014) Adding limestone fines as cement paste replacement to reduce water permeability and sorptivity of concrete, Construction and Building Materials 56, 87–93. http://dx.doi.org/10.1016/j.conbuildmat.2014.01.066

[18] TiloProske, Stefan Hainer, MoienRezvani, Carl-Alexander Graubner (2013) Eco-friendly concretes with reduced water and cement contents — Mix design principles and laboratory tests, Cement and Concrete Research 51, 38–46. http://dx.doi.org/10.1016/j.cemconres.2013.04.011

[19] Jones M, Dhir R, Newlands M, Abbas A. (2000) A study of the CEN test method formeasurement of the carbonation depth of hardened concrete. Materials and Structures 33, 135–42. http://dx.doi.org/10.1007/BF02484168.

[20] Q.T. Phung, N. Maes, D. Jacques, E. Bruneel, I.V. Driessche, G. Ye, G.D. Schutter (2015) Effect of limestone fillers on microstructure and permeability due tocarbonation of cement pastes under controlled CO_2 pressure conditions, Construction and Building Materials 82, 376–390. http://dx.doi.org/10.1016/j.conbuildmat.2015.02.093

[21] Abdurrahman A. Elgalhud, Ravindra K. Dhir, Gurmel S. Ghataora (2017) Carbonation resistance of concrete: limestoneaddition effect, Magazine of Concrete Research 69(2), 84–106. http://dx.doi.org/10.1680/jmacr.16.00371

[22] Daman K. Panesar, Runxiao Zhang (2020) Performance comparison of cement replacing materials in concrete: Limestone fillers and supplementary cementing materials – A review, Construction and Building Materials 251, 118866. https://doi.org/10.1016/j.conbuildmat.2020.118866

[23] Federica Lollini, Elena Redaelli, Luca Bertolini (2014) Effects of Portland cement replacement with limestone on the properties of hardened concrete, Cement& Concrete Composites 46, 32–40, http://dx.doi.org/10.1016/j.cemconcomp.2013.10.016

[24] Muhammad Khokhar, Emmanuel Rozière, Frédéric Grondin, Ahmed Loukili.(2007) Effect of Mineral Additiveson Some of Durability Parameters of Concrete. 2nd International Conference on Advances inCement Based Materials and its Application to Civil Infrastructure, 2007, Lahore, Pakistan. https://hal.science/hal-01008100

[25] M. Collepardi, S. Collepardi, J.J. OgoumahOlagot, F. Simonelli(2004) The influence of slag and fly ash on the carbonation of concretes, in: Eighth CANMET/ACI Int. Conf. Fly Ash, Silica Fume, Slag, Nat. Pozzolans Concr., Proccedings ACI SP-221-29, Las Vegas, Nevada, USA, 2004, pp. 23–29.

[26] Mohammed SeddikMeddah, Mukesh C. Lmbachiya, Ravindra K. Dhir (2014) Potential use of binary and composite limestone cements in concrete production, Construction and Building Materials 58, 193–205. http://dx.doi.org/10.1016/j.conbuildmat.2013.12.012

[27] L.J. Parrott (1996) Some effects of cement and curing upon carbonation and reinforcement corrosion in concrete, Materials and Structures 29, 164–173.

[28] Sebastian Palm, TiloProske, MoienRezvani, Stefan Hainer, Christoph Müller,Carl-Alexander Graubner(2016)Cements with a high limestone content – Mechanical properties, durability and ecological characteristics of the concreteConstruction and Building Materials 119, 308–318. http://dx.doi.org/10.1016/j.conbuildmat.2016.05.009

[29] Radović, A., Hafez, H., Tošić, N., Marinković, S., de la Fuente, A. (2022) ECO2 framework assessment of limestone powder concrete slabs and columns. Journal of Building Engineering 57, 104928. https://doi.org/10.1016/j.jobe.2022.104928

[30] Robalo, K., Soldado, E., Costa, H., do Carmo, R., Alves, H., Júlio, E. (2021) Efficiency of cement content and of compactness on mechanical performance of low cement concrete designed with packing optimization. Construction and Building Materials 266, 121077. https://doi.org/10.1016/j.conbuildmat.2020.121077

[31] Marques, P.F., Chastre, C., Nunes, Â.(2013) Carbonation service life modelling of RC structures for concrete with Portland and blended cements. Cement and Concrete Composites 37, 171–184. https://doi.org/10.1016/j.cemconcomp.2012.10.007

[32] Leemann, A., Nygaard, P., Kaufmann, J., Loser, R. (2015) Relation between carbonation resistance, mix design and exposure of mortar and concrete. Cement and Concrete Composites 62, 33–43. https://doi.org/10.1016/j.cemconcomp.2015.04.020

[33] Chao Jiang, Xianglin Gu, Weiping Zhang, Wei Zou (2015) Modeling of carbonation in tensile zone of plain concrete beams damaged by cyclic loading, Construction and Building Materials 77, 479–488. http://dx.doi.org/10.1016/j.conbuildmat.2014.12.088

[34] Xiao-Hui Wang, Dimitri V. Val, Li Zheng, M. Roderick Jones (2018) Influence of loading and cracks on carbonation of RC elements made of different concrete types,Construction and Building Materials 164, 12–28. https://doi.org/10.1016/j.conbuildmat.2017.12.142

[35] Vedran Carević, Ivan Ignjatović (2019) Influence of loading cracks on the carbonation resistance of RC elements, Construction and Building Materials 227, 116583. https://doi.org/10.1016/j.conbuildmat.2019.07.309

[36] Jun Liu, QiwenQiu, Xiaochi Chen, Feng Xing, NingxuHan, Yijian He, Yueshan Ma (2017) Understanding the interacted mechanism between carbonation and chloride aerosol attack in ordinary Portland cement concrete, Cement and Concrete Research 95, 217–225. http://dx.doi.org/10.1016/j.cemconres.2017.02.032

[37] Vedran Carević, Ivan Ignjatović, Jelena Dragaš (2019) Model for practical carbonation depth prediction for high volume fly ash concrete and recycled aggregate concrete,Construction and Building Materials 213, 194–208. https://doi.org/10.1016/j.conbuildmat.2019.03.267

[38] KritsadaSisomphon, Lutz Franke (2007) Carbonation rates of concretes containing high volume of pozzolanic materials, Cement and Concrete Research 37, 1647–1653.doi:10.1016/j.cemconres.2007.08.014

[39] QiwenQiu (2020)A state-of-the-art review on the carbonation process in cementitious materials: Fundamentals and characterization techniques, Construction and Building Materials 247, 118503. https://doi.org/10.1016/j.conbuildmat.2020.118503

[40] Xiao-Yong Wang (2017) Modeling of Hydration, Compressive Strength, and Carbonation of Portland-Limestone Cement(PLC) Concrete, Materials 10, 115; doi:10.3390/ma10020115

[41] Vagelis G. Papadakis (2000) Effect of supplementary cementing materials on concrete resistance against carbonation and chloride ingress, Cement and Concrete Research 30, 291–299.

[42] V.G. Papadakis, C.G. Vayenas, M.N. Fardis(1991) Fundamental modelling andexperimental investigation of concrete carbonation, ACI Material Journal 88, 363–373.

[43] Keun-Hyeok Yang, Eun-A Seo, Sung-Ho Tae (2014)Carbonation and CO_2 uptake of concrete, Environmental Impact Assessment Review 46, 43–52. http://dx.doi.org/10.1016/j.eiar.2014.01.004

[44] fib, Model code 2010 final draft, vol. 2. fib Bulletin, N. 66, Lausanne, 2012.

[45] fib. Model code for service life design. fib Bulletin, N. 34, Lausanne, 2006.

[46] H. Cui, W. Tang, W. Liu, Z. Dong, F. Xing (2015) Experimental study on effects of CO_2concentrations on concrete carbonation and diffusion mechanisms, Construction and Building Materials 93, 522–527. https://doi.org/10.1016/j.conbuildmat.2015.06.007.

[47] J.H.M. Visser (2014) Influence of the carbon dioxide concentration on the resistance to carbonation of concrete, Construction and Building Materials 67, 8–13. https://doi.org/10.1016/j.conbuildmat.2013.11.005

Building Materials and Structures

GUIDE FOR AUTHORS

In the journal *Building Materials and Structures*, the submission and review processes take place electronically. Manuscripts are submitted electronically (online) on the website **https: // www.dimk.rs**. The author should register first, then log in and finally submit the manuscript which should be in the form of editable files (e.g. Word) to enable the typesetting process in journal format. All correspondence, including Editor´s decision regarding required reviews and acceptance of manuscripts, take place via e-mail.

Types of articles

The following types of articles are published in *Building Materials and Structures:*

Original scientific article. It is the primary source of scientific information, new ideas and insights as a result of original research using appropriate scientific methods. The results are presented briefly, but in a way to enable readers to assess the results of experimental or theoretical/numerical analyses, so that the research can be repeated and yield with the same or results within the limits of tolerable deviations.

Review article. It presents the state of science in particular area as a result of methodically systematized, analyzed and discussed reference data. Only critical review manuscripts will be considered as providing novel perspective and critical evaluation of the topics of interest to broader BMS readership.

Preliminary report. Contains the first short notifications of research results without detailed analysis, i.e. it is shorter than original research paper.

Technical article. Reports on the application of recognized scientific achievements of relevance to the field of building materials and structures. Contain critical analysis and recommendations for adaption of the research results to practical needs.

Projects Notes. Project Notes provide a presentation of a relevant project that has been built or is in the process of construction. The original or novel aspects in design or construction should be clearly indicated.

Discussions. Comment on or discussion of a manuscript previously published in *Building Materials and Structures*. It should be received by the Editor-in-Chief within six months of the online publication of the manuscript under discussion. Discussion Papers will be subject to peer review and should also be submitted online. If Discussion Paper is selected for publication the author of the original paper will be invited to respond, and Discussion Paper will be published alongside any response that the author.

Other contributions

Conference Reports. Reports on major international and national conferences of particular interest to *Building Materials and Structures*. Selected and/or awarded papers from the ASES Conferences are published in Special issues.

Book Reviews. Reviews on new books relevant to the scope of *Building Materials and Structures*.

Manuscript structure

The manuscript should be typed one-sided on A4 sheets. Page numbers should be included in the manuscript and the text should be single spaced with consecutive line numbering - these are essential peer review requirements. The figures and tables included in the single file should be placed next to the relevant text in the manuscript. The corresponding captions should be placed directly below the figure or table. If the manuscript contains Supplementary material, it should also be submitted at the first submission of the manuscript for review purposes.

There are no strict rules regarding the structure of the manuscript, but the basic elements that it should contain are: Title page with the title of the manuscript, information about the authors, abstract and keywords, Introduction, Materials / Methods, Results and Conclusions.

The front page

The front page contains the title of the manuscript which should be informative and concise; abbreviations and formulas should be avoided.

Information about the authors are below the title; after the author's name, a superscript number is placed indicating his/her affiliation, which is printed below the author's name, and before the abstract. It is obligatory to mark the corresponding author with superscript *) and provide his/her e-mail address. The affiliation should contain the full name of the institution where the author performed the research and its address.

Abstract

Abstract should contain 150-200 words. Motivation and objective of the conducted research should be presented; main results and conclusions should be briefly stated as well. References and abbreviations should be avoided.

Keywords

Keywords (up to 10) should be listed immediately after the abstract; abbreviations should be used only if they are generally accepted and well-known in the field of research.

Division into chapters

The manuscript should be divided into chapters and sub-chapters, which are hierarchically numbered with Arabic numbers. The headings of chapters and sub-chapters should appear on their own separate lines.

Appendices

The manuscript may have appendices. If there is more than one appendix, they are denoted by A, B, etc. Labels of figures, tables and formulas in appendices should contain the label of the appendix, for example Table A.1, Figure A.1, etc.

Acknowledgments

At the end of the manuscript, and before the references, it is obligatory to list institutions and persons who financially or in some other way helped the presented research. If the research was not supported by others, it should also be stated in this part of the manuscript.

Abbreviations

All abbreviations should be defined where they first appear. Consistency of abbreviations used throughout the text should be ensured.

Math formulae

Formulae should be in the form of editable text (not in the format of figures) and marked with numbers, in the order in which they appear in the text. The formulae and equations should be written carefully taking into account the indices and exponents. Symbols in formulae should be defined in the order they appear, right below the formulae.

Figures

- figures should be made so that they are as uniform in size as possible and of appropriate quality for reproduction;
- the dimensions of the figures should correspond to the format of the journal: figures with a width approximately equal to the width of 1 column (± 80 mm width), width of 2 columns (± 170 mm width) or width of 1.5 columns (± 130 mm width);
- figures should be designed so that their size is not disproportionately large in relation to the content;
- the text on the figures should be minimal and the font used should be the same on all figures (Arial, Times New Roman, Symbol);
- figures should be placed next to the appropriate text in the manuscript and marked with numbers in the order in which they appear in the text;
- each figure should have a caption that is placed below the figure - the caption should not be on the figure itself.

In cases of unadequate quality of reproduction the author should be required to submit figures as separate files. In this case, the figure should be saved in TIFF (or JPG) format with a minimum resolution of 500 dpi.

Tables

- tables should be in the form of editable text (not in the format of figures);
- tables should be placed next to the appropriate text in the manuscript and marked with numbers in the order in which they appear in the text;
- each table should have a caption that is placed below the table;
- the tables should not show the results that are already presented elsewhere in the manuscript - duplicating the presentation of results should be avoided;
- tables are without vertical lines as boundaries between cells and shading cells.

References

Citation in the text

Each reference cited in the text should be in the reference list (and vice versa). It is not recommended to list unpublished results or personal communications in the reference list, but they can be listed in the text. If they are still listed in the reference list, the journal style references are used, with 'Unpublished results' or 'Personal communication' instead of the date of publication. Citing a reference as ‘in press’ means that it is accepted for publication.

Web references

Web references are minimally listed with the full URL and the date when the site was last accessed. These references can be included in the reference list, but can also be given in a separate list after the reference list.

Reference style

In text: References are given in the text by a number in square brackets in the order in which they appear in the text. Authors may also be referred to directly, but the reference number should always be given.

In reference list: References marked with a number in square brackets are sorted by numbers in the list.

Examples

Reference to a journal publication:

[1] V.W.Y. Tam, M. Soomro, A.C.J. Evangelista, A review of recycled aggregate in concrete applications (2000-2017), Constr. Build. Mater. 172 (2018) 272-292. https://doi.org/10.1016/j.conbuildmat.2018.03.240.

Reference to a book:

[3] A.H. Nilson, D. Darwin, C.W. Dolan, Design of Concrete Structures, thirteenth ed., Mc Graw Hill, New York, 2004.

Reference to a chapter in an edited book:

[4] J.R. Jimenez, Recycled aggregates (RAs) for roads, in: F Pacheco-Torgal, V.W.Y. Tam, J.A. Labrincha, Y. Ding, J. de Brito (Eds.), Handbook of recycled concrete and demolition waste, Woodhead Publishing Limited, Cambridge, UK, 2013, pp. 351–377.

Reference to a website:

[5] WBCSD, The Cement Sustainability Initiative, World. Bus. Counc. Sustain. Dev. http://www.wbcsdcement.org.pdf/CSIRecyclingConcrete-FullReport.pdf, 2017 (accessed 7 July 2016).

Supplementary material

Supplementary material such as databases, detailed calculations and the like can be published separately to reduce the workload. This material is published ‘as received’ (Excel or PowerPoint files will appear as such online) and submitted together with the manuscript. Each supplementary file should be given a short descriptive title.

Ethics in publishing

Authors are expected to respect intellectual and scientific integrity in presentation of their work.
The journal publishes manuscripts that have not been previously published and are not in the process of being considered for publication elsewhere. All co-authors as well as the institution in which the research was performed should agree to the publication in the journal. The authors are obliged not to publish the research which is already published in this journal (electronically or in print) in the same form, in English or any other language, without the written consent of the Copyright owner.

Authors are expected to submit completely original research; if the research of other researchers is used, it should be adequately cited. Authors who wish to include in their manuscript images, tables or parts of text that have already been published somewhere, should obtain permission from the Copyright owner and provide a proof in the process of submitting the manuscript. All material for which there is no such evidence will be considered the original work of the author. To determine the originality of the manuscript, it can be checked using the Crossref Similarity Check service.

The Journal and Publishers imply that all authors, as well as responsible persons of the institute where the research was performed, agreed with the content of the submitted manuscript before submitting it. The Publishers will not be held legally responsible should there be any claims for compensation.

Peer Review

This journal uses a single blind review process, which means that the authors do not know the names of the reviewers, but the reviewers know who the authors are. In the review process, the Editor-in-Chief first assesses whether the contents of the manuscript comply with the scope of the journal. If this is the case, the paper is sent to at least two independent experts in the field, with the aim of assessing its scientific quality and making recommendation regarding publication. If the manuscript needs to be revised, the authors are provided with the reviewers' remarks. The authors are obliged to correct the manuscript in accordance with the remarks, submit the revised manuscript and a special file with the answers to the reviewers within the given deadline. The final decision, whether the paper will be published in journal or not, is made by the Editor-in-Chief.

After acceptance

Once accepted for publication, the manuscript is set in the journal format. Complex manuscript is sent to the authors in the form of proof, for proof reading. Then, authors should check for typesetting errors, and whether the text, images, and tables are complete and accurate. Authors are asked to do this carefully, as subsequent corrections will not be considered. In addition, significant changes to the text and authorship at this stage are not allowed without the consent of the Editor-in-Chief. After online publication, changes are only possible in the form of Erratum which will be hyperlinked for manuscript.

Copyright

Authors retain copyright of the published papers and grant to the publisher the non-exclusive right to publish the article, to be cited as its original publisher in case of reuse, and to distribute it in all forms and media.

The published articles will be distributed under the Creative Commons Attribution ShareAlike 4.0 International license (CC BY-SA). It is allowed to copy and redistribute the material in any medium or format, and remix, transform, and build upon it for any purpose, even commercially, as long as appropriate credit is given to the original author(s), a link to the license is provided, it is indicated if changes were made and the new work is distributed under the same license as the original.

Users are required to provide full bibliographic description of the original publication (authors, article title, journal title, volume, issue, pages), as well as its DOI code. In electronic publishing, users are also required to link the content with both the original article published in *Building Materials and Structures* and the licence used.

Authors are able to enter into separate, additional contractual arrangements for the non-exclusive distribution of the journal's published version of the work (e.g., post it to an institutional repository or publish it in a book), with an acknowledgement of its initial publication in this journal.

Open access policy

Journal *Building Materials and Structures* is published under an Open Access licence. All its content is available free of charge. Users can read, download, copy, distribute, print, search the full text of articles, as well as to establish HTML links to them, without having to seek the consent of the author or publisher.

The right to use content without consent does not release the users from the obligation to give the credit to the journal and its content in a manner described under *Copyright*.

Archiving digital version

In accordance with law, digital copies of all published volumes are archived in the legal deposit library of the National Library of Serbia in the Repository of SCIndeks - The Serbian Citation Index as the primary full text database.

Cost collection to authors

Journal Building Materials and STtructures does not charge authors or any third party for publication. Both manuscript submission and processing services, and article publishing services are free of charge. There are no hidden costs whatsoever.

Disclaimer

The views expressed in the published works do not express the views of the Editors and the Editorial Staff. The authors take legal and moral responsibility for the ideas expressed in the articles. Publisher shall have no liability in the event of issuance of any claims for damages. The Publisher will not be held legally responsible should there be any claims for compensation.

Financial support

MINISTRY OF EDUCATION, SCIENCE AND TECHNOLOGICAL DEVELOPMENT OF REPUBLIC OF SERBIA

INSTITUTE FOR TESTING OF MATERIALS-IMS INSTITUTE, BELGRADE

SERBIAN CHAMBER OF ENGINEERS

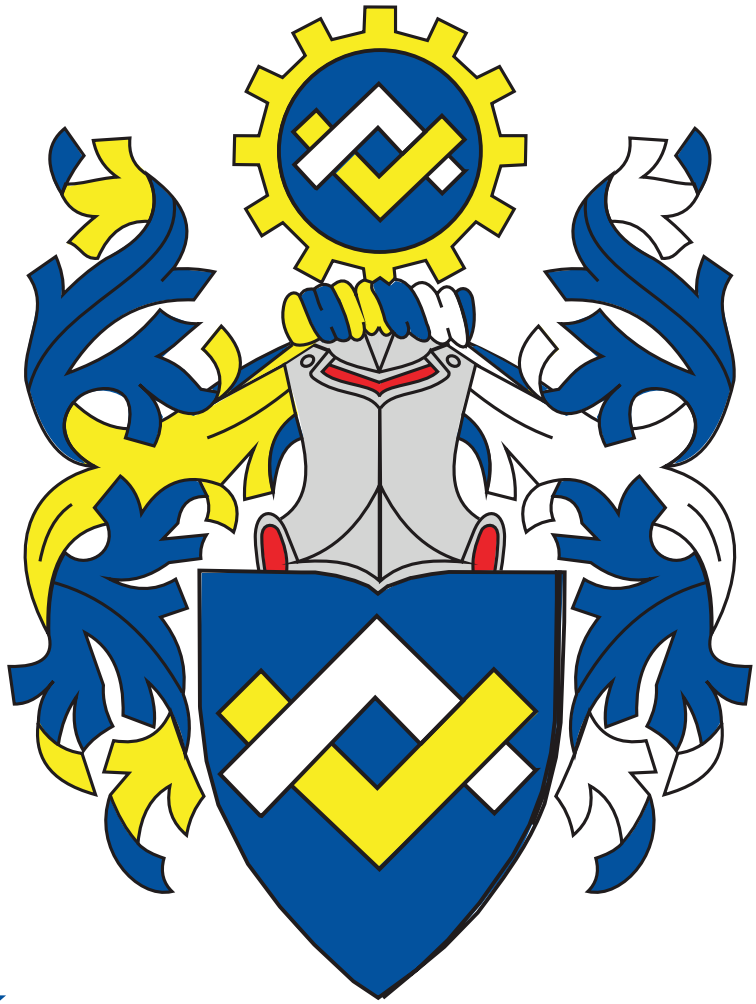

INŽENJERSKA KOMORA SRBIJE

Ringlock

Doka modularni sistem skela.

Bezbedno i efikasno rešenje za skele. Široka oblast primena.

PROVIDING ATPAC COMPLETE SCAFFOLDING SOLUTIONS

Pristupne skele

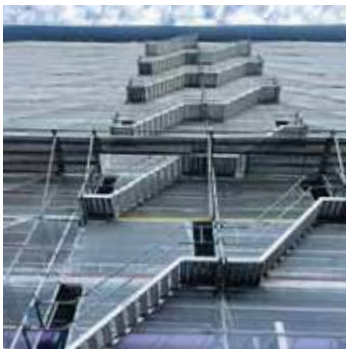

Skele za stambene objekte

Skele za poslovne objekte

Stepenišni toranj

Doka Serb d.o.o. | Svetogorska 4 | 22310 Šimanovci | Srbija | **T** +381 (0)22 400 100 | serb@doka.com | **www.doka.com/rs**

ACO. The future of drainage.

ACO

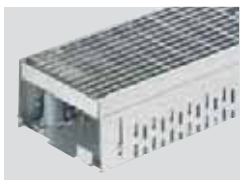

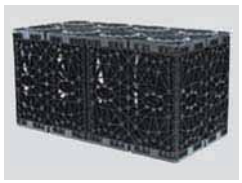

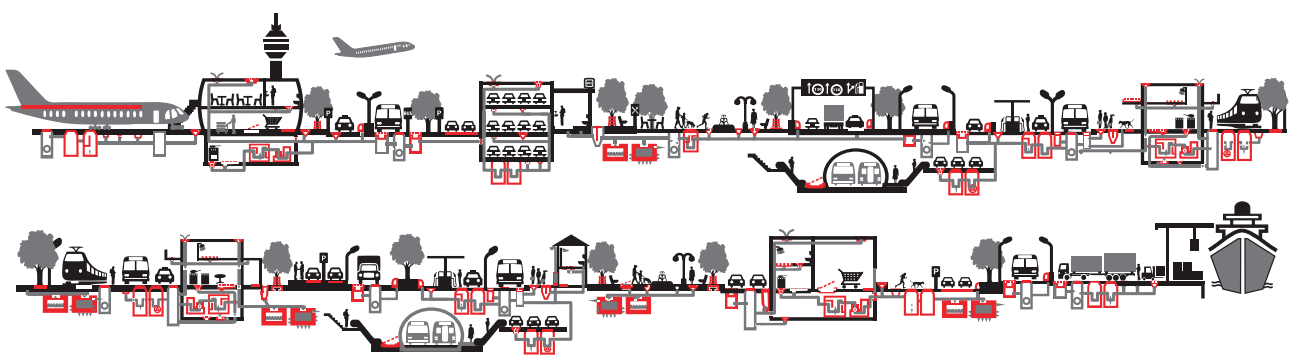

aco.rs

INSTITUT IMS AD
BEOGRAD

CENTAR ZA PUTEVE I GEOTEHNIKU

U okviru centra posluju odeljenja za geotehniku, nadzor i terenska ispitivanja, projektovanje saobraćajnica, laboratorija za puteve i geotehniku. Značajna aktivnost centra usmerena je ka terenskim i laboratorijskim geološko - geotehničkim istraživanjima i ispitivanjima terena za potrebe izrade projekno - tehničke dokumentacije, za različite faze i nivoe projektovanja objekata visokogradnje, niskogradnje, saobraćaja i hidrogradnje, kao i za potrebe prostornog planiranja i zaštite životne sredine. Stručni nadzor, kontrola kvaliteta tokom građenja, rekonstrukcije i sanacije objekata različite namene, izrada studija, ekspertiza, konsultantske usluge, kompletan konsalting u oblasti geotehničkog inženjeringa, neke su od delatnosti centra.

Ispitivanje šipova

- **SLT metoda (Static load test)**
- **DLT metoda (Dynamic load test)**
- **PDA metoda (Pile driving analysis)**
- **PIT (SIT) metoda (Pile (Sonic) integrity testing)**
- **CSL - Crosshole Sonic Logging**

- **Ispitivanje šipova**
  - **Geotehnička istraživanja i ispitivanja – in situ**
    - **Laboratorija za puteve i geotehniku**
      - **Projektovanje puteva i sanacija klizišta**
        - **Nadzor**

Tondach

Krovni sistemi

Najlepši krov u komšiluku

Continental Plus Natura je premium crep u natur segmentu! Dobro poznatog oblika, trajan i veoma otporan, a povrh svega pristupačan, naprosto oduzima dah svima. Čak i vašim komšijama!

Continental Plus Natura crep potražite kod ovlašćenih Tondach partnera.

Wienerberger

PUT INŽENJERING

Put inženjering d.o.o punih 25 godina radi kao specijalizovano preduzeće za izgradnju infrastrukture u niskogradnji i visokogradnji, kao i proizvodnjom kamenog agregata i betona. Preduzeće se bavi i transportom, uslugama građevinske mehanizacije i specijalne opreme.

Za spravljanje betona koristimo drobljeni krečnjački agregat sa našeg kamenoloma, deklarisanih frakcija, kontrolisane vlažnosti. Kompletan proces proizvodnje i kontrole kvaliteta vršimo prema važećim standardima.

Kao generalni izvođač radova, vršimo koordinaciju svih učesnika na projektu, planiranje, praćenje i nabavku materijala, kontrolu kvaliteta izvedenih radova, poštujući zadate vremenske rokove i finansijski okvir investitora.

Obradu armature vršimo brzo, stručno i kvalitetno, sa kompjuterskom preciznošću i dimenzijama po projektu.

Osnovi princip našeg poslovanja zasniva se na individualnom pristupu svakom klijentu i pronalaženje najoptimalnijeg rešenja za njegove transportne i logističke potrebe.

Koristeći inovativne tehnike i kvalitetan građevinski materijal iz sopstvenih resursa, spremni smo da odgovorimo na mnoge zahteve naših klijenata iz oblasti niskogradnje.

Naša kompanija u oblasti visokogradnje primenjuje sistem prefabrikovnih betonskih elemenata koji u odnosu na klasičnu gradnju ima brojne prednosti.

Usluge građevinskom mehanizacijom vršimo tehnički ispravnim mašinama, sa potrebnim sertifikatima kako za rukovaoce građevinskim mašinama tako i za same mašine.

Osnovna prednost prefabrikovane konstrukcije jeste brzina kojom konstrukcija može biti projektovana, proizvedena, transportovana i namontirana.

Prednapregnute šuplje ploče su konstruktivni elementi visokog kvaliteta, proizvedeni u fabrički kontrolisanim uslovima.

Raspolažemo opremom i mašinama za sve zemljane radove, kipere i dampere za rad u teškim terenskim uslovima, automiksere i pumpe za beton, autodizalice, podizne platforme.

Izvodimo hidrograđevinske radove u izgradnji kanalizacionih mreža za odvođenje atmosferskih, otpadnih i upotrebljenih voda, izvođenjem hidrograđevinskih radova u okviru regulacije rečnih tokova, kao i izvođenjem hidrotehničkih objekata.

Izrađujemo betonske "New Jersey profile" koji se u svetu koriste za preusmeravanje saobraćaja i zaštitu pešaka u toku izgradnje puta, kao i Betonblock sistem betonskih blokova.

Sakupljanje i privremeno skladištenje otpada vršimo našim specijalizovanim vozilima i deponujemo na našu lokaciju sa odgovarajućom dozvolom. Kapacitet mašine je 250 t/h građevinskog neopasnog otpada.

Površinski kop udaljen je 35 km od Niša. Savremene drobilice, postrojenje za separaciju i sejalica efikasno usitnjavaju i razdvajaju kamene agregate po veličinama. Tehnički kapacitet trenutne primarne drobilice je 300 t/h.

Uslugu transporta vršimo automikserima, kapaciteta bubnja od 7 m³ do 10 m³ betonske mase. Za ugradnju betona posedujemo auto-pumpu za beton, radnog učinka 150 m³/h, sa dužinom strele od 36 m.

NIŠ
Knjaževačka bb, 18000 Niš - Srbija
+381 18 215 355
office@putinzenjering.com

BEOGRAD
Jugoslovenska 2a, 11250 Beograd – Železnik
+381 11 25 81 111
beograd@putinzenjering.com

MOBECO

www.putinzenjering.com

Mapei proizvodi i rešenja su izbor onih koji znaju da prepoznaju kvalitet, posvećenost svakom detalju i višedecenijsko iskustvo u građevinskoj industriji.

Zato birajte pažljivo. Birajte kvalitet.

Mapei, svetski lider u proizvodnji građevinskih lepkova, hidroizolacija i masa za fugovanje.

Saznaj više na **www.mapei.rs**

MAPEI®

ŽIVI KVALITETNO

MATEST
YOUR PARTNER IN TESTING

iT TECH

INELAS ERECO d.o.o

MATEST "iT TECH" KONTROLNA JEDINICA

JEDNA TEHNOLOGIJA MNOGO REŠENJA

IT Touch Techlogy je Matestov najnoviji koncept koji ima za cilj da ponudi inovativna i user-friendly tehnologiju za kontrolu i upravljanje najmodernijom opremom u domenu testiranja građevinskih materijala

Ova tehnologija je srž Matestove kontrolne jedinice, software baziran na Windows platformi i touch screen sistem koji je modularan, fleksibilan i obavlja mnoge opcije

iT TECH pokriva
- INOVATIVNOST
- INTERNET KONEKCIJA
- INTERFEJS SA IKONICAMA
- INDUSTRIJALNA TEHNOLOGIJA

SISTEM JEDNOG RAZMIŠLJANJA JEDNOM SHVATIŠ - SVE TESTIRAŠ

NAPREDNA TEHNOLOGIJA ISPITIVANJA ASFALTA

- GYROTRONIC - Gyratory Compactor
- ARC - Electromechanical Asphalt Roller Compactor
- ASC - Asphalt Shear Box Compactor
- SMARTRACKER[tm] - Multiwheels Hamburg Wheel Tracker, DRY + WET test environment
- SOFTMATIC - Automatic Digital Ring & Ball Apparatus
- Ductilometers with data acquisition system

MULTIFUNKCIONALNI RAMOVI ZA TESTIRANJE

- CBR/Marshall digital machines
- Universal multispeed load frames
- UNITRONIC 50kN or 200kN Universal multipurpose compression/flexural and tensile frames

OPREMA ZA GEOMEHANIČKO ISPITIVANJE

- EDOTRONIC - Automatic Consolidation Apparatus
- SHEARLAB - AUTOSHEARLAB - SHEARTRONIC Direct / Residual shear testing systems
- Triaxial Load Frame 50kN

MIXMATIC - Automatic Programmable Mortar Mixer

INELAS ERECO D.O.O
Tošin bunar 274a, 11070 , Novi Beograd tel. +381 11 2284 574 email. info@inelasereco.rs

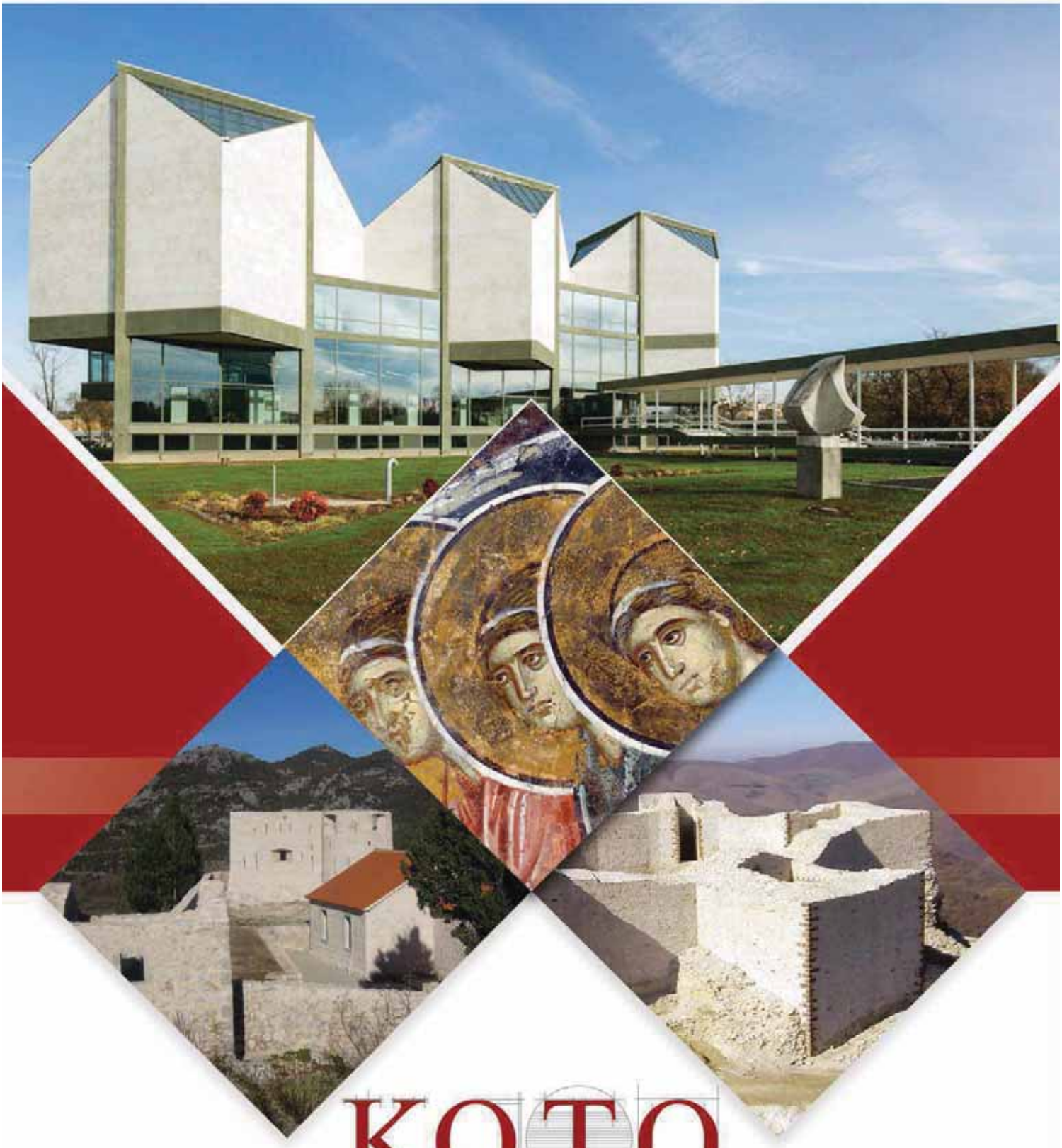

KOTO

www.koto.rs | office@koto.rs | 011 309 7410 | Vojvode Stepe br. 466, Beograd